Reviews in Mineralogy & Geochemistry
Vol. 89 pp. 147-206, 2023

Magmatic Evolution II: A New View of Post-Differentiation Magmatism

Charles Shearer[1,2†], Clive R. Neal[3†], Timothy D. Glotch[4], Tabb C. Prissel[2], Aaron S. Bell[5], Vera Assis Fernandes[6], Lisa R. Gaddis[7], Bradley L. Jolliff[8], Matthieu Laneuville[9], Tomáš Magna[10], Justin Simon[11]

[1]Institute of Meteoritics, University of New Mexico, Albuquerque, NM 87122, USA
[2]Lunar & Planetary Institute, Universities Space Research Association, Houtson, TX 77058, USA
[3]Department of Civil and Environmental Engineering and Earth Science University of Notre Dame Notre Dame, IN 46556, USA
[4]Department of Geosciences, Stony Brook University, Stony Brook, NY11794
[5]Geological Sciences, University of Colorado, Boulder, CO 80309, USA
[6]University of Manchester, Manchester, UK
[7]Astrogeology Science Center United States Geological Survey, Flagstaff, AZ 86001-1637, USA
[8]Department of Earth and Planetary Sciences, Washington University St. Louis, Saint Louis, Mo 63103-4899, USA
[9]Earth-Life Science Institute, Tokyo Institute of Technology, Tokyo, Japan
[10] Czech Geological Survey, Prague, Czech Republic
[11]NASA Johnson Space Center, Houston TX 77058, USA

[†]Designated chapter co-leads: cshearer@unm.edu; neal.1@nd.edu

1. INTRODUCTION AND SCOPE

1.1 Introduction

Just as the use of new tools revolutionized lunar science in 1610 (Galileo's telescope), 1840 (photography), and 1960s–1970s and 1990s (over 45 robotic and human missions to the Moon), data from science-driven, international lunar missions that have flown since 2000 (Gaddis et al. 2023, this volume) and technology-driven sample observations and computational methods have provided a 21st century perspective for the thermal and magmatic evolution of the Moon. In this chapter, we integrate all these observations to reexamine the steps forward that have been taken since publication of the New Views of the Moon 1 (NVM1) in 2006 (Jolliff et al. 2006). This chapter provides a summary of post-differentiation magmatism, describes new observations, and integrates and interprets these observations for renewed understanding of the thermal evolution of the Moon, the first stages of post-differentiation magmatism (Mg-suite, alkali-suite), continued periods of basaltic magmatism with an evolved trace element signature (i.e., elevated abundances of K, REE, P, U, Th, hereafter "KREEP"), mare magmatism, and felsic–silicic magmatism.

1.2 Summary of post-differentiation lunar magmatism in New Views of the Moon (NVM1, Jolliff et al. 2006)

NVM1 summarized both the pre-Apollo and Apollo view of the thermal and magmatic evolution of the Moon (Shearer et al. 2006), and expanded on these views of the Moon based on missions (Galileo, Clementine, Prospector), new samples (e.g., meteorites, clasts in the Apollo collection), improved and recently developed analytical methods (e.g., SIMS, TIMS), and computational and theoretical approaches (e.g., numerical hydrocode simulations).

1529-6466/23/0089-0004$10.00 (print)
1943-2666/23/0089-0004$10.00 (online)
http://dx.doi.org/10.2138/rmg.2023.89.04

Important observations and conclusions concerning post-differentiation magmatism identified in Jolliff et al. (2006) include (1) the lunar magma ocean (LMO) cumulate stratigraphy (and the sources for post-differentiation magmatism) was disrupted due to its density and temperature profile (cumulate overturn). (2) post-LMO highlands magmatism (e.g., Mg-suite) may consist of KREEP-rich rocks in the Procellarum-KREEP terrane, and KREEP-poor lithologies in other lunar terranes. (3) The distribution and duration of lunar volcanism is asymmetrical and is correlated with crustal thickness, the crustal concentration of heat-producing elements, and heat flux. (4) KREEP-rich basaltic magmatism occurred over a wide-range of time from 4380 Ma to < 2900 Ma. (5) Although the Apollo sample collection suggests a bimodal distribution of TiO_2 in mare basalts, remotely sensed data indicate that the high-TiO_2 basalts are rare and the frequency for TiO_2 has a median value of approximately 2.6 wt.% and is skewed to low TiO_2. (6) Mare magmatism may be as young as 1.0 Ga. (7) Pyroclastic glasses in the Apollo collection approach primary mare basalt melt compositions that were derived from the deep lunar mantle (> 400 km) and the crystalline mare basalts were either derived from or reequilibrated at shallower depths. (8) Pyroclastic deposits are more numerous than previously thought and are widely distributed around the Moon.

Missions, samples, analytical methods, and computational observations subsequent to NVM1 have revealed additional insights concerning the role of volatiles in lunar magmatism, the duration, distribution, diversity, and eruptive styles of magmatism, linkages among periods of magmatism, chronology of magmatism and the intimate relationship between thermal history and magma generation.

2. EARLIEST STAGES OF POST-DIFFERENTIATION MAGMATISM

2.1. Introduction

Fundamental details of pre-mare magmatism are presented in Jolliff et al. (2006) and here we summarize recent observations, with emphasis on the provenance of the Mg-suite rocks, the relationship of KREEP to the Mg-suite, and the diversity of ancient magmatism. Studies pertaining to the contemporaneous Alkali-suite receive due attention by Elardo et al. (2023, this volume) and McCubbin et al. (2023, this volume). The latter chapter focuses on constraining the volatile content of ancient magmas and mantle reservoirs.

An important elemental fingerprint associated with the Mg-suite samples returned by the Apollo program is KREEP. Although this section contains some discussion of KREEP, a more thorough discussion of KREEP and its prolonged magmatic history can be found in Gaffney et al. (2023, this volume) and in Sections 3 and 4 of this chapter. A more detailed discussion regarding the current structure and geologic processes responsible for the evolution and modification of the primordial lunar crust can be found in Elardo et al. (2023, this volume).

2.2. Provenance of the highlands Mg-suite

The magnesian-suite (Mg-suite) of rock fragments and clasts includes dunites, troctolites, pink spinel troctolites (PST), norites, and gabbronorites. They are distinguished from other ancient highlands magmatic rocks by Mg′ of mafic silicates and anorthite content of plagioclase (Fig. 1). The PST and troctolites contain the most forsteritic olivine compositions among lunar samples (Mg′ = molar Mg/(Mg + Fe) × 100 = up to Fo_{96}; Snyder et al. 1999), suggesting the Mg-suite parental melt was likely derived from an extremely MgO-rich mantle source (Fig. 1). However, two important observations complicate a simplistic petrogenetic model: The so-called Mg′ problem and an evolved trace element signature paired with primitive mineralogy (e.g., Hess 1994). In most basaltic systems, a substantial amount of olivine must crystallize prior to plagioclase saturation (decreasing the Mg/Fe of the residual system) and thus, the

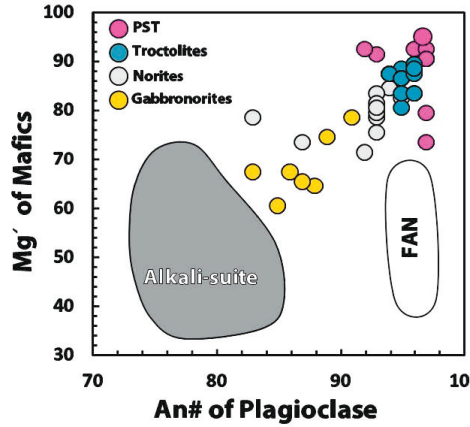

Figure 1. Mg′ of mafic silicates vs. the An# of plagioclase in the Mg-suite, Alkali-suite, and FAN. Pink spinel troctolites (PST) contain the most forsteritic olivine among lunar samples. After Prissel and Gross (2020).

pairing of highly forsteritic olivine and anorthitic plagioclase within lunar troctolites is an unexpected crystallization assemblage of mantle-derived melts. The other issue is an evolved trace element signature (i.e., KREEP) observed within the Mg-suite rocks relative to Ferroan Anorthosites, which suggests derivation from an evolved parent, but chemically contradicts the primitive mineralogy.

Several models have been proposed to explain the unique chemical characteristics of the Mg-suite samples: (1) an impact origin (Vaughan et al. 2013; Vaughan and Head 2014), (2) products of magma ocean crystallization, (3) re-melting and remobilization of late-stage KREEP-bearing magma ocean cumulates, (4) MgO-rich magmas derived from primary mantle cumulates enriched in Al and incompatible trace elements through assimilation of KREEP, anorthositic crust, or both (e.g., Prissel et al. 2016a; Prissel and Gross 2018, 2019, 2020), and (5a) melting of mixed and hybridized cumulate sources either in the deep or (5b) shallow lunar mantle (e.g., Shearer et al. 2006; Longhi et al. 2010; Elardo et al. 2011). Recent advances pertaining to models (1), (4), and (5a,b) are discussed herein. Further discussion regarding the alternative models above can be found in NVM-1 (Jolliff et al. 2006) and references therein, and the review here follows closely that of Shearer et al. (2015) updated with contributions since the time of their review.

Although the impact model for the origin of the Mg-suite has been generally disregarded (e.g., Hess 1994; Shearer and Papike 2005), it has been reevaluated by Vaughan et al. (2013). A recognized attribute of this model is that it provides an instantaneous heat source to produce large volumes of melt capable of crystallizing Mg-suite-like assemblages, depending on the precise contributions of target material. Considering shock melting during impacts, differentiation of voluminous impact melt sheets have been modeled for Orientale (thickness ≥ 15 km, Vaughan et al. 2013) and South Pole Aitken basin (diameter ≥ 350 km, Hurwitz and Kring 2014; Vaughan and Head 2014). Assuming an impact melt sheet was sufficiently insulated, slow cooling and crystallization could reproduce expected Mg-suite rock types and plutonic textures. Ultimately, Vaughan et al. (2013) concluded that the impact process could not specifically account for the petrogenesis of plutonic Mg-suite rocks, and several lines of reasoning present significant hurdles for this hypothesis. As discussed in Section 2.4, crystallization ages of the Mg-suite rocks are > 4100 Ma, and therefore no sample evidence exists to link petrogenesis of Mg-suite rocks in the current collections to many of the younger large impact basins preserved on the lunar near side (e.g., Orientale ~3750 Ma). Since a substantial olivine-dominated mantle component

must be incorporated during the impact to explain the high MgO-content required for the Mg-suite parent, large-quantities of olivine-dominant mantle lithologies should have been excavated and incorporated into the lunar regolith. There is little evidence for the excavation of olivine-dominated upper mantle within the current sample set and only small-scale exposures of olivine-rich lithologies within the remote sensing databases (e.g., Yamamato et al. 2010; Melosh et al. 2017). Incorporation of large proportions of anorthositic crust during impact would produce Al-rich parental melts prior to crystallization, which have been experimentally shown to yield PST mineralogy—inconsistent with the rarity and small volume of PST in the sample collection (Prissel et al. 2016a).

Petrogenetic models (4) and (5a,b) require a high-Mg′ mantle source component. New chemical constraints on the Mg-suite source are provided by several investigations on the crystallization sequence of bulk Moon compositions (for details see Gaffney et al. (2023, this volume). Elardo et al. (2011) experimentally verified that proposed LMO bulk compositions initially undergoing equilibrium crystallization would produce orthopyroxene (Opx)-bearing (± garnet and spinel) dunitic to harzburgitic mantle cumulates with sufficiently high MgO contents required for the Mg-suite source region. Deep cumulates produced during fractional crystallization of bulk Moon appear to be much more monomineralic, yielding almost pure dunitic deep mantles (e.g., Charlier et al. 2018; Rapp and Draper 2018; Lin et al. 2020). The cumulate mantle overturn hypothesis (CMO) provides a transport mechanism for hot and buoyant LMO cumulates to reach the base of the crust (e.g., Zhang et al. 2013, 2017; Dygert et al. 2016; Boukaré et al. 2018; Yu et al. 2019; Zhao et al. 2019). The MgO-rich cumulates could then be subjected to high-degrees of pressure-release melting during adiabatic ascent, possibly forming the Mg-suite primary melt in model (4), or mixing with evolved and plagioclase-bearing cumulates in (5b) (e.g., Longhi et al. 2010; Elardo et al. 2011; Shearer et al. 2015; Prissel et al. 2016a).

Shearer and Papike (2005) showed that another confusing attribute to the Mg-suite (and its high Mg′ source) was its low-Ni, -Co and -Cr. In response to this observation, Longhi et al. (2010) demonstrated that both Ni and Co behave incompatibly with olivine at pressures corresponding to a deep crystallizing magma ocean. Thus, early LMO mantle cumulates are expected to be poor in Ni and Co relative to later stages of LMO cumulates (e.g., sources for low-Ti mare basalts). Elardo et al. (2011) noted that early LMO cumulates appear to be too rich in Cr to explain the Cr-poor olivine in Mg-suite troctolites, suggesting that estimates of bulk Moon compositions may be too rich in Cr. In order to explain the complexity of primitive mineralogy, high Mg′ in silicates, low Co- and Ni-abundances in olivine, and evolved KREEP signature, a (5b) melting of a shallow-level hybridized mantle was modeled by Longhi et al. (2010). The modeled source was comprised of 85.5% dunite (high Mg′, low Co, Ni), 10% norite and 3% gabbronorite (plagioclase-bearing), and 1.5% KREEP. It was predicted that partial melts from this hybridized mantle reservoir would crystallize assemblages matching many of the geochemical paradoxes associated with Mg-suite lithologies. Incorporation of KREEP into the Mg-suite source region may also facilitate melting (Elardo et al. 2017). The geophysical feasibility of producing such a hybridized mantle during CMO, and the timescales associated with formation and later remelting of said source, has been explored (Section 2.4). Prissel et al. (2016a) experimentally investigated melts produced from a plagioclase-bearing hybridized mantle reservoir (5b). Their experiments demonstrated that partial melts from the hybridized source yield high-Al pink spinel and PST-like mineralogy upon crystallization. Thus, melts derived from the hybridized source suggested by Longhi et al. (2010) have difficulty explaining the production of chromite-bearing troctolites or troctolites without pink spinel. Prissel and Gross (2018, 2019) demonstrated that olivine-saturated melts derived from primary dunite cumulates can crystallize olivine and reach plagioclase co-saturation consistent with the lower Mg′ of common lunar troctolites.

2.3. Incorporation of lunar meteorites and remote sensing methods

While the Apollo samples represent the chemistry and mineralogy of lithologies within and adjacent to the Procellarum KREEP Terrane (PKT), lunar meteorites and orbital remote sensing provide a broader sampling of the Moon and excavated lithologies (e.g., Korotev et al. 2009; Pieters et al. 2014). As discussed above, many petrogenetic models infer that KREEP is inherent to the Mg-suite source region, or that KREEP was acquired during secondary processes (e.g., magma–wallrock interactions, magma-mixing at the base of or within the lunar crust). Thus, the presence and detection, or recovery of lunar Mg-suite samples collected outside of the PKT could elucidate the production and global extent of KREEP during LMO differentiation, and the global or regional role of KREEP in Mg-suite petrogenesis.

Classifying Mg-suite lithologies from lunar meteorites remains difficult due to the often-brecciated nature of candidate clasts presenting a significant challenge to establishing pristinity and interpreting true parentage and whole rock chemistry. Furthermore, the small size of many of the clasts probably do not represent the bulk mineralogy (as is also the case for some Apollo Mg-suite samples). Nonetheless, notable meteorite clasts containing similar geochemical characteristics as Apollo Mg-suite samples are available, but with a KREEP-poor chemical signature (see Joy et al. 2023, this volume).

Some examples of KREEP-poor troctolitic clasts containing primitive mineralogy consistent with Mg-suite samples are found within lunar meteorites Dhofar 489 and NWA 10401 (Takeda et al. 2006; Gross et al. 2020). Lunar meteorites MIL 090034/70/75 and MIL 090036 contain clasts and mineral fragments thought to be related Mg-suite lithologies (Liu et al. 2011), where the most primitive compositions are nearly identical to the most primitive troctolites observed from Apollo 17 (Shearer et al. 2015). Liu et al. (2011) and Shirai et al. (2012) reported bulk rock chemistry with a significant KREEP component, consistent with Apollo Mg-suite lithologies, though it is unknown if the individual clasts themselves contain a KREEP signature (Shearer et al. 2015). Gross and Treiman (2011) examined a pink spinel troctolite-like clast within lunar meteorite ALHA 81005,9, though the Mg′ of olivine and pyroxene, as well as the pink spinel (Mg′ 75, 78, and 65, respectively), are lower than most Apollo Mg-suite troctolites and pink spinel troctolites. Gross and Treiman (2011) concluded that such a clast could originate from either differentiation of an impact melt or interaction between picritic magma (with lower Mg′ than Mg-suite) and anorthositic crust. No age or trace element data have been reported to date on this clast.

The presence of KREEP-poor troctolitic clasts is consistent with being derived from the feldspathic highlands but could be derived from Mg-suite reservoirs outside of the PKT to explain the low abundance of REE. If true, it implies KREEP may not be a required component of Mg-suite lithologies (Takeda et al. 2006; Shearer et al. 2015; Prissel et al. 2016a). Prissel and Gross (2020) further challenged the Mg′ problem by sub-dividing the lunar troctolites based on spinel chemistry, and demonstrated that KREEP-free mantle-derived melts can crystallize substantial amounts of olivine (> 45%) and still reproduce the generally lower forsterite content of common lunar troctolites when co-saturated with plagioclase (i.e., those without pink spinel). Considering the substantial amount of latent heat released during this prolonged olivine crystallization model, the authors suggest revisiting the thermodynamic and compositional parameters of magma–wallrock interactions on the Moon. In general, the addition of latent heat released during olivine crystallization aids the efficiency of the assimilation process (Treiman et al. 2019).

Remote sensing methods have been used to globally assess the overall composition of the feldspathic highlands, as well as to identify ancient extrusive materials, intrusive lithologies exposed at the central peaks or basin walls of impact structures, and possible igneous structures that intruded into and solidified within the lunar crust (e.g., Cahill et al. 2009;

Pieters et al. 2011, 2014; Ohtake et al. 2012; Yamamoto et al. 2012; Andrews-Hanna et al. 2013; Prissel et al. 2016b). Near-infrared (NIR) wavelengths are sensitive to compositional variability among olivine-, pyroxene-, spinel-, and plagioclase-bearing assemblages (Cheek and Pieters 2014) but characterizing and quantifying the precise Mg′ of mafic silicates, a distinguishing characteristic of the Mg-suite, is challenging. Cahill et al. (2009) incorporated NIR spectral data to identify central peaks containing mafic exposures with Mg′ >78. These candidate exposures of Mg-suite are widely distributed across the lunar surface. More recently, NASA's Moon Mineralogy Mapper (M^3) mission aboard India's Chandrayaan-1 spacecraft collected reflectance spectra at visible to near-infrared (VNIR) wavelengths to identify surface exposures bearing low-Ca pyroxene (Klima et al. 2011) and olivine (e.g., Isaacson et al. 2011), and depending on the precise composition may also be Mg-suite. Similarly, data from the Spectral Profiler on the Japanese Kaguya mission have also been used to study exposures of pyroxene and olivine-bearing compositions (Yamamoto et al. 2012) and to show the farside highlands have a more Mg-rich signature compared to the near side, suggesting these materials crystallized from a less evolved LMO and would be KREEP-free (Ohtake et al. 2012).

The identification of a potentially new lunar rock type, pink spinel anorthosite (PSA: Pieters et al. 2011), may provide a robust method in remotely identifying Mg-suite magmatism on a global scale (e.g., Pieters et al. 2014; Prissel et al. 2014, 2016b). PSA may form by impact melting crustal material with MgO-rich cumulates (Treiman et al. 2019), or by magma–wallrock interactions between anorthositic crust and MgO-rich mantle melts (Gross and Treiman 2011; Prissel et al. 2014). Regardless, a strong compositional link was experimentally determined between Mg-suite and PSA spinel detected remotely (Prissel et al. 2014), meaning Mg-suite cumulates or Mg-suite parental melts (or both) were involved in producing spinel-rich lithologies. If true, remotely detected outcrops of PSA can be used as a proxy for the global extent of Mg-suite magmatic activity on the Moon (Prissel et al. 2014).

A summary of notable Mg-suite candidate locations across the Moon is provided in Figure 2. In general, Mg-suite-like lithologies appear to be globally distributed across the feldspathic highlands (e.g., Pieters et al. 2014; Prissel et al. 2016b), the inner ring of the

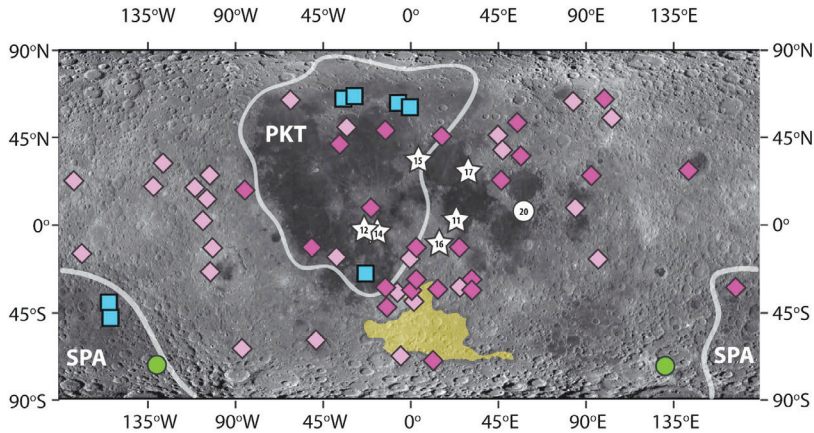

Figure 2. Global lunar mosaic from LROC WAC images with candidate Mg-suite exposures. **Dark pink diamonds** = Mg-spinel detections from Pieters et al. (2014). **Light pink diamonds** = Mg-spinel detections from Sun et al. (2017). **Green circles** = olivine-rich exposures from Yamamoto et al. (2012) and Kramer et al. (2013). **Blue squares** Mg-suite candidate exposures from Klima et al. (2011, 2013). **Yellow field** = predicted region for shallow-level emplacement or eruption of Mg-suite magmas from Prissel et al. (2016b). **Stars** represent Apollo landing sites labeled with mission number, and circle is Luna 20 landing site (spinel troctolite samples (e.g., Snyder et al. 1999). Approximate boundaries are shown for the PKT and SPA regions.

Apollo Basin (eastern SPA), and northern rim of the Imbrium Basin (Yamamoto et al. 2010; Klima et al. 2011). The global distribution of possible Mg-suite lithologies detected remotely is not consistently correlated with the PKT, or specifically associated with any crustal terrane. Though far from conclusive, the apparent disassociation between surface exposures of Th and possible Mg-suite lithologies supports the hypothesis that KREEP is not a defining characteristic of all Mg-suite samples.

Magnesian anorthosite-clasts observed in many lunar meteorites (and some Apollo samples) may represent a widespread crustal lithology on the lunar far side (e.g., Takeda et al. 2006; Treiman et al. 2010; Gross et al. 2014). Their precise relationship to the LMO or earliest stages of post-differentiation magmatism is undetermined. Some studies suggest that a predominance of magnesian anorthositic crust would imply LMO differentiation was not the sole process responsible for producing the primordial lunar crust. Magnesian anorthosites therefore may be related to an episode of post-differentiation serial magmatism similar to layered basic intrusions and massif anorthosites on Earth (Treiman et al. 2010; Gross et al. 2014). Charlier et al. (2018) presented experimental constraints on LMO solidification, showing that the high Mg′ of pyroxenes coinciding with the onset of plagioclase-saturation is consistent with the mineralogy of magnesian anorthosite clasts. The experimental constraints suggest alternative processes to LMO solidification, such as serial magmatism, are not necessary to explain the presence of a primary magnesian anorthositic crust (Charlier et al. 2018).

2.4. Updated chronology and new criteria for age assessment

The age data available for Mg-suite rocks provide a complex picture of their emplacement history. Summaries of ages and interpretations are found in Jolliff et al. (2006), Table 1 and Electronic Annex [EA]-4-1, Shearer and Papike (1993, 2005), Shearer et al. (2006, 2015), Carlson et al. (2014), Borg et al. (2015), Boyet et al. (2015), and Gaffney et al. (2023, this volume). More recent ages and their interpretation are presented by Carlson et al. (2014) and Borg et al. (2015). What is most striking of the more recent data is that the ^{147}Sm–^{143}Nd ages of the Mg-suite samples overlap with those from the ferroan anorthosite suite and that the duration of Mg-suite magmatism is limited (e.g., Carlson et al. 2014; Borg et al. 2015) (Fig. 3).

Radiometric ages for the troctolites are few in number (Table 1 and EA-4-1). Edmunson (2007) was able to date a troctolitic anorthosite clast (also referred to a magnesian anorthosite) in sample 76335 and obtain a Sm–Nd age of 4.278 ± 0.06. Troctolite 76535 has been dated with multiple chronometers (Table 1 and EA-4-1). Borg et al. (2017) derived ^{147}Sm–^{143}Nd, ^{146}Sm–^{142}Nd, and Rb–Sr ages of 4307 ± 11 Ma, 4299 $^{+29}/_{-35}$ Ma, and 4279 ± 52 Ma, respectively. They also reported an Ar–Ar age of 4320 ± 20 Ma. Despite its pristinity, this troctolite has a complex thermal history (Elardo et al. 2012, Borg et al. 2017), which has led to multiple interpretations of the radiometric age data. Papanastassiou and Wasserburg (1976) interpreted the discordant ages of earlier work to represent different, mineral-specific, isotopic closure ages in which the Rb–Sr isochron dates the crystallization age via the isolation of Rb-rich inclusions in olivine. Younger ages determined by many of the other isotopic systems have been interpreted to represent the subsolidus event that is represented by cation ordering in the Opx, and symplectite formation along plagioclase-olivine boundaries (e.g., Elardo et al. 2012). Conversely, Premo and Tatsumoto (1992) and Borg et al. (2017) concluded that this troctolite formed between 4.23 and 4.37 Ga.

The norite lithologies have considerably more radiometric age data than other Mg-suite lithologies because of the availability of samples with a large mass and their abundance of pyroxene (Table 1). Carlson et al. (2014) determined ages from norite for 77215: Rb–Sr = 4450 ± 270 Ma, ^{147}Sm–^{143}Nd = 4283 ± 23 Ma and Lu–Hf = 4421 ± 68 Ma. The data define an initial ^{146}Sm/^{144}Sm ratio of 0.00193 ± 0.00092 corresponding to ages between 4348 and 4413 Ma depending on the half-life and initial abundance used for ^{146}Sm. Gaffney et al.

(2015) concluded that the best age for a norite clast in breccia 15445 is 4330 ± 80 Ma, as recorded by the ^{147}Sm–^{143}Nd system. This age is in between the discordant ages for the same clast derived from Shih et al. (1993): 4460 ± 70 Ma (,17) and 4280 ± 30 Ma (,247). Norite clast 15445,17 is the oldest dated norite, but the Sm–Nd isochron may be disturbed. Shih et al. (1993) recognized that 15445,17 and ,247 represent the same clast, and they interpreted that this contrast in ages represented two distinct norite lithologies in a single clast. However, after examining the mineralogy of the clast with both EPMA and SIMS, Shearer et al. (2012) concluded that this clast represented only one lithology. Mg-suite norite 78238 was dated using the Sm–Nd, Rb–Sr, and U–Pb isotopic systems (Edmunson et al. 2009). 78238 yields a ^{207}Pb–^{206}Pb age of 4333 ± 59 Ma, which is concordant with the Sm–Nd crystallization age of 4334 ± 37 Ma. Two Rb–Sr isochrons were obtained, 4366 ± 53 Ma, which is concordant with the Sm–Nd and ^{207}Pb–^{206}Pb ages, and the other 4003 ± 95 Ma age is concordant with an Ar–Ar age for a plagioclase separate from daughter sample 78236 (Aeschlimann et al. 1982). Isotopic re-equilibration during shock metamorphism may have resulted in the discordant isochrons. Edmunson et al. (2009) argued that younger ages using U–Pb isotopic systems (^{235}U–^{207}Pb = 4010 ± 60 Ma; ^{238}U–^{206}Pb = 3520 ± 290 Ma) were disturbed during sample handling and leaching of mineral fractions.

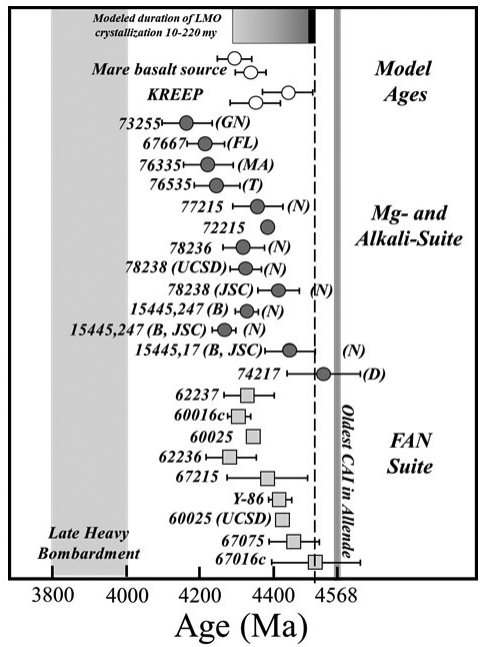

Figure 3. Ages of the Mg-suite and alkali-suite placed within the context of a lunar timeline (age of the oldest CaAl inclusions in Allende, maximum age of lunar differentiation (dashed line) from Kruijer and Kleine (2017), LMO crystallization models (e.g., Elkins-Tanton et al. 2011), Fan crystallization ages, model ages for the mare basalt sources and KREEP, and the late heavy bombardment from Ryder (2002). The modeled duration of LMO crystallization ranges from 10 Myr (crystallization) to 220 Myr (crystallization with tidal heating in FAN lid). Numbers adjacent to symbols are sample numbers. The 'c' adjacent to sample number denotes the sample was a clast. Norite clast B in 15445 represent a single lithology (Gaffney et al. 2015; Shearer et al. 2015). Multiple analyses of individual samples are noted. JSC = analyses at Johnson Space Center, UCSB (University of California Santa Diego). Rock types for Mg-suite samples are abbreviated: D = dunite, N = norite, T = troctolite, MA = magnesian anorthosite, FL = feldspathic lherzolite, GN = gabbronorite. (Modified from Marks et al. 2019).

Table 1. Chronology of Mg-suite, Alkali-suite, and evolved magmatic-derived samples prior to 2000. (modified from Snyder et al. 2000). All ages in Ma.

Lithology and sample number	$^{40}Ar/^{39}Ar$	K/Ca	Rb–Sr	Sm–Nd	U–Pb zircon	U–Pb	Refs
Mg-suite							
Norites							
14305,91					4211 ± 5		[1]
15445,17				4460 ± 70			[2]
15445,247				4280 ± 30			[2]
15455,228	3830		4590 ± 130	4500 ± 300			[2]
72255	3940 ± 30		4170 ± 50				[3,4]
73215,46,25	4190 ± 10						[5]
77215	3980 ± 30		4420 ± 40	4370 ± 70			[6,7]
78155	4170 ± 30					4170 ± 32	[8]
	4150 ± 40						[9]
78235						4426 ± 65	[10]
78236	4390		4380 ± 20	4430 ± 50			[11]
	4110 ± 20			4340 ± 40			[12,13]
Gabbronorites							
14306,60						4200 ± 39	[14]
67667				4180 ± 70			[15]
73255,27,45				4230 ± 50			[13]
Troctolites							
14306150						4245 ± 75	[1]
78535			4485 ± 75	4330 ± 64		4236 ± 15	[16]
	4190 ± 20						[17, 18]
							[19, 20]
	4160 ± 40						[21]
	4270 ± 80						[22]
Dunite							
72417			4550 ± 100				[23]
Alkali-suite and evolved rocks							
Anorthosites							
14066,47					4141 ± 5		[1]
14304,267			4334 ± 81	4108 ± 53			[24]
14321,16					4028 ± 6		[1]

Lithology and sample number	$^{40}Ar/^{39}Ar$	K/Ca	Rb–Sr	Sm–Nd	U–Pb zircon	U–Pb	Refs
			Gabbronorite				
67975,131					4339 ± 5		[1]
			Quartz monzodiorite				
15405,57					4370 ± 30		[25]
15405,145					$4309^{+120}/_{-85}$		[25]
14405,88						4000 ± 100	[26]
			Granites				
12013,141	4010 ± 70	3760 ± 720	3990 ± 50				[27, 28]
			4010 ± 90				[28]
12033,507	796 ± 10	3620 ± 110	2200 ± 650		3883 ± 3		[25, 29, 30]
12034,106					3816 ± 17 to 3986 ± 18		[25]
14082,49					4216 ± 7		[25]
14393,204	3830 ± 30	4040 ± 640	3950 ± 380		4325 ± 12		[25, 29, 30]
					4308 ± 3		[25]
14311,90					4250 ± 2		[25]
14321 B1					4010 ± 2		[25]
14321,1027	3880 ± 30	4060 ± 70	4090 ± 119	4110 ± 200	$3965^{+20}/_{-30}$		[25, 30, 31]
73215,43	3870 ± 10		3990 ± 50				[5, 32]
73217					4360 ± 20		[11]
73235,60A					4218 ± 4		[25]
73235,63					4320 ± 2		[25]
73235,73					4156 ± 3		[25]
73255,27,3	3890 ± 30						[33]

References: [1] Meyer et al. (1989); [2] Shih et al. (1993); [3] Leich et al. (1975); [4] Compston et al. (1975); [5] Jessberger et al. (1977); [6] Stettler et al. (1974); [7] Nakamura et al. (1976); [8] Oberli et al. (1979); [9] Turner and Cadogan (1975); [10] Premo and Tataumoto (1991); [11] Nyquist et al. (1981); [12] Aeschlimann et al. (1982); [13] Carlson and Lugmair (1981a); [14] Compston et al. (1984); [15] Carlson and Lugmair (1981b); [16] Premo and Tatsumoto (1992); [17] Husain and Schaeffer (1975); [18] Papanastassiou and Wasserburg (1976); [19] Lugmair et al. (1976); [20] Hinthorne et al. (1975); [21] Huneke and Wasserburg (1975); [22] Bogard et al. (1975); [23] Papanastassiou and Wasserburg (1975); [24] Snyder et al. (1995); [25] Meyer et al. (1996); [26] Tatsumoto and Unruh (1976); [27] Turner (1970); [28] Lunatic Asylum (1970); [29] Bogard et al. (1994); [30] Shih et al. (1993); [31] Shih et al. (1985); [32] Compston et al. (1977); [33] Staudacher et al. (1979).

Highly relevant to the interpretation of the "crystallization ages" determined for individual Mg-suite rocks are the numerous model ages determined for the formation of potential sources for the Mg-suite: urKREEP and LMO cumulates. Several ur-KREEP Sm–Nd model ages were calculated by Carlson and Lugmair (1979), Nyquist and Shih (1992), and Edmunson et al. (2009) (4600 ± 60, 4420 ± 70 and 4492 ± 61 Ma, respectively). Based on Lu–Hf isotopic analyses of KREEP-enriched breccias (Sprung et al. 2013) and a suite of igneous rocks with KREEP signatures (Gaffney and Borg 2013), model ages for urKREEP formation of 4402 ± 23 Ma and

4353 ± 37 Ma, respectively, were determined. Lunar zircons are thought to be crystallization products from highly enriched KREEP magmas and coupled U–Pb and Lu–Hf studies have been reported (Taylor et al. 2009; Barboni et al. 2017; Crow et al. 2017). The ^{207}Pb–^{206}Pb age distributions for zircons from Apollo 14, 15, and 17 breccia and soil samples show a peak at ~4330 Ma. A majority of zircons appear to have crystallized before ~4100 Ma (Crow et al. 2017). The ^{176}Lu–^{176}Hf model ages of lunar zircons from Apollo 14 polymict breccias 14304, 14305, and 14321 indicated separation of the KREEP source had occurred by ~4480 Ma (Taylor et al. 2009). Barboni et al. (2017) revisited lunar zircon from the Apollo 14 breccias, and with improved precision using isotope dilution thermal ionization mass spectrometry and were able to remove zircon domains affected by Pb loss. This resulted in more accurate ^{207}Pb–^{206}Pb crystallization ages, which were used to determine a Lu–Hf model age for LMO solidification of ~4.51Ga. This model age is > 120 Myr older than the Sm–Nd and Pb–Pb isochorons measured on Mg-suite and ferroan anorthosites (Borg et al. 2011; Carlson et al. 2014).

Model ages for the mare basalt source region have been estimated using the ^{146}Sm–^{142}Nd isotope system. Ages of 4329 $^{+40}/_{-56}$ Ma (Nyquist et al. 1995), 4352 $^{+23}/_{-21}$ Ma (Rankenburg et al. 2006), 4313 $^{+25}/_{-30}$ Ma (Boyet and Carlson 2007), and 4340 $^{+20}/_{-24}$ Ma (Brandon et al. 2009) determined by this method yields a weighted average age for mare basalt source formation of 4337 ± 28 Ma (Borg et al. 2015). Mare basalts from Apollo 12, 15, and 17 were also analyzed using the Sm–Nd isotopic system (McLeod et al. 2014). Depending on the choice of chondritic vs. superchondritic Sm/Nd (and μ^{142}Nd), closure ages for the mare basalt mantle source reservoir were 4450 $^{+10}/_{-09}$ Ma (assuming a 68 Myr half-life for ^{146}Sm) or 4390 $^{+16}/_{-14}$ Ma (assuming a 103 Myr half-life) and 4410 $^{+10}/_{-08}$ or 4340 $^{+15}/_{-14}$ Ma, respectively (McLeod et al. 2014). Evidence from Hf–W chronology indicates that LMO solidification occurred after the extinction of ^{182}Hf and therefore later than 60 Myr after CAI formation (Kleine et al. 2009).

Numerous (and conflicting) interpretations have been reached concerning the chronology of the Mg-suite and its relationship to other highlands lithologies (e.g., FANs, alkali suite) and lunar differentiation. Assuming that the ages determined for the Mg-suite rocks represent the time at which the rocks crystallized, the range of Mg-suite rock ages (4610 ± 70 to 4170 ± 20 Ma) compiled by Nyquist and Shih (1992), Snyder et al. (1995, 2000), Nyquist et al. (2001), and Borg et al. (2015) represents an extensive period of Mg-suite magmatism (~300–400 Myr). Clearly, some of the older ages for the Mg-suite (e.g., 4610 ± 70 Ma) should be disregarded as they represent ages older than the Solar System. Borg et al. (2015) proposed an approach for evaluating the quality of reported ages.

Borg et al. (2015, 2017) concluded that the oldest ages determined with confidence on FAN and Mg-suite highland rocks are ~4350 Ma (Fig. 3), based upon concordance of different chronometers. This age is concordant with ^{142}Nd model ages of mare source formation (Nyquist et al. 1995; Rakenburg et al. 2006; Boyet and Carlson 2007; Brandon et al. 2009), a peak in zircon ages (Pidgeon et al. 2007, 2011; Nemchin 2008, 2011; Grange et al. 2011; Crow et al. 2017), and the Lu-Hf model KREEP formation age from Gaffney and Borg (2013). However, this is challenged by older model ages from lunar zircons (Taylor et al. 2009; Barboni et al. 2017). The 4350 Ma age records either the primordial solidification of the Moon or a major, Moon-wide thermal event such as CMO, or a major basin forming event. In the scenario that the 4350 Ma age represents a differentiation event, FAN magmatism may precede Mg-suite magmatism, but only by a few million years. In the second scenario, the Moon-wide thermal event completely resets the isotopic systems in the mantle and ancient primordial crust (FANs). The episode of Mg-suite magmatism at 4350 Ma partially manifests this thermal event. The older LMO solidification ages obtained on lunar zircon of ~4510 Ma may be interpreted as indicating Sm–Nd ages are compromised by later disturbances, reflect the time of slow cooling and low Sm–Nd closure temperatures, or that a re-examination of the LMO is due (Borg et al. 2011; Barboni et al. 2017). Regardless, multiple chronometers for and sophisticated modeling of the early lunar thermal history of additional ferroan anorthosite, Mg-suite, alkali-suite, and

samples not within proximity to the geochemically anomalous PKT (e.g., lunar meteorites, far side highlands sample return) are needed to resolve or refine current interpretations.

2.5. Synthesis of recent observations

Experimental and model simulations of LMO solidification demonstrate that primordial ultramafic cumulates are sufficiently MgO-rich to serve as a mantle source for Mg-suite magmatism (Elardo et al. 2011; Elkins-Tanton et al. 2011; Charlier et al. 2018; Rapp and Draper 2018; Lin et al. 2020). The CMO hypothesis provides a transport and melting or mixing mechanism for these primitive mantle sources (e.g., Zhang et al. 2013, 2017; Dygert et al. 2016, 2017; Boukaré et al. 2018; Zhao et al. 2019). Mg-suite parental melts may be partial melts of a plagioclase- and KREEP-bearing hybridized mantle source (e.g., Longhi et al. 2010; Elardo et al. 2011), or partial melts of primitive mantle cumulates (± KREEP) during decompression melting and CMO (e.g., Prissel et al. 2016a; Prissel and Gross 2018, 2019, 2020). The preponderance of Mg-suite ages centering around ~4350 Ma records either the primordial solidification of the Moon, or a major Moon-wide thermal event (e.g., CMO, major basin forming event) (e.g., Borg et al. 2011, 2015; Shearer et al. 2015; Barboni et al. 2017).

Remote detection of pink spinel anorthosites appear to be chemically linked to Mg-suite either by impact melting of crust and Mg-suite cumulates (Treiman et al. 2019), or by magma–wallrock interactions between Mg-suite parental melts and lunar crust (e.g., Gross and Treiman 2011; Prissel et al. 2014). In both cases, pink spinel anorthosites could provide a proxy for Mg-suite magmatism on a global scale (Pieters et al. 2014; Prissel et al. 2014). Finally, the integration of lunar meteorites and remote sensing databases into the returned sample collection is imperative to our overall understanding of the earliest stages of post-differentiation magmatism, the relationship between Mg-suite and KREEP, and the diversity of active magmatic systems > 3.85 Ga including ancient mare basaltic volcanism (cryptomare, e.g., Terada et al. 2007; Whitten and Head 2015; Snape et al. 2018).

3. KREEP BASALTS

3.1. Introduction

KREEP basalts are distinct from mare basalts (Section 5.4) in that they generally have higher Al_2O_3 and lower CaO contents and, therefore, lower Ca/Al ratios, which reflect lower modal abundances of Ca-rich pyroxene (e.g., Warren 1988) (Fig. 4). KREEP basalts have been termed “non-mare” or “very high alumina (VHA)” because of these compositional differences (e.g., Hubbard and Gast 1971; Hubbard et al. 1974). Such basalts have been returned by the Apollo 14, 15, 16, and 17 missions. The Apollo 14 KREEP basalts are distinct from the Apollo 14 high-Al mare basalts that contain a KREEP signature in that the incompatible trace element contents are much higher. It is evident that the Apollo 17 KREEP basalts are distinct from those returned by Apollo 14, 15, and 16 in terms of the slope of their REE profile (Fig. 5). These trace element systematics could be due to differences in the degree of partial melting of a more-or-less homogeneous incompatible trace element [ITE]-enriched source or due to differences in ITE concentrations in the mantle source(s) (e.g., Salpas et al. 1987). Regardless of the variations observed in the basalts, their enriched source(s) have similar long-term Rb/Sr and Sm/Nd ratios (Shih et al. 1992).

The origin of KREEP basalts has been debated almost since the first lunar samples were returned. One petrogenetic model is for an origin as primary melts (e.g., Powell et al. 1973; Ryder 1976, 1987, 1988; Ryder and Martinez 1991; Borg et al. 2004). These appear to be the products of primitive melts that assimilated urKREEP (e.g., Warren 1988) followed by low-pressure crystal fractionation (e.g., Ryder 1987). An alternative model has KREEP basalts forming as impact melts. The impact process mixed evolved, KREEP-rich materials with

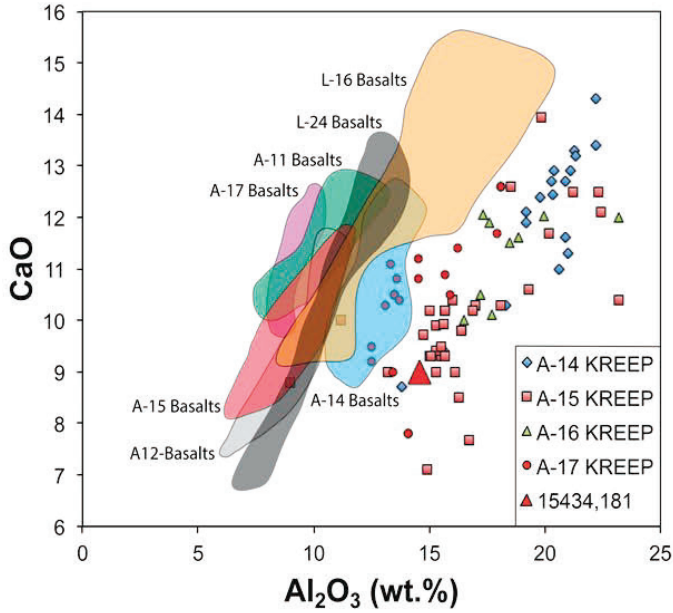

Figure 4. CaO vs. Al_2O_3 for mare basalts and KREEP basalts. Data from Mare Basalt Database (https://www3.nd.edu/~cneal/Lunar-L/) and references cited therein.

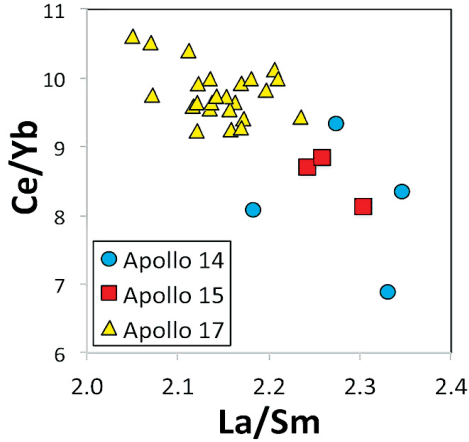

Figure 5. Differences between KREEP basalts from Apollo 17 and those from Apollo 14, 15, and 16. Apollo 17 KREEP basalt data from Salpas et al. (1987); Apollo 14 KREEP basalt data from Laul et al. (1972), Hubbard et al. (1973), McKay et al. (1978, 1979), Ma et al. (1980), Neal and Kramer (2006); Apollo 15 KREEP basalt data from Helmke et al. (1973), Hubbard et al. (1973), Ryder et al. (1988), Simon et al. (1988), Ryder and Martinez (1991), Neal and Kramer (2006); Apollo 16 KREEP basalt data from Hubbard et al. (1973).

more primitive lithologies (e.g., McKay et al. 1978, 1979). The Imbrium event itself has been frequently invoked to produce the KREEPy impact melts and, in some cases, induce KREEP volcanism (Ryder 1987). Variants on these models have been postulated. For example, Ryder (1988) reported evidence in sample 15438 that was consistent with a partially solidified KREEP basalt flow being hit by a meteoroid impact. Jolliff (1991), Marvin et al. (1991), and Ryder and Martinez (1991) also described extreme fractional crystallization products of a KREEP magma, quartz monzodiorite. Such magmas experienced silicate liquid immiscibility that suggests there is a relationship between KREEP and lunar granite/felsite (Ryder 1976; Martinez and Ryder 1989; Jolliff 1991). Borg et al. (2004) suggested the high levels of radioactive elements in KREEP allowed prolonged magmatism on the Moon. Thus, the youngest basalts that occur in the Imbrium-Procellarum region of the Moon (Hiesinger et al. 2011) should be KREEP-rich.

KREEP basalt samples from Fra Mauro (Apollo 14) and the Descartes highlands (Apollo 16) are impact generated (e.g., McKay et al. 1978), whereas those from the Apollo 15 and 17 sites appear to be the products of partial melting of the lunar interior. The pristine nature of the KREEP basalts is based on petrographic evidence (e.g., Ryder 1988), where a two-stage cooling regime was proposed to account for the presence of Opx phenocrysts in some Apollo 15 KREEP basalt samples. However, petrographic and experimental studies demonstrated that porphyritic textures could develop with just one cooling regime if one phase has a significant cooling interval before others come on the liquidus (e.g., Dowty et al. 1976). Cronberger and Neal (2017) showed that the Opx phenocrysts in 15434 were actually xenocrysts from an unrelated magma.

The Apollo 15 KREEP basalts are either at or close to multiple phase saturation as such compositions cluster along the plagioclase–Opx cotectic of the olivine–silica–plagioclase pseudoternary system (e.g., Dymek 1986; Ryder 1987). Taylor et al. (2012) examined 27 Apollo 15 KREEP basalt fragments from 6 thin sections and demonstrated that these basalts were derived from multiple source regions by plotting the Ab contents of the most calcic plagioclases against the Mg′ in the most magnesian pyroxenes. If derived from the same source, the data on such a plot would show little variation, but this was not the case. Taylor et al. (2012) noted that the most magnesian Opx crystals would have crystallized from parent magmas with a Mg′ of 79–90, which in turn requires the source regions to have been dominated by phases that crystallized early from the LMO (e.g., Snyder et al. 1992; Elkins-Tanton et al. 2011). To form the Apollo 15 KREEP source a cumulate overturn event would be needed to mix the early- and late-stage cumulates to form a hybrid source (e.g., Elardo et al. 2011). Alternatively, the KREEP component could have been assimilated after the initial high-Mg parent magma was generated by the melting of a source dominated by early LMO cumulates. The current state of knowledge is that it is not possible to distinguish between these two petrogenetic models. However, recent work suggests the early formed Opx crystals in KREEP basalts were derived from a liquid much more enriched than urKREEP (i.e., the high-K KREEP composition of Warren 1989), which has been termed "über-KREEP" (Cronberger and Neal 2018, 2019a)

3.2. Ages of KREEP basalt formation

Rb–Sr ages predominate for KREEP volcanism and have been determined on a number of samples from Apollo 14 (impact melts 14073 and 14310—Papanastassiou and Wasserburg 1971; 14150,7—McKay et al. 1979), Apollo 15 (15382—Papanastassiou and Wasserburg 1976; 15386—Nyquist et al. 1975; Carlson and Lungmair 1979; 15434,73—Nyquist et al. 1975), and one Apollo 17 sample (72275,543—Shih et al. 1992). The Apollo 14 and 15 basalts indicate similar ages around 3900 ± 40 Ma, but the Apollo 17 sample is slightly older (4130 ± 80 Ma; Sm–Nd age = 4080 ± 70 Ma). This indicates that Apollo 17 KREEP basalts are not only compositionally distinct from those returned by Apollo 14 and 15 (Fig. 5), but also have a distinct age.

While Apollo 14 KREEP basalts are impact melts, it has been generally accepted that Apollo 15 KREEP basalts are endogenous melts of the lunar interior. Usually it is the elevated abundances of highly siderophile elements in lunar samples that indicate an impact melt origin, but often samples are too small to determine such abundances. Neal et al. (2015) developed a textural method that can distinguish impact melts from mantle derived melts based on plagioclase and olivine crystal size distributions (CSDs). Cronberger and Neal (2019b) showed that while 15382 plotted close to the impact melts field for plagioclase CSDs, it had experienced subsequent textural coarsening through thermal metamorphism, similar to that described in 14053 (Taylor et al. 2004; Webb and Neal 2019), which moved the plagioclase CSD to the impact melt field.

More recently analysis of lunar zircons has yielded ages that define the earliest evolution of the Moon (3900–4400 Ma). As ion probes have continued to be developed, a wealth of U–Pb ages have been reported for KREEP-rich breccias from Apollo 14, 15, and 17 samples. These data (e.g., Pidgeon et al. 2007; Nemchin et al. 2008, 2011; Grange et al. 2013; Crow et al. 2017) and their implications are discussed in Section 5.2.4 and summarized in EA-4-1. In addition to the zircon ages derived from the breccas, Meyer et al. (1996) reported a zircon U–Pb age for the Apollo 15 Quartz Monzodiorite 15405 of 4294 ± 26 Ma, with a thermal (impact) event at 1320 ± 280 Ma.

In addition to the Apollo samples, lunar meteorite NWA 773 also appears to fit within the criteria for a KREEP basalt. It has geochemical characteristics that are similar to the KREEP basalts returned by Apollo (e.g., La/Lu). In addition, it plots along the KREEP evolution line in ε_{Nd}-age and $^{87}Sr/^{86}Sr$-age diagrams. The crystallization age for NWA 773 is 2993 ± 32 Ma (Borg et al. 2009). However, Shaulis et al. (2017) reported average baddeleyite ^{207}Pb–^{206}Pb ages for NWA 773 and its paired meteorites of 3119.4 ± 9.4 Ma.

Combining age and remote sensing data indicate that magmatism with a KREEPy signature occurred over a period of over 3.4 billion years from approximately 4380–<1000 Ma (i.e., Hiesinger et al. 2003, 2011). This style of magmatism overlaps in duration with the earliest stages of post-differentiation magmatism (Mg-suite) and mare basalt magmatism.

4. MARE BASALTIC MAGMATISM

4.1. Introduction

Mare basalts cover roughly 18% of the lunar surface and are primarily relegated to the filling of multi-ringed impact basins and irregular depressions (e.g., Whitten and Head 2015). Mare volcanism is asymmetric with only small volumes on the far side, even in large basins such as the South Pole Aitken basin. The mare basalts exhibit a considerable range in several chemical characteristics that often reflect characteristics and origins of their mantle sources. Therefore, they provide a window into the lunar interior. Fundamental characteristics of mare basalts have been known since the Apollo Program and are outlined in NVM1 (Shearer et al. 2006). Recent observations have produced some reluctance in fully accepting some of these characteristics of mare basalts (e.g., dry magmas). These will be discussed below.

4.2. Summary of observations

4.2.1. Distribution and descriptions

4.2.1.1. Mare basalt volcanism. The descriptions of volcanic landforms and the relative chronology of mare basalt magmatism are discussed in detail in Head et al. (2023, this volume). Recent work has better defined the characteristics, distribution, and duration of mare volcanism than described in Shearer et al. (2006). A substantial volume of mare basalts was erupted

between 3100 and 3900 Ma. However, there was a substantial volume of "cryptomare" basalts (covered or hidden mare deposits that are obscured by emplacement of subsequent deposits—Head and Wilson 1992) erupted prior to 3850 Ma, and numerous pulses of basalts were erupted after 3100 Ma (e.g., Hiesinger et al. 2011). A precise timeline of rock types representing pre-mare magmatism (~4500–3850 Ma) continues to be blurred but growing evidence from samples and orbital remote sensing supports mare basaltic volcanism pre-dating 3850 Ma (e.g., Neal and Kramer 2006; Hui et al. 2013; Whitten and Head 2015; Snape et al. 2018). Schultz and Spudis (1983) and Hiesinger et al. (2003) suggested ages as young as 1000 Ma. More recent analysis (Stadermann et al. 2015) of LROC-WAC images of the youngest lunar flows near Aristarchus crater (unit P60) are consistent with the young ages from Hiesinger et al. (2003). Periods of magmatism may be younger than 1000 Ma, but this is still a point of debate. For example, Braden et al. (2014) suggest the existence of irregular mare patches (IMPs) younger than 100 Ma, although an opposing view has these as being > 3000 Ma (Wilson and Head 2017b; Qiao et al. 2018, 2019, 2020). The younger periods of basaltic volcanism appear to be focused within the PKT and are associated with high concentrations of heat-producing elements.

4.2.1.2. Pyroclastic volcanism. Explosively emplaced or pyroclastic volcanic deposits provide clues to the nature of the early lunar interior, especially as related to endogenic volatiles (e.g., Delano 1986; Shearer et al. 2006) and to the distribution of potential resource materials (Duke et al. 2006; see also Crawford et al. 2023, this volume). Although the Moon is largely volatile-depleted, analyses of lunar pyroclastic samples suggest that water and other magmatic volatiles (i.e., F, Cl, S, Zn) have played an important role in lunar magmatic processes (e.g., Saal et al. 2008; Hauri et al. 2011; McCubbin et al. 2023, this volume).

Analyses of color data for lunar pyroclastic deposits from Earth and from orbit have helped to identify the characteristic components of some of these deposits (e.g., Pieters et al. 1973; Weitz et al. 1998, 2017; Gaddis et al. 2000, 2003; Wilcox et al. 2006), to characterize the distribution of lunar volcanic deposits (Head 1974; Gaddis et al. 2003), and to constrain the styles of eruption and emplacement of basalts on the Moon (Wilson and Head 1981, 2003, 2017a; see also Head et al. 2023, this volume). The compositions of lunar pyroclastic deposits have been related to their size, inferred modes of formation, and eruption styles (e.g., Hawke et al. 1989; Coombs et al. 1990; Gaddis et al. 2000, 2003).

The small localized pyroclastic deposits, often found in floor-fractured craters in the lunar highlands, contain magmatic mineral phases (glass alone or clinopyroxene–Cpx–mixed with glass) and pyroxenes derived from entrained country rock (Coombs et al. 1990), which are consistent with an origin by Vulcanian eruptions (Head and Wilson 1978). The amount of pyroxene present may be related to the depth of plug formation and subsequent explosion (Hawke et al. 1989). However, the exact nature of the magmatic component of such deposits is poorly understood because both olivine and glass could account for the observed spectra (McCord et al. 1981; Gaddis et al. 2000, 2016; Horgan et al. 2014).

The compositions of larger regional pyroclastic deposits are dominated by iron-bearing glass, ilmenite, and olivine (Pieters et al. 1973; Gaddis et al. 2000, 2003). Telescopic spectra of the ilmenite-bearing black crystalline and orange glass beads at the Apollo 17 landing site (Pieters et al. 1973*)* suggested that these compositions are glassy and crystalline varieties of the same melt. The degree of crystallization of pyroclasts is thought to be determined by the density of the erupting plume (Weitz et al. 1998); melt droplets in denser plumes will undergo cooling at slower rates and will begin to crystallize, while droplets in thin plumes and at the margins of plumes will quench quickly and become glassy. On the Moon, plume density is largely determined by magma volatile content (e.g., Wilson and Head 1981), so the crystallinity of pyroclastic deposits has been related directly to volume flux and gas content (e.g., volatile content of source magmas) (Weitz et al. 1998).

While the larger pyroclastic deposits likely erupted with an initial explosive event and then more steadily (i.e., as a fire-fountain eruption), the intermittently explosive or Vulcanian eruptions are most likely driven by gas exsolving ahead of rising magma, building up under a cap-rock, and periodically exploding, entraining magmatic components and/or country rock (e.g., Head and Wilson 1979; Hawke et al. 1989; Wilson and Head 2017a). Carbon monoxide (CO) has been considered to be the primary volatile, produced by reduction reactions between graphite and species such as FeO, TiO_2 and Cr_2O_3 in the source magma (e.g., Fogel and Rutherford 1995). The CO content in returned samples is estimated to range from ~500 to 2000 ppm by mass (e.g., Rutherford and Papale 2009), but ~14000 ppm may have been needed to emplace the largest pyroclastic deposits (Wilson et al. 2011). This suggests that there is enrichment in CO and/or the involvement of additional volatile species. H_2O has been identified in lunar pyroclastic glasses at 260–1410 ppm (Saal et al. 2008; Hauri et al. 2011).

SELENE data from the Multiband Imager (MI), Spectral Profiler (SP) and NASA Moon Mineralogy Mapper (M^3) data (Bennett et al. 2016) were used to characterize the locations and compositions of more than a dozen pyroclastic deposits in the Oppenheimer crater floor. These pyroclastic deposits (Bennett et al. 2016) are mixtures of Opx and minor Cpx sourced from the crater floor, magmatic Cpx, and magmatic iron-rich glass. A Vulcanian eruption should cause significant country rock to be incorporated into the pyroclastic deposit, but M^3 data indicate that large areas of the deposits show spectra consistent with high abundances of immature volcanic material and only some floor material. These data support a Strombolian or more continuous fire-fountain eruption at high effusion rates.

Different results were observed at Alphonsus with M^3 data (Gaddis et al. 2016). Compositional modeling showed a wide distribution of crater-floor-like Opx away from the vent that is consistent with an energetic initial explosion, followed by fire-fountaining to form glass-rich deposits. Near-vent spectra indicated a presence of Cpx, which could be present as especially thick, possibly coherent pyroclastic deposits, thin flows, or fragmented basalt from within the source dike. These observations are in contrast with those at Oppenheimer crater, which exhibited little to no evidence for a country rock component within the deposits. Taken together, the contrasting but similarly complex mineral assemblages of Alphonsus and Oppenheimer attest to the complex nature of eruptions of small lunar volcanoes and suggest that small lunar pyroclastic deposits may have a more complex origin and mode of emplacement than previously thought.

With the availability of global remote sensing data (see Gaddis et al. 2023, this volume), more than 40 previously unrecognized lunar pyroclastic deposits have been identified in the last decade.Building on the global map of Gaddis et al. (2003), Gustafson et al. (2012) used orbital color data and images from the Lunar Reconnaissance Orbiter's Narrow Angle Camera (LROC NAC; ~50 cm to 2 m/pixel) to identify 12 previously unrecognized pyroclastic deposits at sites along the margins of major impact basins. Recent work for Alphonsus and Oppenheimer floor-fractured crater dark deposits using MI, NAC, M^3 and Diviner data (Horgan et al. 2015; Bennett et al. 2016) resulted in the identification of 2 and 8 new vents, respectively. An updated distribution map for the global population of 148 lunar pyroclastic deposits is shown in Figure 6.

4.2.2. Composition and implications for petrogenesis

4.2.2.1. Major elements. Lunar mare basalts and associated picritic glasses display a uniquely wide range in major element compositions (e.g., Papike et al. 1976, 1998; BVSP 1981; Delano 1986; Neal and Taylor 1992; Longhi 1992; Shearer and Papike 1993; Shearer et al. 2006) (Fig. 7). Their compositions and compositional diversity are fundamental to our interpretation of their mantle sources. The pyroclastic glasses are the closest approximation for primary magmas (magmas in equilibrium with their mantle sources) and therefore their

chemistry provide insights into numerous characteristics of their sources (e.g., Delano 1986). Shearer et al. (2006) summarized the following observations concerning the mare basalt sources from major elements.

- The compositions of many of the mare basalts represented by Apollo, Luna, and meteorite samples reflect fractional crystallization of magmas derived from a variety of mantle sources (Fig. 7a). The magmas crystallized at approximately IW-1. They were derived from mantle sources that were at similar reducing conditions. The picritic glasses are *generally* at higher Mg′ and lower incompatible element concentrations than the crystalline mare basalts. Longhi (1992) illustrated that the picritic glasses had compositions lying on the higher Mg′ end of liquid lines of descent. Therefore, the analysis of source depth and mineralogy are best made using the primitive picritic glasses. However, the crystalline mare basalts do provide insights into mantle sources using radiogenic and stable isotopes and post-magma generation evolutionary processes (e.g., Neal and Kramer 2006).

- Due to low TiO_2, Al_2O_3, and CaO and limited correlation between TiO_2 and Al_2O_3–CaO in the very low-Ti picritic glasses, a primitive lherzolitic mantle is not an appropriate source (Fig. 7). In the VLT glasses, Al_2O_3 and CaO are buffered to near constant values. The VLT melts are undersaturated with potential Al and Ca buffering phases such as plagioclase and high-Ca Cpx (i.e., these two phases are commonly 100 °C below liquidus). Only Opx and garnet are possible residual phases that can buffer Al_2O_3 and CaO during melting. Either of these minerals as a liquidus phase indicates derivation from deep within the lunar mantle. Garnet is a liquidus phase only at pressures above 3 GPa (i.e., below 500 km; Neal 2001, and references therein).

- The FeO content of the VLT glasses range from 16 to 23% (Delano 1986; Shearer and Papike 1993). This variation may be attributed to either the source compositions varying a similar amount or a dominant residual phase. In the latter case, between 0 and 40% partial melting must occur if the FeO is being controlled by Opx. This much variation in melting is not consistent with the near constant Al_2O_3 and CaO. The observed variation in FeO, Al_2O_3 and CaO is consistent with a variable FeO source, similar degrees of partial melting, and Opx + olivine residual phases.

- For the high-Ti picritic glasses, the range in TiO_2 and FeO likely reflect variation in source region rather than degree of partial melting using the same arguments as above. The high TiO_2 and FeO most likely reflect ilmenite in the source. Hess (2000) illustrated that high-Ti glass compositions projected along an olivine–Opx boundary in the system (Mg,Fe)O–SiO_2–TiO_2 at 1.5 GPa and therefore suggests that ilmenite is not a residual phase and does not buffer the TiO_2 content of the melt. The Al_2O_3 and CaO in the high-Ti glasses overlap or are substantially lower than in the VLTs. In addition, the CaO/Al_2O_3 ratio changes more significantly in the high-Ti glasses than the VLT glasses. This could be due to the pressure dependence of Al in Opx, suggesting that high-Ti magmas derived from higher pressure should have lower concentrations of Al_2O_3. In the few examples that the relationship between Al_2O_3 and multiple saturation depth can be compared, this appears to not be the case. For example, the Apollo 15 red glass has both a higher Al_2O_3 and multiple saturation depth than the Apollo 17 orange glass. This argues for differences in source composition and mineralogy.

- There is an interesting discrepancy between sample-based pyroclastic glass observations and orbital and telescopic examinations of pyroclastic deposits. As noted above, volcanic glasses derived from pyroclastic eruptions are near-primary magmas (e.g., Mg-rich olivine as the sole liquidus phase, high-liquidus temperature, high Mg′, low CaO and Al_2O_3), whereas many of the pyroclastic deposits documented from orbit are clearly

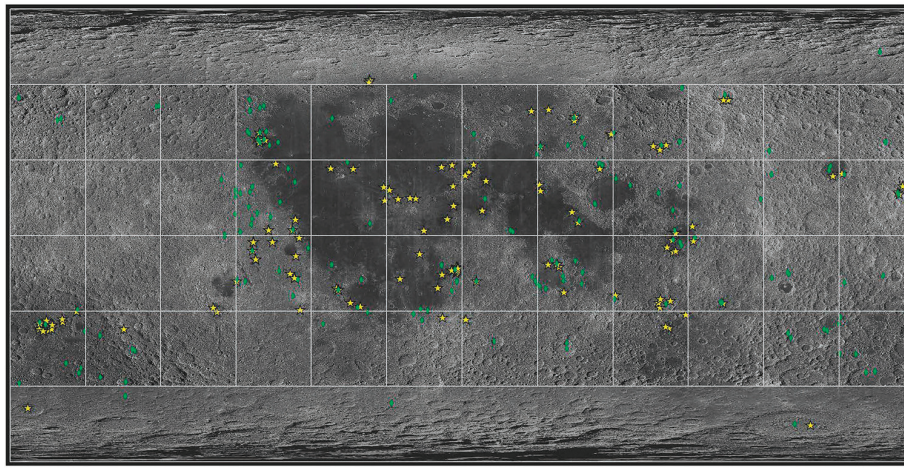

Figure 6. Global distribution of 148 lunar pyroclastic deposits, updated June 2018. Pyroclastic deposits (**yellow stars**) are observed in the highlands adjacent to mare-filled basins and are often associated with floor-fractured craters (**green diamonds**, after Jozwiak et al. 2017 and references within).The base image is the LROC WAC global mosaic at 100 m/pixel (Speyerer et al. 2011).

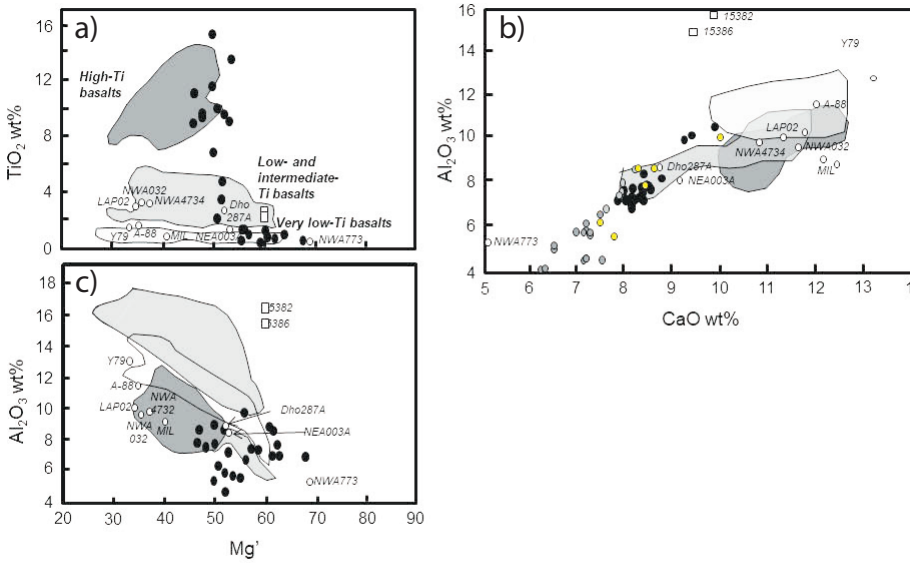

Figure 7. (a) Plot of Mg′ versus TiO_2 for fields of mare basalts, pyroclastic glasses (**black points**) and recent lunar meteorites (**open points**). **(b)** Plot of Mg′ versus Al_2O_3 for fields of mare basalts, pyroclastic glasses (**black points**) and recent lunar meteorites (**open points**). **(c)** CaO versus Al_2O_3 for fields of mare basalts, pyroclastic glasses (**black points** for very low-Ti glasses, **yellow points** for intermediate-Ti glasses, **gray points** for high Ti glasses) and recent lunar meteorites (**open points**). Data from Mare Basalt Database (https://www3.nd.edu/~cneal/Lunar-L/) and references cited therein and Shearer et al. (2006) and references cited therein.

more evolved magmas (e.g., Cpx as an important liquidus phase and Fe-rich volcanic glass imply lower liquidus temperatures and higher concentrations of CaO and Al_2O_3). In addition, orbital data documents that the pyroclastic deposits are spatially and perhaps petrogenetically associated with thin flows and fragmented basalt.

Within the context of these observations and conclusions, what are the spatial, temporal, and petrogenetic relationships among the near-primary magmas (picritic glasses) and mare basalts? Most of the mare basalts plot at lower Mg′ than the picritic glasses. Based simply on the higher Mg′ of the picritic glasses a conclusion that could be reached is that the picritic glasses represent parental magmas to the mare basalts in the returned samples and meteorites. This simple relationship is not correct. Longhi (1987), Shearer and Papike (1993), and Neal (2018) illustrated the calculated liquid lines of descent for the picritic glasses cannot reproduce the crystalline basalts returned by the Apollo program. The parental liquids for the crystalline mare basalts have higher CaO and Al_2O_3 than the picritic glasses. For example, primitive high-Ti crystalline basalts (Mg′ = 50) that approximate liquid compositions have Al_2O_3 and CaO concentrations of 7–12% and 10–11%, respectively, whereas picritic glasses with only somewhat higher Mg′ have lower concentrations of both oxides (e.g., Al_2O_3 = 4–8%, CaO = 6–8%). Several conclusions can be reached from these observations. The parental magmas for the crystalline mare basalt have a similar range of Mg′ and TiO_2 as the picritic glasses and are derived from sources with similar characteristics with regards to these elements. As it is likely that the primary magmas for all of these basalts leave behind Opx and olivine residual upon extraction, the differences in Al_2O_3 and CaO between the picritic glasses and crystalline mare basalts reflect differences in source composition for these elements. Similar conclusions can be reached from the trace elements (Sc, REE Co, Cr) and will be discussed below.

The lunar mare basaltic meteorite suite exhibits a far more limited range in TiO_2 than observed in the Apollo collection (Fig. 7). This more limited variation in TiO_2 in lunar basaltic meteorites is further suggested through the examination of fragments of crystalline basalts in feldspathic lunar meteorites by Robinson et al. (2012). Using back calculated melt compositions from pyroxenes in these clasts, they concluded that the basalt clasts in these meteorites are dominated by low- and very low-Ti basalts with very few high-Ti basalts (Robinson et al. 2012; Joy and Arai 2013; Xue et al. 2019). Further, they concluded that the TiO_2 concentration frequency in this clast population was nearly identical to the basalt population obtained from remotely sensed data rather than the population collected by the Apollo missions. Unlike TiO_2, the ranges in CaO and Al_2O_3 of the mare basalt meteorites overlaps with the Apollo basalts for the very low- and intermediate-Ti basalts returned by the Apollo missions (Fig. 7c).

4.2.2.2. Trace elements. Shearer et al. (2006) summarized characteristics and interpretations of trace element chemistry of mare basalts. In particular, REE patterns have long been used to interpret the source regions for mare basalts (Fig. 8). For example, the negative Eu anomaly observed in most lunar basalts (crystalline mare basalts, picritic glasses, basaltic meteorites) have been interpreted as representative of the source region because the more primitive basalts are far from being saturated in plagioclase at any pressure (BVSP 1981, Longhi 1992). These negative Eu anomalies and the low Al_2O_3 contents of mare basalts have been attributed to the flotation of plagioclase during LMO crystallization (e.g., Smith et al. 1970; Wood et al. 1970; Taylor and Jakes 1974; Warren 1985). The more mafic silicates that sink during LMO during plagioclase flotation incorporate it into the mare basalt source region. Negative anomalies in many lunar basaltic meteorites suggest that this process was a global phenomenon (Fig. 8). The extent of the negative Eu anomaly is commonly correlated to the overall REE concentration. This correlation may be generated by later stages of the LMO becomingly increasingly enriched in incompatible elements and being influenced by increasingly higher abundances of plagioclase being removed by flotation. It is also likely that plagioclase fingerprint was superimposed on cumulates that were formed prior to LMO

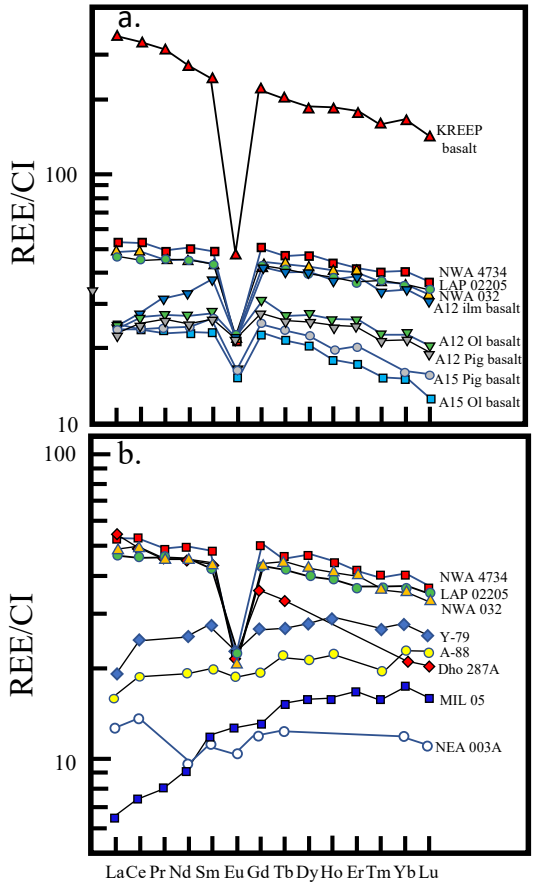

Figure 8. (a) REE plots of low- and intermediate-Ti basalts from Apollo sites. **(b)** REE plots of low- and intermediate-Ti basalts and gabbros represented by lunar meteorites (after Shearer et al. 2006; Elardo et al. 2014).

plagioclase saturation by hybridization through CMO with an evolved component that witnessed plagioclase removal (Snyder et al. 1992; Shearer et al. 2006).

Using major elements, picritic glasses and crystalline mare basalts appear to be derived from distinctly different sources. Trace element characteristics also illustrate this point. Plotting Fe (wt.%) versus Sc (Fig. 9a) illustrates that the picritic glasses are distinct from the crystalline mare basalts. This difference reflects source region differences, and not by crystallization processes involving liquidus or near-liquidus phases (olivine or pyroxene). Basaltic meteorites do not behave quite as well in this type of plot. This may suggest that their source regions are more varied in FeO–Sc. Alternatively, there may be other magmatic processes that control their position on this plot (e.g., accumulation of Sc- and Fe-poor phases, such as plagioclase, or terrestrial weathering processes). Figures 9b–d illustrate this point perhaps better. Using these 3 diagrams Neal (2018) pointed out that even in a very local setting (Apollo 17 Taurus-Littrow Valley), high-Ti basalts exhibit derivation from slightly different mantle sources. Crystalline high-Ti basalts exhibit subtle differences that most likely reflect source differences and not post-magma generation processes. In particular, the high-Ti orange glasses are significantly different from the crystalline mare basalts. These observations are consistent with the B, Be, Li data on the mare basalts and picritic glasses that also indicate different sources.

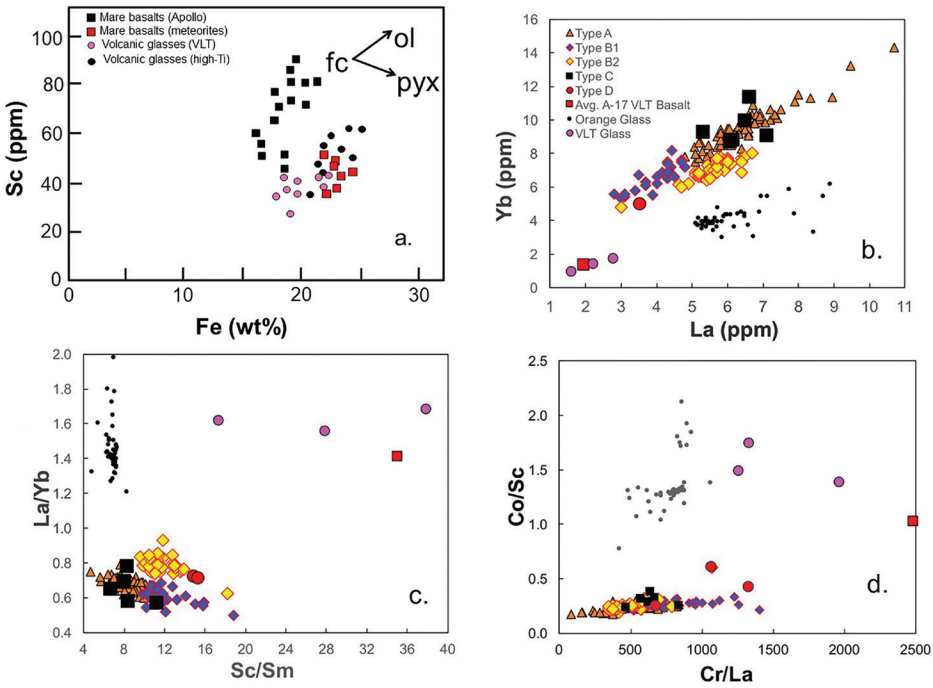

Figure 9. (a) Plot of FeO versus Sc for picritic glasses, mare basalts, and lunar basaltic meteorites (after Shearer et al. 2006). **(b)** Plot of La versus Yb for Apollo 17 basalts (from Neal 2018). **(c)** Plot of Sc/Sm versus La/Yb for Apollo 17 basalts (from Neal 2018). **(d)** Plot of Cr/La versus Co/Sr for Apollo 17 basalts (Neal 2018).

Highly siderophile elements (HSE) and chalcophile elements in mare basalts and their behavior in these magmas have been recently summarized in several studies (e.g., Day et al. 2016a; Steenstra et al. 2018).Their importance in understanding the origin of the Earth–Moon system is discussed in detail in Canup et al. (2023, this volume). Day et al. (2016a) observed that the HSE are in very low abundances (< 0.0001 × CI-chondrites), the high-MgO mare basalts have relatively flat, chondritic-relative patterns, whereas the low-MgO mare basalts have strongly fractionated HSE patterns. The HSE patterns in mare basalts have been interpreted and modeled as products of crystallization and partial melting processes (e.g., Day et al. 2016a). Steenstra et al. (2018) concluded that most mare basalts were not sulfide saturated and therefore differences in siderophile and chalcophile element among mare basalts reflected differences in mantle sources.

Another set of intriguing observations is the occurrence of trace to major abundances of H-species (e.g., OH) in both mare basalts (in apatite) and picritic volcanic glasses. This occurrence is discussed in detail in the McCubbin et al. (2023, this volume). There are still disagreements about the amount and distribution of water (and other volatiles) in the lunar mantle and mare basalts and the state of the H-species. Several recent studies suggest 100s of ppm water in the mantle and undegassed mare basalts (Saal et al. 2008; Hauri et al. 2011). On the other hand, modeling by Elkins-Tanton and Grove (2011) and Renggli et al. (2017) indicate the lunar interior contains upward of 10 ppm water and that most of the hydrogen species in the basalt and release gases are OH, and H_2, respectively.

The solubility of water, *sensu stricto*, in magmatic liquids is, to the first order, directly controlled by the water fugacity (i.e., fH_2O) of the system of interest.The dissolution a water into silicate liquids as a function of fH_2O has been thoroughly studied experimentally in terrestrial magmas over the last 30 years (e.g., Burnham 1975; Stolper 1982; Newcombe et al. 2017). In terrestrial magmatic liquids, the bulk dissolved hydrogen content is present as either hydroxyl groups bound to bridging oxygens or as molecular water. The picture for hydrated lunar magmas, however, is more complicated. At relatively low fO_2 that are characteristic of lunar magmas (e.g., Sato 1976), molecular hydrogen becomes an important component of the O–H fluid system. In H-bearing magmatic systems the prevailing fO_2 controls the relative fH_2O and fH_2 via the following expressions:

$$H_2O = 0.5\,O_2 + H_2$$
$$fH_2/fH_2O = K \times (fO_2)^{-0.5}$$

These expressions indicate that lunar magmas are characterized by relatively high fH_2 to fH_2O ratios, and thus in some sense can be described as inherently "dry" systems. Under these conditions the dissolution of molecular hydrogen into silicate melts must also be considered when describing "hydrated" magmatic liquids. Several studies have experimentally investigated the molecular hydrogen solubility in silicate liquids saturated with an O–H vapor phase at high pressures; Hirschmann (2012) showed that the solubility of molecular H_2 was proportional the fH_2 imposed on the system. Extrapolating these results to the low pressures of the shallow lunar crust, Hirschmann (2012) predicted an H_2 solubility of less than 0.5 ppm. The conclusion was echoed in Newcombe et al. (2017) where the authors concluded that hydroxyl is the dominant hydrogen species dissolved in lunar magmas. The authors of this study estimated an upper limit for H_2 solubility of 4 ppm for volatile saturated magmas at low pressure conditions. At present, it seems likely that OH is by far the most important hydrogen species present in hydrous lunar magmas. Here it should be stressed that this conclusion does not nullify the potential importance of molecular H in exsolved magmatic volatile phases, where thermodynamic constraints dictate that the equilibrium volatile phase must be rich in H_2. The speciation difference between H in the melt and its conjugate fluid phase may have important consequences for understanding the redox evolution of lunar magmas.

In light of new data on endogenous lunar volatiles within the mare basalts and pyroclastic glasses (e.g., Saal et al. 2008; McCubbin et al. 2010, 2011, 2023, this volume; Hauri et al. 2011), Needham and Kring (2017) calculated the effect of volatile release during the peak period of lunar magmatism between 3.8 and 3.2 Ma (Head and Wilson 1992, 1997). They calculated the peak of mare basalt eruption was ~3.5 Ga and, based upon the volatile abundances of the returned basalts, the lunar atmosphere was calculated to be 1.5 times that of the current atmosphere of Mars (Pa, atmospheric surface pressure). This transient atmosphere could have been preserved in polar cold traps and would have taken up to 70 m.y. to dissipate (Needham and Kring 2017).

4.2.2.3. Radiogenic isotopes. Radiometric crystallization ages for mare magmatism are far more restricted than implied by remotely sensed observations (i.e., crater count ages – see Hiesinger et al. 2023, this volume). In addition to ages summarized by Nyquist and Shih (1992), Papike et al. (1998), Snyder et al. (2000), and Shearer et al. (2006), recent published basalt crystallization ages are presented in EA-4-1. Individual mare basalt samples returned by the Apollo Program range in age from approximately 3900 to 3160 Ma (Shearer et al. 2006). Older basalts have been identified in in breccias returned by Apollo and in lunar meteorites.

Basalt clasts (aluminous mare-like basalts) in lunar breccias are as old as 4330 Ma (Taylor et al. 1983; Dasch et al. 1987; Nyquist and Shih 1992). High-Al basalts appear to be common and globally distributed across the Moon based on Clementine UVVIS data, and Lunar Prospector gamma-ray spectrometer data (constrained by FeO, Th, TiO_2 abundances

within collected samples) (Kramer et al. 2008a,b). The Apollo 14 Group A high-Al basalts have ages extending to 4330 ± 130 Ma, and the Rb–Sr radiometric age of Apollo 14 Group B high-Al basalt 14321,1353 is 4030 ± 40 Ma (e.g., Dasch et al. 1987; Neal and Kramer 2006; Hui et al. 2013). Similar clasts have been reported among the lunar meteorite collection such as Miller Range (MIL) 13317 (Snape et al. 2018; Curran et al. 2019). A $^{207}Pb/^{206}Pb$ isochron of 4332 ± 2 Ma was determined using several basaltic clasts of MIL 13317 (Snape et al. 2018). The ancient age, paired with trace element analysis, is consistent with the oldest ages and compositions of the Apollo 14 Group A high-Al basalts (Snape et al. 2018; Curran et al. 2019). Terada et al. (2007) describe a very low-Ti and low-Al mare basalt clast with low incompatible trace element concentrations within lunar meteorite Kalahari 009, interpreted to represent sampled cryptomare. U–Pb dating of phosphates yield an age of 4350 ± 150 Ma, and Lu–Hf data from mineral separates define a crystallization age of 4286 ± 95 Ma. (Terada et al. 2007; Sokol et al. 2008). A more precise $^{207}Pb/^{206}Pb$ isochron of 4369 ± 7 Ma was obtained from the analysis of five phosphate grains in Kalahari 009 (Snape et al. 2018).

The youngest dated mare basalt is currently the paired stones Northwest Africa (NWA) 032 and 479, with a Sm–Nd age of 2931 ± 92 Ma and a concordant Rb–Sr age of 2947 ± 16 Ma (Borg et al. 2009). The mare basaltic meteorites collected from the LaPaz Icefield (LAP) 02205 and its pairings (Sm–Nd: 2992 ± 85 Ma; Rb–Sr: 2991 ± 14 Ma; Rankenburg et al. 2007), NWA 4734 (Sm–Nd: 3024 ± 27 Ma; Rb–Sr: 3083 ± 42 Ma; Elardo et al. 2014), NWA 773 (Sm–Nd: 2993 ± 33 Ma; Borg et al. 2009) and Northeast Africa (NEA) 003A (Sm–Nd: 3089 ± 64 Ma; Haloda et al. 2009) produce similarly young and overlapping ages. A summary of all recent mare basalt ages is presented as age-ε_{Nd} and age-$^{87}Sr/^{86}Sr$ in Figure 10 (also see EA-4-1).

Most of the mare basalts are derived from time-integrated depletions in their sources ($\varepsilon_{Nd} > 0$) and $^{87}Rb/^{86}Sr$ less than 0.038. Only basalts with a significant KREEP component have enriched isotopic signatures. For example, the Apollo 17 high-Ti basalts and the Apollo 12 ilmenite basalts are the most depleted and the Apollo 15 pigeonite and olivine basalts are the least depleted of the mare basalts. The KREEP basalts from Apollo 15 are the most enriched. This indicates that during the peak eruptive flux of mare magmatism between 3.8 and 3.2 Ma (Head and Wilson 1992; Head and Coffin 1997) basalts were produced through melting of a variety of enriched and depleted sources. The youngest basalts represented by the lunar meteorites were produced after the peak flux of mare magmatism (Head and Wilson 1992; Head and Coffin 1997). During this episodic period of mare magmatism in which the mantle produced smaller volumes of magma, a variety of mantle sources were still being melted to produce incompatible element enriched basalt (e.g., NWA 773) and highly incompatible element depleted basalts (e.g., NWA 032). It is difficult to produce this range in ε_{Nd} in a crystallizing lunar magma ocean because the Sm/Nd should not be dramatically fractionated for over ~80% of LMO crystallization, as low-Ca pyroxene and olivine are the dominant cumulate phases (e.g., Snyder et al. 1992, 2000). Most likely this reflects the mixing of two components: a primitive cumulate component with a near constant Sm/Nd ratio and a volumetrically smaller second component that is enriched in Nd and Sm and a lower Sm/Nd ratio. Snyder et al. (1994) suggested that this second component is a trapped intercumulus liquid. This liquid is in very small volumes and could be an instantaneous liquid composition or a migrating melt squeezed out of cumulates during a reduction in porosity. Alternatively, Borg et al. (2009) suggested that the high incompatible-element abundances, lower Sm/Nd and higher Th/Sm component added to the cumulate source was a product of late-stage LMO crystallization (i.e., urKREEP). It is clear that the majority of mare basalt sources are not LMO primitive cumulates but a product of hybridization of mantle lithologies (e.g., Kesson and Ringwood 1976; Shearer et al. 1991; Snyder et al. 1994; Singletary and Grove 2008; Sakamaki et al. 2010; Ling et al. 2015). This results in a wide diversity of mantle sources for not only mare basalts, but also all lunar magmatism (e.g., Gaffney et al. 2007).

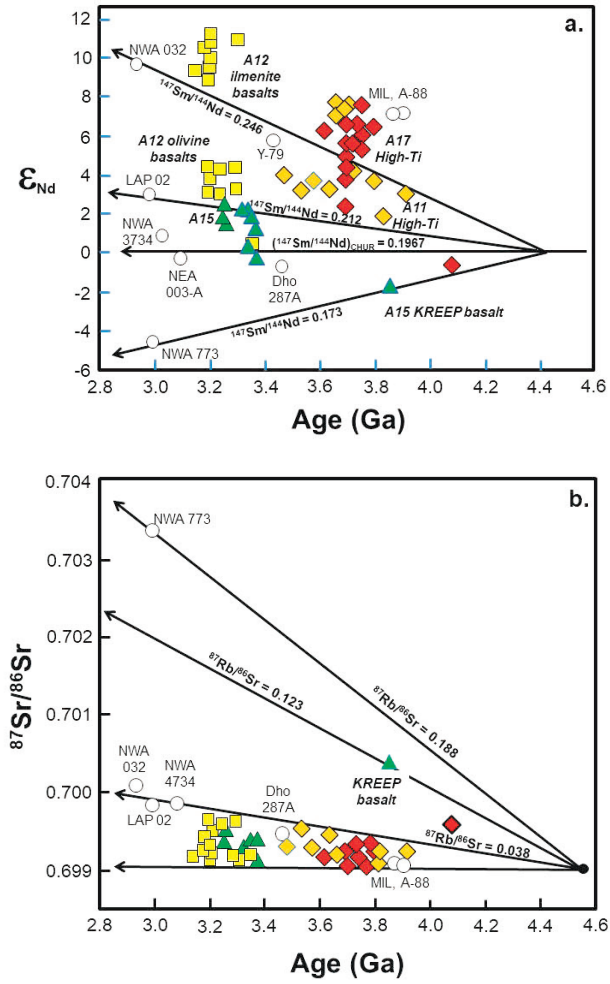

Figure 10. (a) Age versus εNd for mare basalts. **(b)** Age versus $^{87}Sr/^{86}Sr$ for mare basalts (modified after Shearer et al. 2006; Elardo et al. 2014 and references within).

Mare basalt Lu–Hf systematics (combined with Sm–Nd) have been examined in numerous studies starting with the work of Unruh et al. (1984). However, recent work has provided model ages for the mantle sources of the mare basalts (Fig. 3; Sprung et al. 2013; Carlson et al. 2014; Gaffney and Borg 2014; Borg et al. 2015). These studies derive a Lu–Hf model age for the formation of the mare basalt sources and KREEP that is relatively young (~4350 Ma). There are multiple interpretations for this model age for the mare basalt source and urKREEP: the end of LMO differentiation, closure of the hybridization process (e.g., CMO), or a mantle heating event (Borg et al. 2015; Shearer et al. 2015).

U–Pb studies of pyroclastic glasses have led to an interpretation of lunar Pb and the chronology of a pyroclastic eruption. Nemchin et al. (2011) showed that the radiogenic Pb isotope compositions of the Apollo 14 volcanic glass beads are similar to those commonly determined for mare basalts and are correlated with chemical variations observed in the beads. This indicates that Pb unsupported by in-situ U decay has a similar origin in both glass beads and mare basalt

samples and is likely to reflect variations of $^{238}U/^{204}Pb$ (μ) in the lunar mantle. They interpreted that the complete range of Pb isotope compositions observed in the glass beads and mare basalts is a result of mixing between a LMO produced sulphide-rich reservoir and KREEP.

4.2.2.4. Stable isotopes. The development of multi-collector ICP MS instruments (e.g., Halliday et al. 1998) has enabled high-precision stable isotope measurements of several elements. These have provided a number of answers to some basic questions in the evolution of Moon and the Earth–Moon system. Some stable isotope systems appear to be fractionated between the high-Ti and low-Ti mare basalts (Li, O, Mg, Ti, Cu, Fe) whilst for other systems (Si, S, Cr, Ca, Ga, K, Rb, V, Zn) no differences have been reported to date. Volatile behavior during LMO evolution could be reflected in peculiar signatures of some stable isotope systems (Cl, Cr, Cu, Zn, Ga). Additionally, some stable isotope systems are indistinguishable between the Earth and the Moon (possible B but more work is needed, Ca, Fe, Li—low-Ti basalts, Mg, O, Rb, Si, Ti—low-Ti basalts, V), while others show the Moon is distinct (Cr, Cu, Ga, K, Li—high-Ti basalts, Ti—high-Ti basalts, Zn). Observations made on the basis of results of stable isotope investigations are detailed below. See the McCubbin et al. (2023, this volume) for discussion of Cl and S isotopes.

Lithium elemental/isotope systematics in mare basalts were investigated by Magna et al. (2006), Day et al. (2016b), and Seitz et al. (2006). These studies provided unequivocal evidence for Li isotope dichotomy between low-Ti and high-Ti mare basalts, with cumulative mean $\delta^7Li = +3.8 \pm 0.6‰$ and $+5.2 \pm 1.1‰$ for low-Ti and high-Ti mare basalts, respectively (Day et al. 2016b). The Li isotope composition of the former group largely mimics that of the primitive Earth's mantle (see Tomascak et al. 2016 and references therein). The first-order explanation encompasses the intrinsic mineralogical difference for the source regions of diverse basalt types, with olivine–Opx assemblage dominating the source of low-Ti mare basalts and Cpx-rich source advocated for high-Ti mare basalts (e.g., Snyder et al. 1992, Elkins-Tanton et al. 2011).

Boron isotope compositions has been analyzed in three mare basalts by Zhai et al. (1996). The $\delta^{11}B$ values show overlap at ~−5‰. This is slightly higher than the estimates of $\delta^{11}B$ value for the Earth's primitive mantle at $-7.1 \pm 0.9‰$ (Marschall et al. 2017).

Oxygen isotopes are a sensitive tracer of various processes and components that add to the chemical and isotopic make up of Earth, Moon, Mars and other planetary/asteroidal bodies (see Canup et al. 2023, this volume). Clayton and Mayeda (1996) reported $\delta^{18}O$ values for lunar meteorites of which several were classified as low-Ti basalts/gabbros. Wiechert et al. (2001) revealed the difference in $\delta^{18}O$ values between low-Ti and high-Ti mare basalts, later confirmed by Spicuzza et al. (2007). Although no such difference in $\delta^{18}O$ was detected by Liu et al. (2010), Hallis et al. (2010) observed a marginal difference in $\delta^{18}O$ between low-Ti and high-Ti mare basalts, more recently reinforced by new high-precision O isotope measurements (Herwartz et al. 2014; Young et al. 2016). These O isotope differences were discussed nearly exclusively in the frame of mineralogy-controlled variations in the source mantles (Spicuzza et al. 2007 ; Hallis et al. 2010; Liu et al. 2010), although some internal $\delta^{18}O$ variability (such as that reported for Apollo 17 basalts; Hallis et al. 2010) could have been the result of fractional crystallization. Whether ilmenite could be responsible for the reported variations in $\delta^{18}O$ is yet unclear. The cumulative $\delta^{18}O$ for Bulk Silicate Moon at $5.5 \pm 0.2‰$ indicates an irresolvable difference to Earth's mantle (Liu et al. 2010).

Oxygen isotopes from zircons from Apollo 12 14, 15, and 17 have been reported (Nemchin et al. 2008, 2011; Whitehouse and Nemchin 2009; Valley et al. 2014). Nemchin et al. (2008) and Whitehouse and Nemchin (2009) analyzed Apollo 14 zircons with a range of crystallization ages (~4.4 to 3.9 Ga). All data fall within a narrow range of $\delta^{18}O$ (~1 per mil), indistinguishable from terrestrial mid-ocean ridge basalts. Valley et al. (2014) analyzed zircons from four Apollo

landing sites and reported incredibly constant $\delta^{18}O$ values (5.61 ± 0.07 per mil VSMOW), which is higher than zircons from the Earth's oceanic crust (5.20 ± 0.03 per mil VSMOW). Lunar zircons contain higher Ti contents relative to their terrestrial counterparts, consistent with higher crystallization temperatures.

Magnesium isotopic composition of olivine in several Apollo 12 low- to intermediate-Ti mare basalts were measured by Norman et al. (2006). Their results revealed a largely identical Mg isotope composition with Bulk Silicate Earth. Wiechert and Halliday (2007) showed a dichotomy in $\delta^{26}Mg$ values between low-Ti and high-Ti basalts, while no such Mg isotope difference was reported by Chakrabarti and Jacobsen (2010). The isotope dichotomy in $\delta^{26}Mg$ (−0.33 to −0.02‰ in low-Ti versus −0.61 to −0.37‰ in high-Ti basalts) revealed by Sedaghatpour et al. (2013) provided a strong support for the original observations made by Wiechert and Halliday (2007), although the absolute $\delta^{26}Mg$ values differ beyond the analytical uncertainty. Recent Mg isotope data by Sedaghatpour and Jacobsen (2019) confirm the previous Mg isotope dichotomy between low-Ti and high-Ti basalts, the origin of which is yet unclear. The dichotomy could be related to crystallization of ilmenite or kinetic effects. Olivine-normative basalt 15555 yielded highly negative $\delta^{26}Mg = -0.78‰$, indicating a strong control exerted by inter-mineral Fe–Mg diffusion (Sedaghatpour and Jacobsen 2019). Sedaghatpour et al. (2013) estimated $\delta^{26}Mg = -0.26 \pm 0.16‰$ for the Moon, identical within the uncertainty to that of Earth (Bourdon et al. 2010; Teng et al. 2010; Teng 2017).

Silicon isotope compositions for low-Ti and high-Ti mare basalts do not reveal any resolvable differences among these major lithological groups or between the Moon and Earth (e.g., Fitoussi and Bourdon 2012; Zambardi et al. 2013), pointing to inefficiency of high-temperature processes and/or core segregation to impart any measurable Si isotope fractionation. Apollo 17 mare basalts show a larger $\delta^{30}Si$ variability (~0.1‰), perhaps attesting to overall more complex history of their source region.

Potassium stable isotope compositions collected using ion microprobe showed no difference in $\delta^{41}K$ among lunar basalts (Humayun and Clayton 1995). Recent high-precision K isotope measurements revealed $\delta^{41}K$ difference of ~0.4‰ between the Moon and Earth (Wang and Jacobsen 2016; see Canup et al. 2023, this volume) but available data for low-Ti and high-Ti mare basalts are indistinguishable and no further implications for magmatic evolution can be made at present. However, lunar rocks are significantly (>2σ) enriched in the heavy isotopes of K compared to the Earth and chondrites (by around 0.4 parts per thousand; Wang and Jacobsen 2016).

Calcium isotope datum reported by Simon and DePaolo (2010) for high-Ti mare basalt 10017 represents the first modern Ca isotope anchor relative to Earth, showing no difference to terrestrial mafic lithologies. Valdes et al. (2014) measured Ca isotope composition in four mare basalts (three low-Ti, one high-Ti) with no systematic difference. Simon et al. (2017) reported a mean $\delta^{44/40}Ca = 0.99 \pm 0.14‰$ for seven lunar samples and from a small external error, it can be judged that no resolved Ca isotope variation between low-Ti and high-Ti mare basalts is to be expected.

Titanium stable isotope investigations have recently been applied to low-Ti and high-Ti mare basalts, and the results show a clear dichotomy with isotopically heavier high-Ti basalts and $\delta^{49}Ti$ values for low-Ti basalts that are statistically indistinguishable from the Earth's mantle (Millet et al. 2016; Greber et al. 2017). Given the refractory nature of Ti, a direct consequence of this observation is a compositional similarity between Earth and the Moon-forming impactor. Higher $\delta^{49}Ti$ values in high-Ti basalts are somewhat enigmatic, as ilmenite should preferentially incorporate light Ti, according to stable isotope fractionation theory (e.g., Schauble 2004).

Chromium isotope data was reported by Bonnand et al. (2016) for low-Ti and high-Ti basalts ($\delta^{53}Cr$ values −0.33 to −0.15‰ versus −0.27 to −0.17‰); these values are at the lower

end of δ^{53}Cr values reported for pristine terrestrial materials (e.g., Schoenberg et al. 2008). The Cr isotope overlap between low-Ti and high-Ti basalts has recently been confirmed by Sossi et al. (2018) who have also provided evidence for resolved difference in mean δ^{53}Cr between Earth (−0.11 ± 0.02‰) and Moon (−0.21 ± 0.03‰). Chromium isotopes appear to be fractionated during magmatic process as evidenced by broad correlations with Mg′ but the overall effect of magmatic differentiation appears to be subordinate given the high temperatures of LMO solidification, as also supported by δ^{53}Cr = −0.16‰ found for the late-stage KREEP basalt 15386 (Bonnand et al. 2016). Core formation is unlikely to produce detectable Cr isotope fractionation, and Cr depletion, coupled with slight isotope difference, have been discussed in the frame of partial vapor loss during magma ocean crystallization at temperatures below silicate liquidus (Sossi et al. 2018).

Vanadium stable isotope compositions have recently been explored for 19 low-Ti and high-Ti mare basalts by Hopkins et al. (2019). The results span a δ^{51}V range of nearly ~2.5‰ (from −3.5 to −1.0‰), irrespective whether low-Ti or high-Ti in origin. Considering the lack of V isotope fractionation during magmatic process, Hopkins et al. (2019) revealed strict negative correlation with exposure ages of lunar rocks and explored the possibility of modulating V isotope systematics via Galactic Cosmic Ray (GCR) irradiation, mostly through Fe and Ti as target elements. Pre-irradiation δ^{51}V = −1.05 ± 0.14‰ has been calculated for Bulk Silicate Moon (Hopkins et al. 2019), which is identical within uncertainty with that derived for Earth (Prytulak et al. 2013) and chondrites (Nielsen et al. 2019).

Iron isotope data for mare basalts were first produced Beard and Johnson (1999) for high-Ti basalts using TIMS but their analytical uncertainties (~±0.15–0.23‰) prevented any meaningful discussion. Wiesli et al. (2003) and Poitrasson et al. (2004) reported on the first high-precision (mostly < ±0.06‰) Fe isotope compositions in lunar samples and their cumulative data indicated isotopically lighter low-Ti mare basalts compared to high-Ti basalts. These conclusions were reinforced by Weyer et al. (2005) who suggested that ilmenite could carry isotopically heavy Fe and that remelting of late-stage ilmenite-rich cumulates could introduce a ^{57}Fe-rich component, an idea that was recently confirmed by careful experiments (Sossi and O'Neill 2017). Liu et al. (2010) provided further evidence for Fe isotope dichotomy between low-Ti and high-Ti mare basalts; they also estimated that the mean Fe isotope composition of the lunar upper mantle is within the estimates for the Earth's upper mantle. Recently, Sossi and Moynier (2017) re-confirmed the Fe isotope dichotomy in mare basalts. Poitrasson et al. (2019) measured the Fe isotope compositions for a suite of 33 bulk lunar mare basalts and highland rocks and combined these with published data to produce a compendium of 73 Fe isotope analyses from different lunar samples. The combined data revealed a statistically significant Fe isotope difference between low-Ti and high-Ti mare basalts, yielding average δ^{57}Fe = 0.127 ± 0.012‰ (2SE; n = 27) and δ^{57}Fe = 0.274 ± 0.020‰ (2 SE; n = 25), respectively (relative to the IRMM-14 isotopic reference material). The estimated relative proportion of the low-Ti and high-Ti source mantle indicates that the lunar upper mantle δ^{57}Fe value should be 0.142 ± 0.026‰. However, the δ^{57}Fe values of 15 highland rock analyses cannot distinguish any difference between ferroan anorthosites and Mg-suite rocks. Future experimental studies must address potential Fe isotope fractionation at extremely reducing conditions and low pressures relevant for lunar core formation, because the intrinsic cause of the Fe isotope difference between low-Ti and high-Ti mare basalts remains uncertain. However, bulk Moon δ^{57}Fe is indistinguishable from that of Earth (e.g., Sossi and Moynier 2017; Poitrasson et al. 2019).

Copper isotope compositions for a handful of high-Ti mare basalts were made by Moynier et al. (2006) and Herzog et al. (2009). The δ^{65}Cu ranged from +0.12 to +1.40‰. Preliminary data for five low-Ti mare basalts (2.0 ± 0.2‰; Lindsay et al. 2011) show systematically higher δ^{65}Cu values relative to high-Ti mare basalts, suggesting yet unknown process that results in a

larger difference between Cu isotope composition of Earth and low-Ti mare basalts, considered to broadly represent silicate mantle of the Moon. Copper is a redox-sensitive element and experiments under lunar mantle fugacity conditions could provide further clues to this peculiar observation.

Zinc isotope compositions in Apollo 11 and 17 high-Ti mare basalts (Moynier et al. 2006; Herzog et al. 2009) indicated a large variation in $\delta^{66/64}$Zn values (+0.17 to +1.90‰), departing significantly from pristine terrestrial rocks (e.g., Wang et al. 2017). A follow-up study by Paniello et al. (2012) underscored the earlier findings by analyzing also low-Ti mare basalts ($\delta^{66/64}$Zn from +0.84 to +1.56‰). Kato et al. (2015) re-iterated the general results of these studies with no systematic difference between low-Ti and high-Ti mare basalts. Kato et al. (2015) estimated $\delta^{66/64}$Zn = +1.4 ± 0.5‰ for lunar mare basalts while $\delta^{66/64}$Zn for the Earth's primitive upper mantle is variously estimated between +0.16 ± 0.06‰ and +0.30 ± 0.07‰ (e.g., Wang et al. 2017; Sossi et al. 2018). The effect of mineral phases (e.g., ilmenite, spinel) on Zn isotope systematics, relevant for LMO evolution, remains to be tested. The reason for the Zn isotope difference between Earth and Moon may be related to the energetic impact origin of the Moon and subsequent volatile loss (see Day and Moynier 2014 for discussion). Alternative models (e.g., Dhaliwal et al. 2018) employ evaporative fractionation of Zn by volatilization and/or isolation during LMO crystallization.

Rubidium The pilot study of δ^{87}Rb systematics in mare basalts by Pringle and Moynier (2017) indicated indistinguishable mean δ^{87}Rb values of low-Ti and high-Ti basalts whereas Earth and Moon have different mean δ^{87}Rb values with Moon being isotopically heavier.

Gallium isotopic composition was first reported for low-Ti and high-Ti basalts by Kato and Moynier (2017) reported the first Ga isotope compositions two principal lithological groups have overlapping δ^{71}Ga values, with perhaps somewhat larger δ^{71}Ga variability found for high-Ti basalts (−0.03 to +0.57‰). As with Rb, the overall heavy Ga isotope systematics in lunar samples relative to Earth appear to reflect volatile loss, most likely tied to the giant impact.

4.2.2.5. Experimental petrology. Substantial examination of the phase relations of mare basalts has been made since the return of the first Apollo samples and has brought us considerable insights into their origins. There are numerous summaries of previous work and their interpretations (e.g., BSVP 1981; Longhi 1992; Grove and Krawczynski 2009). From previous work, several conclusions can be reached:

- Mg, Fe silicates are the first minerals to crystallize when near-primary basaltic magma cool to its liquidus. Liquidus temperatures for these basalts are very high (~1400°C) and are similar to many terrestrial komatiites (e.g., Hess 1989, 2000; Longhi 1992). More evolved mare basalts will crystalliz e other phases (e.g., plagioclase, ilmenite, armalcolite) at lower temperatures.
- At pressures up to ~1 GPa olivine is the liquidus phase. At higher pressures olivine is joined and replaced by Opx. At the olivine to Opx transition, there is a point on the liquidus known as the multiple-saturation point where both phases crystallize simultaneously. This point of multiple saturation of olivine and Opx has significance under some conditions, and potentially can be indicative of melting conditions (e.g., the depth, temperature, and minerals in the residue after the melt was extracted).However, under the conditions that a melt experiences fractional crystallization of olivine, the depth of multiple saturation represents a minimum depth of the source. The multiple saturation pressure for mare basalts ranges from 0.5 to 1.5 GPa, whereas for the picritic glasses the multiple saturation pressure is 1.5 to 2.5 GPa, suggesting a deeper origin (e.g., Longhi 1992). There appears to be little correlation between Ti concentration and pressure of multiple saturation.

- The pyroclastic glasses are the closest approximations for primary lunar magmas.
- Plagioclase is not a near-liquidus phase in any basaltic composition. In fact, plagioclase crystallizes only after a significant temperature interval and only at low pressure. The negative Eu anomaly implies that plagioclase should have been retained in the source residue after the melting event, yet olivine and pyroxene are the only high-pressure liquidus phases. This evidence strengthened the arguments that the plagioclase- (and Eu-)rich lunar crust and the plagioclase-poor, ultramafic mantle are complementary cumulate regions formed during a large-scale magma ocean differentiation event.
- The source of the mare lavas was composed of minerals that had been in equilibrium with plagioclase when they crystallized and had inherited their negative Eu anomaly from this prior LMO-processing event. This fingerprint of plagioclase removal to form the lunar crust was probably imparted onto most of the mare basalt source region by hybridization of the cumulate pile (the CMO event).

More recent experiments have focused on phase equilibria of basaltic meteorites at variable pressure and temperature, a unifying model for the interpretation of earlier experiments, as well as LMO crystallization, to better understand the mare basalt source region.

Elardo et al. (2014) examined and compared the phase relationship among lunar basalts represented by meteorite NEA 003A and LAP group. These meteorites represent contrasting bulk compositions with NEA 003A being a primitive basalt (ITE-poor) and the LAP group basalts are evolved (ITE-rich). The liquidus multiple saturation point for NEA 003A is at 1.1 GPa, 1330 °C. In contrast, the liquidus multiple saturation point for the LAP group is < 0.55 GPa and 1150–1200 °C. They proposed distinctly different models for the petrogenesis of these two basalts through the integration of isotopic and chemical characteristics with experimental data. If the primitive NEA 003A liquid composition is a minimally-modified melt, the relatively low Mg′ of its source region (73–75), its lack of a significant Eu anomaly, and its chondritic initial Nd isotopic composition indicate its source region likely escaped mixing during the CMO event. The LAP basalts experienced fractional crystallization and therefore its multiple saturation point may not be related to depth of origin (cf. Grove and Krawczynski 2009). However, the trace element characteristics suggest hybridization of source with a late-stage LMO cumulate, but not a KREEP-rich component.

Previous studies have attempted to place the mare basalt sources within the context of the LMO cumulate pile (e.g., Taylor and Jakes 1974; Longhi 1978; Snyder et al. 1992). More recent studies have examined through experiments and computational methods the potential LMO cumulate sequence and the potential nature of the source region of mare basalts (Elardo et al. 2011; Elkins-Tanton and Grove 2011; Elkins-Tanton et al. 2011; Lin et al. 2017, 2020; Charlier et al. 2018; Rapp and Draper 2018). Results from Lin et al. (2017, 2020), Charlier et al. (2018), and Rapp and Draper (2018) showed varied cumulate sequences based on starting composition and efficiency of crystallization (fractional vs. equilibrium). All of these models illustrate that the source regions modeled for the mare basalts and pyrocastic glasses require mixing of earlier and later stage cumulates.

Experimental investigations of oxygen fugacity (fO_2) influence on the source depths for high-Ti picritic glasses determined new multiple saturation depths for these magmas. Krawczynski and Grove (2012) showed that multiple saturation with olivine and Opx on the liquidus occurs at 1.2 GPa and 1350 °C for the Apollo 15 red glass (13.8 wt.% TiO_2), and 2.5 GPa and 1530 °C for the Apollo 17 orange glass (9.1 wt.% TiO_2) at IW + 1.3. At more reducing conditions, (IW − 2.1) the multiple saturation points shift to higher pressure and are 2.2 GPa and 1450 °C for the red glass, and 3.1 GPa and 1560 °C for the orange glass. Using independent estimates of fO_2 for the orange glass source region of ΔIW − 0.6 (e.g., Nicholis and Rutherford 2009), interpolation of phase stability data yielded a pressure of

multiple saturation of 2.8 GPa. The results confirmed that the red and orange glasses are buoyant with respect to model lunar interior assemblages at their multiple saturation pressures. Brown and Grove (2015) illustrated a similar effect of fO_2 on the intermediate-Ti picritic glasses (yellow glasses from Apollo 14, 15, and 17 landing sites). They concluded that assimilation fractionation and/or melt–wall rock reaction all fail to produce the within-suite compositional variability observed in the Apollo 14, 15, and 17 yellow glasses. Mixing of remelted source cumulates, combined with small amounts of olivine fractionation, are the only mechanisms that can reproduce all three trends. Barr and Grove (2013) examined melt compositions in equilibria with a garnet-lherzolite residual phase assemblage that were produced at 2.35 GPa (1440 and 1420 °C) and at 2.6 GPa (1460 °C). Combining these data with major and trace element data, they concluded that very low-Ti Apollo 15 Green A magmas were derived by melting a source containing primordial lunar mantle and a component of late-stage LMO cumulates.

4.2.3. Synthesis and integration of recent results

The duration of mare magmatism extends from 4350 Ma to 1000 Ma and even younger ages have been proposed (Braden et al. 2014). During this extensive period of magmatism various types and mixtures of mantle sources were melted, often concurrently. The duration of mare magmatism overlapped with KREEPy magmatism (Mg-suite, KREEP basalts).

Pyroclastic deposits are common on the lunar surface. They range in size, eruptive style, and magma composition. The heat generated in the deep lunar mantle and transported by picritic magmas may have resulted in melting at more shallow levels in the mantle. Head et al. (2023, this volume) discuss this possibility.

Mare basalts are predominantly a product of remelting hybridized LMO cumulates. Source components include mixtures of LMO cumulates with similar Sm/Nd ratios (but different mineral assemblages and compositions), a component that may represent either an intercumulus melt or last stages of LMO crystallization (urKREEP), and potentially a remobilized garnet-bearing unprocessed mantle. The model ages for these sources (mafic cumulates, urKREEP) are approximately 4380 Ma. This model age represents a thermal event linked to either primary lunar differentiation, the CMO event, or a large basin forming event.

5. SILICIC–FELSIC MAGMATISM

5.1. Summary of observations

Lunar features classified as “red spots” were initially identified on the Moon during the Apollo era and the following decade. These features typically have low ultraviolet reflectance with respect to the near-infrared and low TiO_2 and FeO abundances (Whitaker 1972; Malin 1974). Of these features, the Gruithuisen domes were the subject of several early studies. These studies suggested that, on the basis of rough surface textures and inferred steep slopes of 15–30°, the domes were produced by felsic lavas with high silica contents and correspondingly high viscosities, perhaps similar to terrestrial rhyolite domes (e.g., Head and Hess 1978; Chevrel et al. 1999).

Mid-infrared data from the LRO Diviner Lunar Radiometer Experiment confirmed the silicic/felsic nature of the Gruithuisen domes, as well as the Mairan domes, Lassell Massif, Hansteen Alpha, Compton Belkovich, and Aristarchus (Glotch et al. 2010, 2011; Jolliff et al. 2011; Ashley et al. 2016; Boyce et al. 2017). However, not all lunar red spots are silicic in composition; the Helmet, Montes Riphaeus, and Darney Chi and Tau are among the originally identified red spots that do not have a silicic signature in Diviner data (Fig. 11).

The interpretations of Diviner data are based on analyses of the silicate Christiansen feature (CF), an emissivity maximum, the position of which is indicative of bulk silicate mineralogy

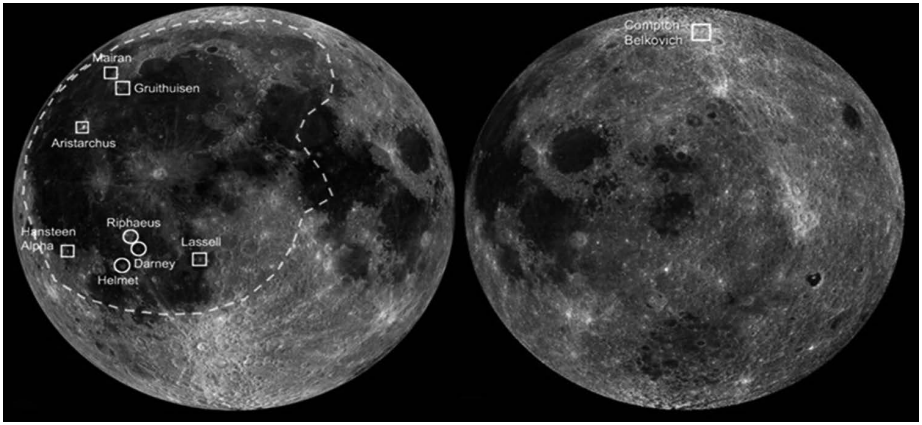

Figure 11. Locations of "red spots" mentioned in the text that have a silica-rich signature in LRO Diviner data (**squares**) and those that are red spots but have no silica enhancement (**circles**). Base map is LROC WAC; **left** image centered at 0° longitude and **right** image, at 90° longitude. **Dashed line** marks approximate boundary of the Procellarum KREEP Terrane.

(e.g., Salisbury and Walter 1989). Three-point Diviner spectra display a concave up spectral shape, which is unique on the Moon, and based on comparison with laboratory mineral and rock spectra, indicates a composition of ≥ ~65 wt.% SiO_2 (Glotch et al. 2010, 2017). This interpretation is supported by visible photometric analyses of LRO Camera Narrow Angle Camera (LROC NAC) images. These data show that lunar silicic regions exhibit unusually high reflectance and single scattering albedos, consistent with the presence of quartz and/or alkali feldspar, and relatively minor mafic mineral abundances (Clegg-Watkins et al. 2017).

Several studies have shown that silicic lunar features are also correlated with elevated Th abundances. Lawrence et al. (2003, 2007) showed that the Compton-Belkovich region has an elevated Th abundance compared to typical feldspathic highlands terrain based on Lunar Prospector Gamma Ray Spectrometer data (LP-GRS Lawrence et al. 2000, 2003). Subsequent analyses showed that four additional red spots—the Gruithuisen domes, Hansteen Alpha, Lassell Massif, and Aristarchus—all have elevated Th abundances (Hagerty et al. 2006, 2009), along with the Mairan domes (Glotch et al. 2011).

The correlation between silicic compositions and Th abundance is reflected in the geographic distribution of silicic lunar silicic features (Fig. 11). All of the features, with the exception of Compton-Belkovich, fall within the PKT (Jolliff et al. 2000). The silicic compositions, high Th content, and geographic distribution all point to these features being the products of evolved magmas.

In addition to the silicic features identified in lunar remote sensing data sets, silicic rocks ranging from complex impact breccias to lithic clasts in impact breccias and small, mm to cm size fragments of rock found in regolith, have previously been identified in samples from the Apollo 11, 12, 14, 15, and 17 sites (e.g., Meyer et al. 1996). These rocks contain intergrowths of K-feldspar and quartz or a high-temperature silica polymorph, i.e., "felsic" assemblages, and correspondingly high-SiO_2 and high-Th compositions (Table 2).

The majority of lunar granitoids are nonpristine, polymict products of impact mixing of multiple lithologies (e.g., Shervais and Taylor 1983; Warren et al. 1983; Jolliff 1991; Warren 1993; Snyder et al. 1995; Bonin et al. 2002). There are, however, *true* granitic rock fragments and clasts in breccia returned from the Apollo missions, including subsamples from 12013 (Quick et al. 1981); 12032, 366-19 (Seddio et al. 2013); 14303,204 and 14321,1027 (Warren et

al. 1983); 15405,12 (Ryder 1976); 15434,10 (Ryder and Martinez 1991); 15459,315 (Marvin et a1. 1991); 72215 to 72275; 73215 and 73235 (Stoeser et al. 1975). These silicic rocks are characterized by up to 75 wt.% SiO_2, up to 8 wt.% K_2O, and high Th abundances (> 60 ppm). Examples of these compositions are presented in Table 2. The high Th content is of particular interest, as this element is easily detectable by orbital gamma-ray spectroscopy and the correspondence of Th "hotspots" on the Moon with spectral indicators of silica-rich exposures of volcanic rocks and impact-excavated intrusive rocks.

Table 2. Granitic lithology bulk major- and trace-element chemical compositions

	12013 ,09,13	**12013 ,163, I-1**	**12023 ,147-10**	**12032 ,366-19**	**14321 ,1027 clast 4**	**73255 ,27/,3**
			oxides (wt.%)			
SiO_2	73.0	70.6	72.7	70.1	74.2	(74.9)
TiO_2	0.60	0.40	0.58	1.07	0.33	0.26
Al_2O_3	11.9	14.5	12.5	13.5	12.5	12.3
Cr_2O_3		0.017	<0.01	<0.03	<0.02	0.01
FeO	1.40	1.60	3.14	4.98	2.32	3.10
MnO	<0.1		0.03	0.07	0.02	0.04
MgO	0.14	0.40	0.24	0.14	0.07	0.20
CaO	1.4	1.8	3.0	3.0	1.3	0.5
BaO	0.70	0.73	0.62	0.68	0.24	0.61
Na_2O	1.40	1.80	1.39	2.47	0.52	0.53
K_2O	6.80	7.70	5.60	4.58	8.60	7.55
P_2O_5	0.10		0.01	0.05		
Sum	97.4	99.5	99.8	100.7	100.1	100.0
Mg/(Mg+Fe)	0.15	0.31	0.12	0.05	0.05	0.10
			trace elements (ppm)			
Sc		6.2	6.3	8.7	3.0	2.3
Co		13.8	0.8	0.8	0.9	1.5
Ni		265	<50	<25	4.9	
Sr		122	134	167	55	215
Rb		184	172	96	210	
Cs		6.5	5.0	3.7	5.7	
La		67	77	79	44	20
Ce		151	184	182	117	50
Nd		65	80	82	58	34
Sm		19.8	23.8	24.6	15.9	6.74
Eu		1.98	2.38	3.01	1.17	2.71
Tb		5.4	6.1	6.6	4.3	1.52
Dy					32	
Yb		41.1	44	52	32.2	10.3
Lu		5.8	6.2	7.4	5.1	1.5

	12013 ,09,13	12013 ,163, I-1	12023 ,147-10	12032 ,366-19	14321 ,1027 clast 4	73255 ,27/,3
Zr	<750	876	970	1500	660	
Nb			154	304		
Hf		37	32	46	13.9	16.0
Ta		9.8			8.3	2.4
Th		60.4	59.5	60.6	65	10
U		19.0	19.5	20.7	23.4	
			ppb			
Ir		0.30	<4		0.05	
Au		4.80	<11		0.04	

References: 12013,09,13: Quick et al. (1981); 12013,163,I-1: Valencia (2017); 12023,147-10: Seddio et al. (2014); 12032,366-19: Seddio et al. (2013); 14321,1027/,1028/1062 clast 4: Warren et al. (1983); 73255,27/,3: Blanchard and Budahn (1979). Blank cells mean values not determined; SiO_2 in parentheses estimated by difference.

In every case, these materials have been excavated by impacts and transported from unknown source regions to their respective sampling locations. Most of the reported granitic samples are small, i.e., < 1 g samples. Sample 12013, however, is an 82.3 g impact breccia with a significant granitic, partially impact-melted component (Fig. 12). Other samples, including 15405,57, 14321 clast 1028, and 12033,507 have masses exceeding 1g (Warren et al. 1983, 1987; Meyer et al. 1996). Some of the granitic samples are fine grained or glassy impactites, whereas others are crystalline and monomict, exhibiting a range of grain sizes (Fig. 13). Apollo 15 breccias 15403 and 15405 contain granitic clasts with grain sizes up to several mm (Warren et al. 1987; Marvin et al. 1991; Meyer et al. 1996), and 12013 contains numerous clasts with cm-size or larger felsic segregations (Fig. 12). Granophyric intergrowths of K-feldspar and silica are common, and a relatively coarse "graphic intergrowth" occurs in 14321,1027 (thin section of 14321,1028: Warren et al. 1983; Meyer et al. 1996).

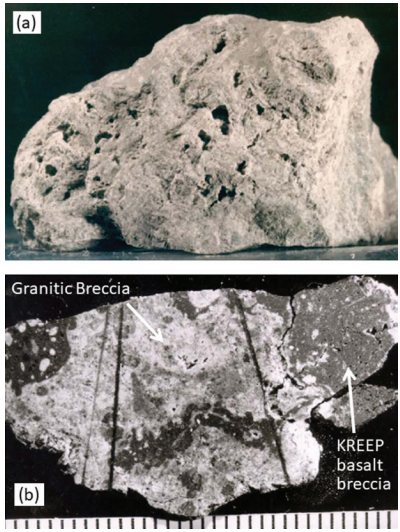

Figure 12. Granitic breccia 12013. **(a)** Photo of 12013,11. Field of view is 4.5 cm. NASA# S70-43636. **(b)** Photo of 12013 slab ,9, mm scale; NASA# S70-40833.

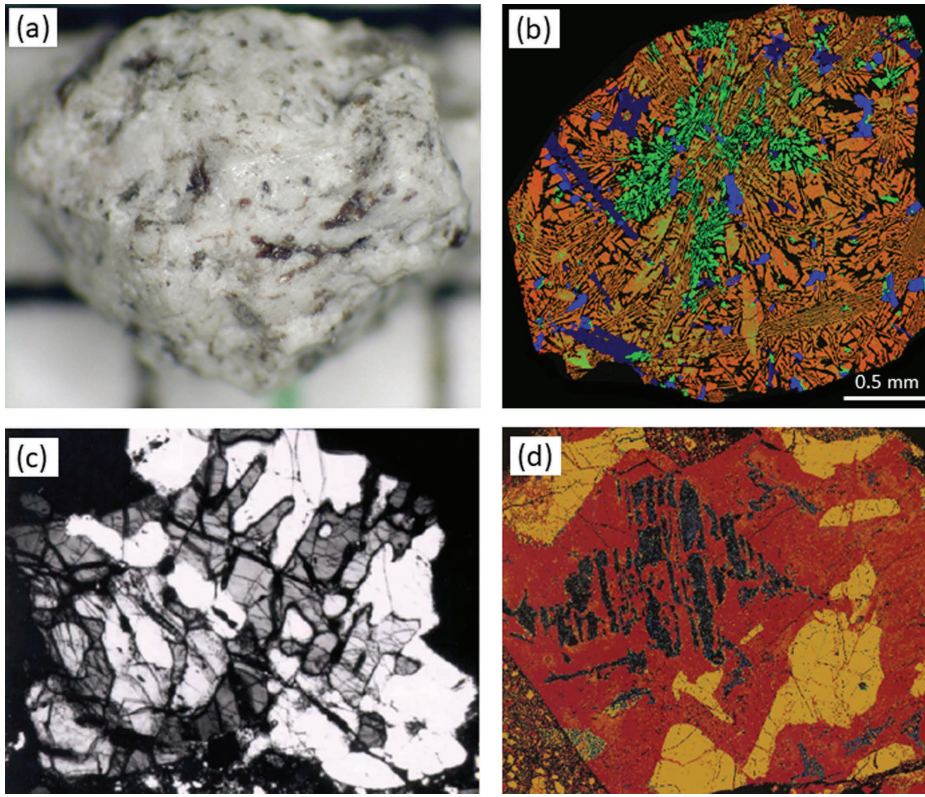

Figure 13. **(a)** Sample 12032,366-19 on a 1 mm grid (see Seddio et al. 2013). K-feldspar, plagioclase, and silica appear **white**. Hedenbergite, fayalite, and ilmenite are **dark**. (b) RGB x-ray composite image of 12032,366-19 with K in the **red** channel, Na in **green**, and Fe in **blue**. K-feldspar appears **orange**, more sodic K-feldspar is **brownish orange**, sodic plagioclase is **green**, olivine is **bright blue**, pyroxene is **darker blue**, and quartz is represented as **black**. After Seddio et al. 2013, their Fig. 4a. **(c)** Thin section photomicrograph of granite clast in 14321,1027 (crossed polars) showing intergrown silica and K-feldspar. K-feldspar is **white**, silica is **gray**, and epoxy is **black**. Thin section is #14321,1047; from Meyer et al. 1996, their Fig. 6. Field of view is 2.3 mm wide. **(d)** False-color BSE of granite clast in breccia 72275 (Meyer et al. 1996). K-feldspar is **red**, plagioclase is **yellow**, and silica is **black**. Field of view is 4 mm. [Reproduced from Meyer at al. (1996) copyright The Meteoritical Society 1996]

The granitic assemblages generally reflect relatively high temperature (for granite), dry crystallization, with final crystallization around 950 to 1000 °C (Valley et al. 2014). A single example of a lunar felsite shows evidence for a low crystallization temperature (~771–810 °C) and oxidizing conditions (Bellucci et al. 2019). Evidence for crystallization of silica as one of the high-temperature polymorphs, cristobalite or tridymite, exists in some samples (Seddio et al. 2015). The "hackly" fracture pattern observed in silica in many granophyric intergrowths is consistent with volume loss on inversion to quartz, where the latter is highlighted by laser Raman spectroscopy. Conversely, primary quartz, observed in some granitic samples, coupled with grain size and the Ti-in-quartz geothermometer has been interpreted to reflect slow cooling and crystallization in an intrusive setting (Robinson et al. 2015; Belucci et al. 2019).

5.1.1. Chronology

Silicic domes on the lunar surface are ancient features, with crater count ages varying from 4.07–3.35 Ga. Hansteen Alpha, the largest of the silicic domes, is composed of several

distinct units with surfaces emplaced between ~3.74 and 3.50 Ga (Wagner et al. 2010; Boyce et al. 2017). The silicic lava flows associated with the dome are embayed by younger mare deposits (Boyce et al. 2017). The Gruithuisen Delta and Gamma domes are slightly older than Hansteen Alpha, having been dated at ~3.74 Ga. As seen at Hansteen Alpha, the silicic domes are considerably older than surrounding plains, which have been dated to ~2.30–3.60 Ga (Wagner et al. 2010; Ivanov et al. 2016). In close proximity to the Gruithuisen Domes are the Mairan Domes. Only the largest "middle" dome has been dated. Boyce et al. (2018) concluded that this dome first erupted at ~3.75 Ga, with a second major episode of volcanism at ~3.35 ± 0.2 Ga. Unlike Hansteen Alpha and the Gruithuisen domes, silicic volcanism in the Mairan Domes region was apparently simultaneous with eruptions of regional mare basalts. The Compton Belkovich Volcanic Complex was active around the same time as the Mairan Domes, with the earliest possible onset of volcanism at ~3.80 Ga, followed by volcanic resurfacing at ~3.50 Ga. (Shirley et al. 2016). The Lassell Massif is the oldest of the lunar silicic domes, with the emplacement of the main unit between 3.95 and 4.07 Ga (Ashley et al. 2016), prior to local mare emplacement at 3.38 Ga (Hiesinger et al. 2003).

Laboratory-based age determinations of felsic rock samples may help ground-truth the surface ages determined by crater counts. Absolute dating of silicic magmatism is limited because of the small sample size and rarity of silicic rock materials available for study. Nevertheless, the radiometric ages for lunar granitic materials fall broadly into two groups—an older group ~4.3 Ga or older, and a younger group, formed ~3.9 Ga (Tables 1 and 3).

Seddio et al. (2014*)* suggested that the younger group might represent an origin following the Imbrium event whereby granitic melt formed as a result of heating and melting and was mobilized and emplaced along an Imbrium-related ring-fracture system. The age of Imbrium basin formation is notably older than the majority of silicic lunar features, which have impact crater model ages ranging from ~4.07–3.38 Ga. Alternatively, the isotopic ages may only partially represent the protracted span of felsic magma formation times, or could reflect the effects of later thermal resetting due to impact events leading to some apparently younger ages (e.g., Bogard et al. 1994; Shuster et al. 2010). A similar span of ages for small fragments of lunar granitoids has been determined by *in situ* U–Th–Pb isotopic analysis of zircon in thin section using ion microprobes (Meyer 1996, Nemchin et al. 2008). Likewise, the refined K–Ca and Rb–Sr internal isochron analyses (Simon et al. 2011), which support a relatively young ~4.05 Ga formation age for silicic clast 14321,1027 (using sub-sample 1062), are consistent with the existing ages determined by zircon dating and other isochrons determined for this well-studied granitoid sample (Warren et al. 1983; Shih et al. 1993) (Fig. 14).

With this relatively small, but robust data set, it is notable that the dated silicic samples appear systematically older than the dated silicic surface features. Given the apparent age difference between the range of dated sample materials and surface deposit ages, one might question whether the silicic features observed on the lunar surface are the source regions for the silicic lithologies that have been studied in the Apollo samples. It is possible that the samples represent more ancient crustal lithologies that have been destroyed or obscured by younger crustal features. If true, direct comparisons between the samples and observed surface features may not be entirely appropriate and would require targeted sample returns from the silicic areas identified from orbital data.

To date, no examples of young (<1 Ga) silicic samples or surface features are known. While some examples of extremely young lunar volcanism have been proposed (Braden et al. 2014), measurements by Diviner and the Moon Mineralogy Mapper indicate these are basaltic features.

Table 3. Age determination for granitic rock and silicic features

Sample*	Age (Ma)	2σ	Material	Description	Reference
12013	4318		older population of zircon in matrix breccia	mean Pb–Pb zircon age	Thiessen et al. (2018)
12033	4320		felsic clast	mean Pb–Pb zircon age	Nemchin et al. (2008)
	800	30		Ar–Ar closure age	Bogard et al. (1994)
14303	4312	7	felsic clast	mean Pb–Pb zircon age	Meyer et al. (1996) Nemchin et al. (2008)
	3830	30		Ar–Ar closure age	Shih et al. (1994)
14082	4216	14	felsic clast	mean Pb–Pb zircon age	Meyer et al. (1996)
14321	4031	74	felsic clast	K–Ca isochron	This chapter Shieh et al. (1994) Simon et al. (2011)
	4052	81		Rb–Sr isochron	This chapter Shieh et al. (1994) Simon et al. (2011)
	4110	200		Sm–Nd isochron	Shih et al. (1994)
	3990	48		mean Pb–Pb zircon age	Meyer et al. (1996)
	3880	*30*		Ar–Ar closure age	Shih et al. (1994)
15405	4276	77	felsic clast	mean Pb–Pb zircon age	Meyer et al. (1996)
72235	4230	83	felsic clast	mean Pb–Pb zircon age	Meyer et al. (1996)
Feature**	**Age (Ma)**	**2σ**	**Eruptive period (Ma)**	**Location**	**Reference**
Hansteen	3695	127	3700–3500	Southern margin of Oceanus Procellarum at 12.3° S, 309.8° E	Wagner et al. (2010); Boyce et al. (2017)
Gruithuisen	3785	184		Northeast border ofOceanus Procellarum at the highlands-mare boundary at 36.3° N, 319.8° E	Wagner et al. (2002)
Mariran Domes	3350	200	3750–3350	Northern Oceanus Procellarum at approximately 312.3°E, 41.4°N	Boyce et al. (2017)
Compton Belkovich Volcanic Complex	3600		3800–3500	Northern, far side of the Moon at 61.1°N 99.5°E	Shirley et al. (2016)
Lassell Massif	4010	170		Near the center of Alphonsus A basin in Mare Nubium at 14.65°S, 350.96°E	Ashley et al. (2016)

Notes: * Radioisotopic ages; **Crater size frequency distribution ages; Ages in italics are reset

5.2. Implications for the origin of silicic–felsic magmatism

5.2.1. Source components

The Diviner Lunar Radiometer Experiment (e.g., Glotch et al. 2010) expanded upon evidence obtained by the Lunar Prospector for widespread silicic lithologies on the Moon that are consistent with the compositions of rare, evolved rock clasts found in the Apollo sample collection (e.g., Warren et al. 1983; Jolliff 1991). These global geochemical surveys indicate that granites and other evolved lunar magmas are more common than previously recognized, and

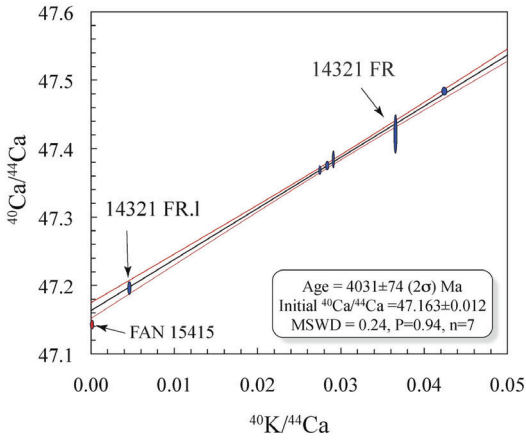

Figure 14. K–Ca internal isochron for lunar granitic clast 14321,1062. New data for feldspar-rich fragment (FR) and leachate (FR.1) results (Simon et al. 2011) are combined with two bulk rock fragments and three color-sorted mineral separates from Shih et al. (1993). The resultant isochron age and initial $^{40}Ca/^{44}Ca$ ratio are calculated using Isoplot (Ludwig 2003), which can be used to test petrogenetic models of lunar granite formation (see main text). The error envelope represents the 95% confidence interval of the regression that is 2× more precise than the previously reported age. The bulk measurement of ferroan anorthosite (FAN) 15415 is thought to be representative of primitive lunar highland rocks.

therefore more important to our understanding of lunar crust formation than previously believed. Traditional models of lunar silicic magma generation (e.g., silicate–liquid immiscibility—SLI) have unequivocally been confirmed by lunar samples (e.g., Neal and Taylor 1989a; Jolliff et al. 1999). However, it is difficult for these models to satisfactorily explain the widespread production of compositionally evolved lithologies or the volume of felsic magma likely needed (e.g., Petford 1996) to produce the silicic volcanic domes and flows that have been shown to exist on the lunar surface (cf. Hess et al. 1975; Hagerty et al. 2006).

The standard model for the generation of evolved magmas on the Moon is one in which they formed in large bodies of KREEP-rich magma undergoing SLI, leading to silicic-rich felsic and ferrobasaltic melts (e.g., Rutherford et al. 1976; Neal and Taylor 1989b; Jolliff et al. 1999). Gravity separation then produces shallow intrusive or volcanic eruptions of the low-density felsic magmas. After sufficient volumes of felsic magma have formed, it has been shown experimentally that it is possible to segregate the highly viscous melts from their source region (Petford 1996). The felsic melts are commonly less dense than their surroundings and therefore buoyant, leading to formation and ascension of silicic plumes and/or dikes (Maaløe and McBirney 1997). It is notable, however, that experimental and natural products of SLI show that U and Th, which are abundant in the lunar felsic samples and seen in the remote sensing data of silicic domes on the Moon (Glotch et al. 2011; Jolliff et al. 2011), are preferentially partitioned into the depolymerized ferrobasaltic magma (Rutherford et al. 1976; Neal and Taylor 1989a). In contrast, after extensive fractional crystallization or during low-degree melting of mafic source regions, incompatible trace elements will be partitioned into silicic melts, producing lithologies enriched in incompatible trace elements such as Th (e.g., Hess 1989; Singoi et al. 1994). Generally, U and Th are expected to partition into mafic melts during SLI (Neal and Taylor 1989b). Jolliff (1991) described Apollo 14 granitic material and monzogabbro that contain complementary concentrations of a range of incompatible trace elements including the REEs. These concentrations were consistent with formation of the monzogabbro as a pyroxene- and REE-merrillite-rich cumulate that lost a residual melt component, possibly as the assemblage was undergoing SLI. In that case, the residual melt would have been richer in Th than the denser cumulate and would have solidified to form granite.

If SLI is not the mechanism that generated the magmas forming the silicic lunar domes, then alternative processes become more viable, but require further testing. For example, if the evolved lunar magmas have formed by extensive fractional crystallization of mantle-derived magmas, then we would expect to find chemically intermediate fractionates commonly found on Earth (e.g., basaltic andesite, monzonite). It is notable that such missing intermediate rocks have been suggested by the K–Ca isotopic studies of Simon et al. (2011). In addition to the geochronology, the novel K–Ca isotope system can be used to determine the composition (i.e., K/Ca ratio) of the felsic rock studied and to estimate the K/Ca of its parental source reservoir (Fig. 15). The isochron approach is the most direct method for estimating the incompatible element (e.g., K) enrichments in the studied felsic materials. This can be accomplished by comparing the abundance of K estimated for the source (i.e., based on the *y*-intercept value defined by an isochron) (Fig. 15) to the abundance of K measured directly for the sample by the isotope dilution method. A similar approach can be applied for the Rb–Sr isotope system if it has not been disturbed. The degree of KREEP enrichment is of significant interest because it can be used to estimate the volatile abundances in the source reservoirs of the felsic rocks (e.g., McCubbin et al. 2010; Mills et al. 2017; Simon et al. 2020, and see below).

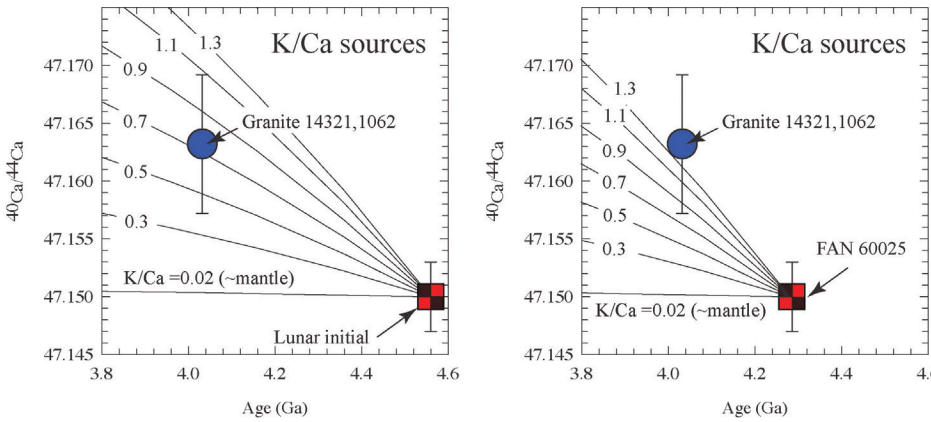

Figure 15. Plots of $^{40}Ca/^{44}Ca$ evolution against time: (left) Growth curves are shown for basaltic (K/Ca = 0.02), intermediate, and evolved (K/Ca ≥1) source materials. The initial $^{40}Ca/^{44}Ca$ composition of Apollo 14 granitoid clast 14321, 1062 when compared to primitive lunar crust (e.g., FAN 15415) indicates that it was derived from a relatively enriched source that has a K/Ca ratio (~0.7) that is equivalent to terrestrial andesite. (right) Growth curves are the same, but the new 4.360 Ma age for FAN 66025 is used (Borg et al. 2011). If this age is representative of FAN this requires that the source of granite 14321 was even more enriched (K/Ca ratio ~1.5) and/or probably not FAN.

5.2.2. Petrogenesis, melting and ascent

The small rocks and rock fragments of felsic lithologies found among the Apollo samples offer clues to their origins in igneous bodies—intrusive and extrusive—on the Moon. Owing to low lunar oxygen fugacity, igneous differentiation of lunar magmas typically leads to FeO enrichment, thus residual melts do not undergo significant SiO_2 enrichment. Instead, the FeO-enrichment commonly results in lunar residual melts undergoing some degree of SLI (e.g., Hess et al. 1975; Rutherford et al. 1976; Neal and Taylor 1989a,b). This phenomenon is observed in mare basalts as well as evolved alkali-suite rocks such as monzodiorite or monzogabbro (Jolliff 1991; Marvin et al. 1991; Jolliff et al. 1999). These observations led to the inference that perhaps SLI was involved in the segregation of felsic materials from more mafic parent melts such as KREEP basalt in the formation of lunar felsic rocks (Hess et al. 1975; Ryder 1976; Neal and Taylor 1989b).

Associated with some of the lunar granitic samples or assemblages are more mafic, possibly cogenetic or "complementary" assemblages known among the lunar samples as quartz monzodiorite or monzogabbro, e.g., samples 15403 and 15405 (Ryder 1976; Marvin et al. 1991; Meyer et al. 1996). These lithologies have FeO concentrations ranging from 9 to over 16 wt.% FeO, and low Mg′, ranging from 0.6 to 0.3. These lithologies are also highly evolved. Their occurrence together in breccias or among proximally located samples (Apollo 14, Apollo 15) suggests a possible petrogenetic relationship with granitic materials. Bulk major-element compositions support a petrologic relationship by SLI wherein the felsic assemblages represent the silicic fraction, and the mafic assemblages the FeO-rich fraction (e.g., Rutherford et al. 1976; Neal and Taylor 1989b; Jolliff 1991; Marvin et al. 1991).

It is not clear, however, that the detailed trace-element compositions of the granitic and possibly related mafic materials support a relationship via SLI. High-field-strength elements (HFSE) such as Ta and Th should be strongly partitioned into the mafic liquid (e.g., Gullikson 2016), yet these elements are most strongly enriched in the felsic rocks (Jolliff 1991). Intrusive sample 14161,7373, with coarse-grained, exsolved pyroxene and unmistakingly a product of SLI, solidified in a shallow intrusive setting (crustal, maybe within 1–2 km of the surface*;* Jolliff et al. 1999).There is nothing about the sample that requires or hints at a direct mantle origin. Therefore, an alternative model to consider is partial melting of pre-existing lunar crust (e.g., Hagerty et al. 2006). A major advantage of this model is that, based on terrestrial examples, it can overcome two of the major issues associated with the SLI model: voluminous melt production and Th enrichment in a silicic melt. Hagerty et al. (2006) proposed that partial melting of the lunar crust could be initiated as the result of basaltic underplating. Basaltic underplating on Earth occurs when hot basaltic magma intrudes country rock that is at an ambient crustal temperature (e.g., Bergantz 1989). Once extensive near-solidus partial melting of mafic crust has been initiated, relatively large amounts of silicic melt can be generated over geologically short timescales (10^2–10^3 years, cf. Simon et al. 2008, 2014) compared with other mechanisms for silicic melt generation (Petford and Gallagher 2001; Sisson et al. 2005). After a *voluminous* silicic melt is formed, it becomes rather straightforward to efficiently segregate the highly viscous melts from their source region (Petford 1996; Jónasson 2007). The silicic melts are positively buoyant, leading to formation of silicic plumes and/or dikes (Maaløe and McBirney 1997). During partial melting of mafic crust, incompatible trace elements such as Th are partitioned into silicic partial melts, producing extrusive lithologies and satisfying the Th-rich criterion that the SLI model cannot. Experiments indicate that silicic rocks can be produced from monzogabbro and alkali gabbronorite by partial melting at < 1000 °C (Gullickson et al. 2016).

A long-standing problem with any model of granitic melt collection and emplacement is the high viscosity of dry granitic melt and the difficulty of collecting and moving such melt a significant distance through the lunar crust. An implication is that silicic intrusive or volcanic materials likely formed not far from where they were ultimately emplaced, their emplacement was enabled by movement of melt along extensional fractures associated with impact basins, or their viscosity was lower as a result of a higher water content. Extended fractional crystallization to produce granitic derivatives is not indicated for iron-rich residual melts, and evidence for intermediate rocks between basalt/gabbro and rhyolite/granite is generally lacking, with the exception being the inference shown in Figure 15. An origin for melt bodies that could produce large volcanic constructs, such as the Gruithuisen domes, by SLI is difficult to imagine. Partial melting by basaltic underplating of a fertile source rock such as KREEP basalt appears to be the most plausible hypothesis at this time (Hagerty et al. 2006; Gullikson et al. 2016).

5.2.3. Potential role of volatiles in melting and eruption

The presence of volatiles can have a profound effect on the solidus temperatures and viscosities of igneous rocks (e.g., Johannes and Holtz 1996 and Dingwell et al. 1985,

respectively). Although the lack of hydrous silicate phases and hydrothermal alteration in lunar samples were used to suggest that the Moon is depleted in hydrogen (and other volatile elements), recent sample studies have reported measurable abundances of OH in apatite and nominally anhydrous phases (see McCubbin et al. 2023, this volume). On Earth, water and other volatile species of igneous rocks generally correlate with other incompatible elements like K, Rb, Th and U (e.g., Stolper and Newman 1994). Recent spectroscopic data from the Moon (Klima et al. 2013) support this trend, with a positive correlation between water and Th. However, there are relatively few published studies of volatile abundances in lunar felsic materials. Magmatic water estimates based on apatite measurements (Boyce et al. 2010; McCubbin et al. 2010; Barnes et al. 2014; Robinson and Taylor 2014), including lunar granite 14321,1028 (sub-sample 1047), range from as low as 0.001 to ~0.04 wt. % H_2O (Fig. 16). In contrast, measurements by Mills et al. (2017) of nominally anhydrous alkali feldspar in KREEP-rich granitoid clast 15405,78 implies magmatic water as high as 0.5–2 wt. % (Fig. 16) at the time of alkali feldspar crystallization. The latter work is notable because M^3 data for the Compton Belkovich region have been interpreted to indicate that the volcanic complex is possibly a location of OH^--bearing pyroclastic activity (Bhattacharya et al. 2013; Petro et al. 2013). Additionally, the inferred magmatic water contents based on OH^- in lunar apatite have recently been shown to be complicated by the co-dependent compatibilities of F, Cl, and OH^- (Boyce et al. 2014). Evolved magmas with high Cl/F can crystallize apatite that generally excludes OH^-, regardless of the water content of the magma (McCubbin et al. 2011; Boyce et al. 2014). To help resolve these discrepancies, further studies are required of OH^-/H_2O content in both apatite and feldspar in the same felsic clasts along with F and Cl measurements to address the issue of OH^- exclusion from apatite.

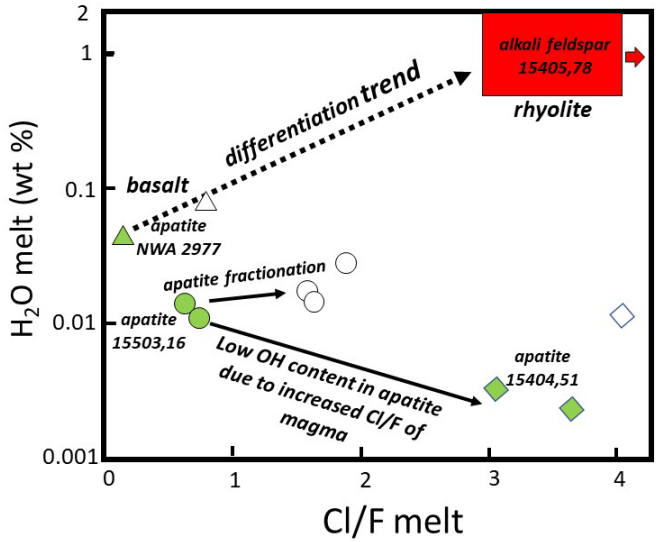

Figure 16. Plot of the estimated Cl/F ratio of magma versus estimated water content for lunar magmas (after Mills et al. 2017). Apatite data and their magmatic water estimates are from McCubbin et al. (2010), except for apatites from lunar granite 14321,1047 measured by Robinson and Taylor (2014). The calculated H_2O melt composition of older 15405,78 granitoid clast (Mills et al. 2017) appears much higher than apatite-based estimates for younger felsic lunar material.

6. THERMAL EVOLUTION OF THE MOON AND ITS BEARING ON LUNAR MAGMATISM

6.1. Introduction

As some of the unique features of lunar magmatic observations imply (long duration, near and far side dichotomy), the evolution of volcanic activity through space and time can be used as a strong constraint to numerical evolution models of the lunar interior. Here, we begin just after cumulate overturn (see Gaffney et al. 2023, this volume) and consider only implications linked to magmatism. However, numerical models of global evolution should also be considered in the context of magnetism (see Wieczorek et al. 2023, this volume) and interior structure (see Andrews-Hanna et al. 2023, this volume).

6.2. Long term evolution—post-magma ocean

There has been progress in characterization of maria ages, volumes and compositions, as well as in surface temperature and interior heat flow. The mantle bulk composition, and in particular the presence of water content is also a key uncertainty that has been highlighted from recent research.

Advances in secondary ion mass spectrometry during the last decade allowed for a re-analysis of Apollo samples. Saal et al. (2008) found unexpectedly high-water contents in Apollo 15 green and Apollo 17 orange volcanic glasses that may have originated from mantle sources with a minimum of 260 ppm water (95% confidence level). Assessment of how widespread this water content is an ongoing process, but regardless of the answer, it will have a large influence on thermal evolution models. Indeed, any water level is known to sharply reduce the viscosity of solids and would favor faster cooling of the mantle than currently believed. This could help explain a long-lasting, thermally-driven dynamo by increasing the core-mantle boundary heat flow for a long period of time (see Wieczorek et al. 2023, this volume), but would also make it harder to explain the long-lasting duration of mare volcanism. Indeed, if the mantle cools quickly, it would reach global subsolidus temperature faster.

One way to address these considerations is to have stronger constraints on mare depth of origin as a function of time. Elardo et al. (2014) performed high-temperature experiments over a range of pressures to constrain the petrogenesis of lunar magmas. It is interesting to note that, while some thermo-chemical evolution models of the mantle suggest a deeper source depth of mare basalts with time, the experiments presented in this study are consistent with magmas derived from a constant mantle depth range from ~4 to ~3 Ga. Similarly, some meteorites have a multiple saturation point at < 0.6 GPa at 3 Ga, which is in contradiction with the predicted thick lithosphere from thermo-chemical models at that time. In addition, the existence of samples with low Mg′ and lack of Eu anomaly suggests that at least part of the mantle did not experience the CMO mixing event or did not witness plagioclase removal during LMO crystallization, which could help constrain this early stage of lunar evolution (Elardo et al. 2014). However, these data must be carefully interpreted and incorporated into thermal models for the Moon as primary melts (melts in equilibrium with their mantle source) will provide the most useful information concerning the depths (multiple saturation) and chemistries of mantle sources.

In an effort to understand the evolution of mare basalt volcanism, Kato et al. (2017) studied the correlation between Ti content and eruption age of mare basalt. While the depth to Ti content correlation is unclear, there seems to be a distinct evolution with time. They found that the mare basalt production rate outside of the PKT region has a single peak at ~3.7 Ga, while including the PKT maria leads to the apparition of a second peak at ~2 Ga. That second peak is also linked to a sharp increase in average Ti content, suggesting a different magma source. These different mantle sources could be the result of incomplete overturning of an ilmenite-rich layer. The oldest maria would result from top down warming of the mantle by

part of the KREEP layer that remained in the upper mantle, while the later high-Ti maria would be the product of at least partial upwelling from the portion of the dense ilmenite layer that sunk around the core–mantle boundary. In general, these multi-dimensional constraints on volcanic activity should be integrated in thermo-chemical evolution models in order to discuss plausible evolution scenarios.

Finally, observations of the lunar surface by the Diviner instrument onboard the Lunar Reconnaissance Orbiter mission were able to place better constraints on mantle heat flow. Paige and Siegler (2016) used temperature measurements from permanently shadowed regions to calculate an upper limit on mantle heat flow at the polar regions. Here, the observed surface thermal emission is balanced directly by heat flow from the interior. Depending on assumptions about the properties of the crust, they estimated a mantle heat flow of 3–6 mW/m^2. This is consistent with a locally enriched mantle–crust column below the PKT region, where the Apollo 15 heat flow probe found relatively high heat flow (e.g., Siegler and Smrekar 2014 and references therein), while the remaining mantle and crust have much lower concentrations of heat sources. Such observations help constrain the distribution of heat sources among different lunar regions that serve as initial conditions for global evolution models.

6.3. Integrated mantle modeling

The KREEP-rich signature on the near side is key to understanding global lunar evolution, yet it remains uncertain whether it is the cause or consequence of early mare volcanism. Assuming the ilmenite-bearing cumulate layer reached the core mantle boundary during CMO, Zhang et al. (2013) used an Arrhenius law for viscosity, sampling a range of parameters consistent with Earth upper mantle material. They found that for the lower activation energy (100 kJ/mol), the layer becomes unstable in a few 100 m.y. and rises to the surface as a spherical harmonic degree-1 plume. As the activation energy increases, the upwelling becomes shorter and shorter wavelength, and the layer finally remains stable at 300 kJ/mol. This can change somewhat depending on the initial heat source budget or reference viscosity, but this work clearly showed the importance of rheology in drawing conclusions about the stability of the layer. A key feature of this model is that degree-1 upwelling would generate mare volcanism from ~3.9 Ga. This fits with the few 100 Myrs delay between start of the simulation and upwelling of the layer, but during that time the core is heating up, which may hinder magnetic field generation, which in turn is thought to explain the oldest magnetic field 4.2 Ga ago (see Wieczorek et al. 2023, this volume for more information). Using the new rheologic properties of an ilmenite-rich assemblage from Dygert et al. (2016, 2017), Zhang et al. (2017) re-analyzed this scenario. They found that the reduced viscosity and its increased temperature-dependence both act to suppress upwelling. The new set of models indicates that the layer is unlikely to become unstable over lunar history, and would therefore remain over the core-mantle boundary. Depending on the thickness of the layer, this may have implications for the seismically attenuating layer observed at the base of the lunar mantle (e.g., Harada et al. 2016). However, in itself this model can no longer explain the timing and duration of mare volcanism.

Starting from an entirely different perspective, Laneuville et al. (2013, 2018) studied the evolution of the Moon in the case where most of the primordial layer (enriched in ilmenite and radiogenic heat sources) is concentrated below the crust in the Procellarum KREEP Terrane. This scenario could arise from different processes such as degree-1 down welling (e.g., Parmentier et al. 2002) or asymmetric crystallization of the LMO (e.g., Loper and Werner 2002a,b). From this initial condition, the underlying mantle on the near side warms up with the maximum depth of melting increasing with time and the lithosphere remains thin in that same region (*cf.* Snyder et al. 2000). The time required to reach significant depths of partial melting matches first order timing constraints for mare volcanism. In addition, early cooling of the core predicts a direct onset of the thermally-driven dynamo, consistent with paleomagnetic field estimates. One caveat of this model is the predicted thermal anomaly of

the near side mantle. Such an anomaly will influence the gravity signal and topography, but also the temperature-dependent electrical conductivity (e.g., Grimm 2013). Therefore, it is not clear if such a large temperature anomaly in the present near side mantle is consistent with all observables, although it may hint at a lower heat budget below the near side crust. The new rheologic parameters for ilmenite may help reconcile both views by improving models of degree-1 down welling and quantifying the fraction reaching the core-mantle boundary vs. the fraction trapped in the lithosphere (e.g., Li et al. 2016; Zhao et al. 2019).

Following the recent development in the determination of the water concentration in the lunar mantle described above (Saal et al. 2008; Hauri et al. 2011), Evans et al. (2014) studied how that would influence global evolution, and in particular magnetic field generation. They found that addition of water in the lunar mantle (thus reducing its viscosity) would promote a higher rate of cooling and therefore a larger core mantle boundary heat flow, capable of sustaining a thermally driven dynamo beyond 3.56 Ga. They noted that even a modest water enrichment (~20 ppm) in a thin layer on top of the core–mantle boundary would be enough to enhance cooling of the core and sustain a thermal dynamo for longer than dry mantle models. An aspect not considered at this point is how water would influence mantle overturn. In addition, water would change the melting temperature of the mantle, which is usually assumed to be that of dry peridotite KLB-1 in numerical models.

A heat source usually neglected in these studies is impact heating. Impacts can influence evolution in two different ways: through direct addition of heat in the underlying mantle, and by increasing porosity and therefore reducing thermal conductivity of the crust. Rolf et al. (2017) first analyzed the influence of single impacts on mantle evolution and then constructed a sequence of events as expected from observations from the lunar surface. They found that while any single event has a limited influence on global evolution (temperature and heat flux anomalies are limited to ~100 m.y. following the impact), the widespread ejecta blanket, and superposed with the ejecta blankets from the many other events reduces the crustal thermal conductivity enough to have a lasting influence. In particular, they found that it delays cooling enough to favor a period of mantle warming, and therefore crustal expansion as suggested by recent observations of the lunar gravity field (Andrews-Hanna et al. 2013).

6.4. Thermal structure implications

Global evolution models predict the thermo-chemical structure of the Moon, which has an influence on numerous observations. Any single observable can be matched any number of ways, and recent models have shown that in order to constrain evolution scenarios, it is important to consider as many parameters as possible.

For instance, Miljković et al. (2013) found that the thermal anomaly predicted by Laneuville et al. (2013) would affect the thermal structure of the crust enough during the lunar evolution that it would change impact basin formation. The authors studied the differences between impacts on a cold versus hot crust, thought to be representative of the far and near sides, respectively. They found that, for a given set of impactor properties, the basin formed on a relatively hot crust would have up to twice the diameter as the same basin on the cooler far side hemisphere. This is key to understanding impact distribution, which is used in crater counting models. While the lunar near side is thought to have had a statistically larger number of large basins, this study showed that when corrected for the temperature effect, the near and far side distributions are statistically indistinguishable.

Another important implication of global evolution models is their influence on moment of inertia. Siegler et al. (2016) have shown that the formation of the low-density thermal anomaly below the Procellarum KREEP Terrane was large enough to alter the density structure of the Moon and change its moments of inertia. Depending on the assumed lithospheric strength and therefore the amplitude of any crustal uplift caused by the mantle expansion, the axis of rotation

of the Moon may have moved by as much as 10 degrees over lunar history. The rationale of that study was to investigate the origin of the peculiar distribution of polar hydrogen deposits. From orbiting neutron measurements, the polar deposits were found to be antipodal to each other and displaced equally from each pole along opposite longitude. Such a distribution could have been formed if the surface temperature conditions had shifted since volatile delivery on the Moon.

7. QUESTIONS AND FUTURE WORK

There are numerous issues that still need to be explored with regards to the petrogenesis of post-differentiation magmatism, which include (but are not limited to) the following.

- What is the thermal event that is recorded by the mare basalt source region, Mg-suite rocks, and the FANs? Does it represent the termination and closure of the LMO event, overturn of the LMO cumulate pile, or some other large thermal event (giant impact)?
- How is ancient volcanism (> 4000 Ma) related to the Mg-suite? Does the extrusive equivalent to the Mg-suite exist?
- Over the wide duration of KREEP magmatism, what sources are being melted?
- What is the duration of mantle melting and magmatism? Is it as young as 100 Ma as has been recently suggested? What mantle sources are being melted during the oldest stages of mare magmatism (4300 Ma) and the youngest stages of mare magmatism?
- How does lunar magmatism (and mantle sources) differ within and outside the PKT?
- What is the distribution of H-bearing species (and other volatiles) in the lunar mantle and what is their role in magmatism and volcanism?
- What is(are) the age(s) and origin(s) of the silicic complexes now known to exist on the lunar surface?
- What is the degree of silica enrichment associated with the various silicic occurrences? Clegg-Watkins et al. (2017) suggested that some of the volcanic complexes, e.g., the Compton-Belkovich volcanic complex, might include intermediate volcanics as well as late-stage granitic and felsic pyroclastic material.

Numerous sites are compelling candidates for future landed in-situ exploration and sample return that will address these questions. Desirable sites include volcanic and plutonic regions outside the PKT, ancient and young volcanics, large pyroclastic deposits, and silicic intrusive or extrusive materials. Future missions should also test, either in-situ or with sample return, the volatile contents of materials associated with the silicic volcanic complexes and pyroclastic deposits. A coordinated study to identify new lunar magmatic lithologies in Apollo, Luna, or meteorites using XCT imaging would be complimentary to sample return. Previously collected and new orbital data will provide additional insights. For example, low-FeO Mg-suite volcanic deposits (Mg-suite volcanics) may be detected similarly to cryptomaria (e.g., Prissel et al. 2016b), or as positive Bouguer anomalies in gravity and topography data (e.g., Jozwiak et al. 2017).

ACKNOWLEDGMENTS

Analysis of the materials studied herein would not have been possible without the Apollo era scientists, NASA engineers, and astronauts. NASA curation staff are thanked for their commitment to maintain the integrity of the samples and the skillful processing. The authors would like to thank reviewers for providing by edits and insightful additions to this chapter. CKS would like to acknowledge financial and logistical support for his participation in this initiative

through the NASA Lunar Data Analysis Program (grant#80NSSC19K1099), the Institute of Meteoritics at the University of New Mexico, and the Lunar and Planetary Institute. Additional input into the manuscript was provided by JJP and CJS. CRN was partially supported by NASA grants NNX16AR95G and NNX15AH76G. TDG acknowledges support from the Diviner Lunar Radiometer science team and the RISE2 node of NASA's Solar System Exploration Research Virtual Institute. LRG was partially supported by the NASA LDAP program (IAA #NNH17AE091). Brad Jolliff acknowledges support from the Lunar Reconnaissance Orbiter Measurement Investigation (NNG07EK00C) and from the McDonnell Center for the Space Sciences at Washington University. JS was partially supported by the NASA Planetary Science Division, specifically LASER and SSW Programs. TM contributed to the chapter with the support of the Strategic Research Plan of the Czech Geological Survey (DKRVO/CGS 2018-2022). Financial support for VAF through the Deutsche Forschungsgemeinschaft grant FE 1523/3-1 and via a Marie Skłodowska Curie Fellow, funded by the EU-Commission, HORIZON2020 Programme, project number 749815. Financial support for TCP from the Gordon McKay Fellowship with the Lunar and Planetary Institute. ML acknowledges funding by JSPS Grant-in-Aid for Young Scientist (grant 16K17790). Travel and logistics support for the initiative and workshops were provided by the Lunar and Planetary Institute and NASA. We would also like to thank former LPI directors Steve Mackwell and Louise Prockter for their constant and unwavering support of New Views of the Moon 2 initiative.

REFERENCES

Aeschlimann U, Eberhardt P, Geiss J, Grögler N, Kurtz J, Marti K (1982) On the age of cumulate norite 78236: an ^{39}Ar–^{40}Ar study. Lunar Planet Sci Conf 13:1001

Andrews-Hanna JC, Asmar SW, Head JW, Kiefer WS, Konopliv AS, Lemoine FG, Matsuyama I, Mazarico E, McGovern PJ, Melosh HJ, Neumann GA, Nimmo F, Phillips RJ, Smith DE, Solomon SC, Taylor GJ, Wieczorek MA, Williams JG, Zuber MT (2013) Ancient igneous intrusions and early expansion of the Moon revealed by GRAIL gravity gradiometry. Science 339:675–678

Andrews-Hanna JC, Weber RC, Garrick-Bethell I, Evans AJ, Kiefer WS, Grimm RE, Keane JT, Laneuville M, Ishihara Y, Kamata S, Matsuyama I (2023) The structure and evolution of the lunar interior. Rev Mineral Geochem 89:243–292

Ashley J, Robinson MS, Stopar JD, Glotch TD, Hawke BR, Bogert CH, Hiesinger H, Lawrence SJ, Jolliff BL, Greenhagen BT, Giguere TA, Paige DA (2016) The Lassell Massif—a silicic lunar volcano. Icarus 273:248–261

Barboni M, Boehnke P, Keller B (2017) Early formation of the Moon 4.51 billion years ago. Sci Adv 3:e1602365

Barnes JJ, Tartèse R, Anand M, McCubbin FM, Franchi IA, Starkey NA, Russell SS (2014) The origin of water in the primitive Moon as revealed by the lunar highlands samples. Earth Planet Sci Lett 390:244–252

Barr JA, Grove TL (2013) Experimental petrology of the Apollo 15 group A green glasses: Melting primordial lunar mantle and magma ocean cumulate assimilation Geochim Cosmochim Acta 106:216–230

Beard BL, Johnson CM (1999) High precision iron isotope measurements of terrestrial and lunar materials. Geochim Cosmochim Acta 63:1653–1660

Bellucci JJ, Nemchin AA, Grange M, Robinson KL, Collins G, Whitehouse MJ, Snape JF, Norman MD, Kring DA (2019) Terrestrial-like zircon in a clast from an Apollo 14 breccia. Earth Planet Sci Lett 510:173–185

Bennett KA, Horgan BHN, Gaddis LR, Greenhagen BT, Allen CC, Hayne PO, Bell III JF, Paige DA (2016) Complex explosive volcanic activity on the Moon Within Oppenheimer Crater. Icarus 273:296–314

Bergantz GW (1989) Underplating and partial melting: implications for melt generation and extraction. Science 245:1093–1095

Bhattacharya S, Saran S, Dagar A, Chauhan P, Chauhan M, Ajai, Krian Kumar AS (2013) Endogenic water on the Moon associated with non-mare silicic volcanism: implications for hydrated lunar interior. Current Sci 105:685–691

Blanchard DP, Budahn JR (1979) Remnants from the ancient crust: Clasts from Consortium breccia 73255. Proc Lunar Planet Sci Conf 10:803–816

Bogard DD, Nyquist LE, Bansal BM, Wiesmann H, Shih CY (1975) 76535: An old lunar rock. Earth Planet Sci Lett 26:69–80

Bogard DD, Garrison DH, Shih C-Y, Nyquist LE (1994) ^{39}Ar–^{40}Ar dating of two lunar granites: The age of Copernicus. Geochim Cosmochim Acta 58:3093–3100

Bonin B, Bebien J, Masson P (2002) Granite: a planetary point of view. Gondwana Res 5:261– 273

Bonnand P, Williams HM, Parkinson IJ, Wood BJ, Halliday AN (2016) Stable chromium isotopic composition of meteorites and metal–silicate experiments: Implications for fractionation during core formation. Earth Planet Sci Lett 435:14–21

Borg LE, Shearer CK, Asmerom Y, Papike JJ (2004) Prolonged KREEP magmatism on the Moon indicated by the youngest dated lunar igneous rock. Nature 432:209–211
Borg LE, Gaffney AM, Shearer CK, DePaolo DJ, Hutcheon ID, Owens TL, Ramon E, Brennecka G (2009) Mechanisms for incompatible-element enrichment on the Moon deduced from the lunar basaltic meteorite Northwest Africa 032. Geochim Cosmochim Acta 73:3963–3980
Borg LE, Connelly JN, Boyet M, Carlson RW (2011) Chronological evidence that the Moon is either young or did not have a global magma ocean. Nature 477:70–72
Borg LE, Gaffney AM, Shearer CK (2015) A review of lunar chronology revealing a preponderance of 4.34–4.37 Ga ages. Meteorit Planet Sci 50:715–732
Borg LE, Connely JN, Cassata WS, Gaffney AM, Bizzarro M (2017) Chronological implications for slow cooling of troctolite 76535 and temporal relationships between the Mg-suite and the ferroan anorthosite suite. Geochim Cosmochim Acta 201:377–391
Borg LE, Gaffney AM, Kruijer TS, Marks NA, Sio CK, Wimpenny J (2019) Isotopic evidence for a young lunar magma ocean. Earth Planet Sci Lett 523:115706
Boukaré C-E, Parmentier EM, Parman SW (2018) Timing of mantle overturn during magma ocean solidification. Earth Planet Sci Lett 491:216–225
Bourdon B, Tipper ET, Fitoussi C, Stracke A (2010) Chondritic Mg isotope composition of the Earth. Geochim Cosmochim Acta 74:5069–5083
Boyce JW, Liu Y, Rossman GR, Guan Y, Eiler JM, Stolper EM, Taylor LA (2010) Lunar apatite with terrestrial volatile abundances. Nature 466:466–469
Boyce JW, Tomlinson SM, McCubbin FM, Greenwood JP, Treiman AH (2014) The lunar apatite paradox. Science 344:400–402
Boyce JM, Giguere TA, Hawke BR, Mouginis-Mark PJ, Robinson MS, Lawrence SJ, Trang D, Clegg-Watkins RN (2017) Hansteen Mons: An LROC geological perspective. Icarus 283:254–267
Boyce JM, Giguere T, Mouginis-Mark P, Glotch T, Taylor GJ (2018) Geology of the Mairan middle dome: Implications for silicic volcanism on the Moon. Planet Space Sci 162:62–72
Boyet M, Carlson RW (2007) A highly depleted moon or a non-magma ocean origin for the lunar crust? Earth Planet Sci Lett 262:505–516
Boyet M, Carlson RW, Borg LE, Horan M (2015) Sm–Nd systematics of lunar ferroan anorthositic suite rocks: Constraints on lunar crust formation. Geochim Cosmochim Acta 148:203–218
Braden SE, Stopar JD, Robinson MS, Lawrence SJ, Bogert CH, Hiesinger H (2014) Evidence for basaltic volcanism on the Moon within the past 100 million years. Nat Geosci 7:787–791
Brandon AD, Lapen TJ, Debaille V, Beard BL, Rankenburg K, Neal CR (2009) Re-evaluating $^{142}Nd/^{144}Nd$ in lunar mare basalts with implications for the early evolution and bulk Sm/Nd of the Moon. Geochim Cosmochim Acta 73:6421–6445
Brown SM, Grove TL (2015) Origin of the Apollo 14, 15, and 17 yellow ultramafic glasses by mixing of deep cumulate remelts. Geochim Cosmochim Acta 171:201–215
Burnham CW (1975) Water and magmas; a mixing model. Geochim Cosmochim Acta 39:1077–1084
BVSP (Basaltic Volcanism Study Project) (1981) Basaltic Volcanism on the Terrestrial Planets. Pergamon Press, Inc., New York
Cahill JTS, Lucey PG, Wieczorek MA (2009) Compositional variations of the lunar crust: Results from radiative transfer modeling of central peak spectra. J Geophys Res Planets 114:E09001
Canup RM, Righter K, Dauphas N, Pahlevan K, Ćuk M, Lock SJ, Stewart ST, Salmon J, Rufu R, Nakajima M, Magna T (2023) Origin of the Moon. Rev Mineral Geochem 89:53–102
Carlson RW, Lugmair G (1979) Sm–Nd constraints on early lunar differentiation and the evolution of KREEP. Earth Planet Sci Lett 45:123–132
Carlson RW, Lugmair GW (1981a) Time and duration of lunar highlands crust formation Earth Planet Sci Lett 52:227–238
Carlson RW, Lugmair GW (1981b) Sm–Nd age of lherzolite 67667: implications for the processes involved in lunar crustal formation. Earth Planet Sci Lett 56:1–8
Carlson RW, Borg LE, Gaffney AM, Boyet M (2014) Rb–Sr, Sm–Nd and Lu–Hf isotope systematics of the lunar Mg-suite: the age of the lunar crust and its relation to the time of Moon formation. Phil Trans R Soc Ser A 372:20130246
Chakrabarti R, Jacobsen SB (2010) The isotopic composition of magnesium in the inner Solar System. Earth Planet Sci Lett 293:349–358
Charlier B, Grove TL, Namur O, Holtz F (2018) Crystallization of the lunar magma ocean and the primordial mantle–crust differentiation of the Moon. Geochim Cosmochim Acta 234:50–69
Cheek LC, Pieters CM (2014) Reflectance spectroscopy of plagioclase-dominated mineral mixtures: Implications for characterizing lunar anorthosites remotely. Am Mineral 99:1871–1892
Chevrel SD, Pinet PC, Head III JW (1999) Gruithuisen domes region: A candidate for an extended nonmare volcanism unit on the Moon. J Geophys Res 104:16515–16529
Clayton RN, Mayeda TK (1996) Oxygen isotope studies of achondrites. Geochim Cosmochim Acta 60:1999–2017
Clegg-Watkins RN, Jolliff BL, Watkins MJ, Coman E, Giguere TA, Stopar JD, Lawrence SJ (2017) Nonmare volcanism on the Moon: Photometric evidence for the presence of evolved silicic materials. Icarus 285:169–184

Compston W, Foster JJ, Gray CM (1975) Rb–Sr ages of clasts from within Boulder 1, Station 2, Apollo 17. The Moon 14:445–462
Compston W, Foster JJ, Gray CM (1977) Rb–Sr systematics in clasts and aphanites from consortium breccia 73215. Proc Lunar Sci Conf 8:2525–2549
Compston W, Williams IS,Meyer C (1984) Age and chemistry of zircon from late-stage lunar differentiates. Lunar Planet Sci Conf 15:182–183
Coombs CR, Hawke BR, Lucey PG, Owensby PD, Zisk SH (1990) The Alphonsus region: A geologic and remote sensing perspective. Proc Lunar Planet Sci Conf 20:339–353
Crawford IA, Anand M, Barber S, Cowley A, Crites S, Fa W, Flahaut J, Gaddis LR, Greenhagen B, Haruyama J, Hurley D, McLeod CL, Morse A, Neal CR, Sargeant H, Sefton-Nash E, Tartèse R (2023) Lunar resources. Rev Mineral Geochem 89:829–868
Cronberger K, Neal CR (2017) KREEP basalt petrogenesis: Insights from 15434,181. Meteorit Planet Sci 52:827–841
Cronberger K, Neal CR (2018) Origin(s) and evolution of KREEP basalts. Lunar Planet Sci Conf 49:1305
Cronberger K, Neal CR (2019a) KREEP basalt petrogenesis. Lunar Planet Sci Conf 50:2453
Cronberger K, Neal CR (2019b) KREEP basalt 15382: not as pristine as originally thought. Lunar Planet Sci Conf:2444
Crow CA, McKeegan KD, Moser DE (2017) Coordinated U–Pb geochronology, trace element, Ti-in-zircon thermometry and microstructural analysis of Apollo zircons. Geochim Cosmochim Acta 202:264–284
Curran NM, Joy KH, Snape JF, Pernet-Fisher JF, Gilmour JD, Nemchin AA, Whitehouse MJ, Burgess R (2019) The early geological history of the Moon inferred from ancient lunar meteorite Miller Range 13317. Meteorit Planet Sci 54:1401–1430
Dasch E, Shih C, Bansal B, Wiesmann H, Nyquist L (1987) Isotopic analysis of basaltic fragments from lunar breccia 14321: Chronology and petrogenesis of pre-Imbrium mare volcanism. Geochim Cosmochim Acta 51:3241–3254
Day JMD, Moynier F (2014) Evaporative fractionation of volatile stable isotopes and their bearing on the origin of the Moon. Phil Trans R Soc Ser A 372:20130259
Day JMD, Brandon AD, Walker RJ (2016a) Highly siderophile elements in Earth, Mars, the Moon, and asteroids. Rev Mineral Geochem 81:161–238
Day JMD, Qiu L, Ash RD, McDonough WF, Teng FZ, Rudnick RL, Taylor LA (2016b) Evidence for high-temperature fractionation of lithium isotopes during differentiation of the Moon. Meteorit Planet Sci 51:1046–1062
Delano JW (1986) Pristine lunar glasses: Criteria, Data, and Implications. Proc Lunar Planet Sci Conf 16. J Geophys Res Solid Earth 91:D201–D213
Delano JW (1990) Pristine mare glasses and mare basalts: Evidence for a general dichotomy of source regions. *In:* Workshop on Lunar Volcanic Glasses: Scientific and Resource Potential. JW Delano and Gl. Heiken (eds). LPI Tech Rept 90–02, Lunar and Planet Inst, Houston, TX, p 30–31
Dhaliwal JK, Day JMD, Moynier F (2018) Volatile element loss during planetary magma ocean phases. Icarus 300:249–260
Dingwell DB, Scarfe CM, Cronin DJ (1985) The effect of fluorine on viscosities in the system Na_2O–Al_2O_3–SiO_2: implications for phonolites, trachytes and rhyolites. Am Mineral 70:80–87
Dowty S, Keil K, Prinz M, Gros J, Takahashi H (1976) Meteorite-free Apollo 15 crystalline KREEP. Proc Lunar Sci Conf 7:1833–1844
Duke MB, Gaddis LR, Taylor GJ, Schmitt HH (2006) Development of the Moon. Rev Mineral Geochem 60:597–656
Dygert N, Hirth G, Liang Y (2016) A flow law for ilmenite in dislocation creep: Implications for lunar cumulate mantle overturn. Geophys Res Lett 43:532–540
Dygert N, Lin JF, Marshall EW, Kono Y, Gardner JE (2017) A low viscosity lunar magma ocean forms a sratified anorthitic flotation crust with mafic poor and rich units. Geophys Res Lett 44:11282–11291
Dymek RF (1986) Characterization of the Apollo 15 feldspathic basalt suite. *In:* Geology and Petrology of the Apollo 15 Landing Site
Edmunson JE (2007) Evolution of the early lunar crust: Chronology studies of magnesium-suite samples 78238 and 76335. PhD Thesis. The University of New Mexico
Edmunson J, Borg LE, Nyquist LE, Asmerom Y (2009) A combined Sm–Nd, Rb–Sr, and U–Pb isotopic study of Mg-suite norite 78238: further evidence for early differentiation of the Moon. Geochim Cosmochim Acta 73:514–527
Elardo SM, Draper DS, Shearer CK (2011) Lunar Magma Ocean crystallization revisited: Bulk composition, early cumulate mineralogy, and the source regions of the highlands Mg-suite. Geochim Cosmochim Acta 75:3024–3045
Elardo SM, McCubbin FM, Shearer CK (2012) Chromite symplectites in Mg-suite troctolite 76535 as evidence for infiltration metasomatism of a lunar layered intrusion. Geochim Cosmochim Acta 87:154–177
Elardo SM, Shearer CK, Fagan AL, Borg LE, Gaffney AM, Burger PV, Neal CR, Fernandes VA, McCubbin FM (2014) The origin of young mare basalts inferred from lunar meteorites Northwest Africa 4734, 032, and LaPaz Icefield 02205. Meteorit Planet Sci 49:261–291
Elardo SM, Shearer CK, McCubbin FM (2017) The role of KREEP in the production of Mg-suite magmas and its influence on the extent of Mg-suite magmatism in the lunar crust. Lunar Planet Sci Conf 48:2450

Elardo SM, Pieters CM, Dhingra D, Donaldson Hanna KL, Glotch TD, Greenhagen BT, Gross J, Head JW, Jolliff BL, Klima RL, Magna T, McCubbin FM, Ohtake M (2023) The evolution of the lunar crust. Rev Mineral Geochem 89:293–338

Elkins-Tanton LT, Grove TL (2011) Water (hydrogen) in the lunar mantle: Results from petrology and magma ocean modeling. Earth Planet Sci Lett 307:173–179

Elkins-Tanton LT, Burgess S, Yin QZ (2011) The lunar magma ocean: Reconciling the solidification process with lunar petrology and geochronology. Earth Planet Sci Lett 304:326–336

Evans AJ, Zuber MT, Weiss BP, Tikoo SM (2014) A wet, heterogeneous lunar interior: Lower mantle and core dynamo evolution. J Geophys Res Planets 119:1061–1077

Fitoussi C, Bourdon B (2012) Silicon isotope evidence against an enstatite chondrite Earth. Science 335:1477–1480

Fogel RA, Rutherford MJ (1995) Magmatic volatiles in primitive lunar glasses, I: FTIR and EPMA analyses of Apollo 15 green and yellow glasses and revision of the volatile-assisted fire fountain theory: Geochim Cosmochim Acta 59:201–215

Gaddis LR, Hawke BR, Robinson MS, Coombs C (2000) Compositional analyses of small lunar pyroclastic deposits using Clementine multispectral data, J Geophys Res 105:4245–4262

Gaddis LR, Staid MI, Tyburczy JA, Hawke BR, Petro N (2003) Compositions of lunar pyroclastic deposits. Icarus 161:262–280

Gaddis LR, Horgan B, McBride M, Bennett K, Stopar J, Gustafson JO (2016) Alphonsus crater: Compositional clues to eruption styles of lunar small volcanoes. Lunar Planet Sci Conf 47:2065

Gaffney AM, Borg LE (2013) A young age for KREEP formation determined from Lu–Hf isotope systematics of KREEP basalts and Mg-suite samples. Lunar Planet Sci Conf 44:1714

Gaffney AM, Borg LE (2014) A young solidification age for the lunar magma ocean. Geochim Cosmochim Acta 140:227–240

Gaffney AM, Borg LE, Asmerom Y (2007) The origin of geochemical diversity of lunar mantle sources inferred from the combined U–Pb, Rb–Sr, and Sm–Nd isotope systematics of mare basalt 10017. Geochim Cosmochim Acta 71:3656–3671

Gaffney AM, Borg LE, Shearer CK, Burger PV (2015) Chronology of 15445 morite clast B and implications for Mg-suite magmatism. Lunar Planet Sci Conf 46:1443

Gaffney AM, Gross J, Borg LE, Donaldson Hanna KL, Draper DS, Dygert N, Elkins-Tanton LT, Prissel KB, Prissel TB, Steenstra ES, van Westrenen W (2023) Magmatic evolution I: Initial differentiation of the Moon. Rev Mineral Geochem 89:103–145

Glotch TD, Lucey PG, Bandfield JL, Greenhagen BT, Thomas IR, Elphic RC, Bowles NE, Wyatt MB, Allen CC, Donaldson-Hanna KL, Paige DA (2010) Identification of highly silicic features on the Moon. Science 329:1510–1513

Glotch TD, Hagerty JJ, Lucey PG, Hawke BR, Giguere TA, Arnold JA, Williams J, Jolliff BL, Paige DA (2011) The Mairan domes: Silicic volcanic constructs on the Moon. Geophys Res Lett 38:L21204

Glotch TD, Shirley KA, Greenhagen BT (2017) Simulated lunar environment spectra of felsic rock particulates. Lunar Planet Sci Conf 48:1688

Grange ML, Nemchin AA, Timms N, Pidgeon RT, Meyer C (2011) Complex magmatic and impact history prior to 4.1 Ga recorded in zircon from Apollo 17 South Massif aphanitic breccia 73235. Geochim Cosmochim Acta 75:2213–2232

Grange ML, Pidgeon RT, Nemchin AA, Timms NE, Meyer C (2013) Interpreting U–Pb data from primary and secondary features in lunar zircon. Geochim Cosmochim Acta 101:112–132

Greber ND, Dauphas N, Puchtel IS, Hofmann BA, Arndt NT (2017) Titanium stable isotopic variations in chondrites, achondrites and lunar rocks. Geochim Cosmochim Acta 213:534–552

Grimm RE (2013) Geophysical constraints on the lunar Procellarum KREEP Terrane. J Geophys Res 118:768–777

Gross J, Treiman AH (2011) Unique spinel-rich lithology in lunar meteorite ALHA 81005: Origin and possible connection to M3 observations of the farside highlands. J Geophys Res Planets 116:E10009

Gross J, Treiman AH, Mercer CN (2014) Lunar feldspathic meteorites: Constraints in the geology of the lunar highlands, and the orgin of the luar crust. Earth Planet Sci Lett 388:318–328

Gross J, Hilton A, Prissel TC, Setera JB, Korotev RL, Calzada-Diaz A (2020) Geochemistry and Petrogenesis of Northwest Africa 10401: A New Type of the Mg-Suite Rocks. J Geophys Res Planets 125:E2019JE006225

Grove TL, Krawczynski MJ (2009) Lunar mare volcanism: Where did the magmas come from? Elements 5:29–34

Gullikson AL, Hagerty JJ, Reid MR, Rapp JF, Draper DS (2016) Silicic lunar volcanism: Testing the crustal melting model. Am Mineral 101:2312–2321

Gustafson JO, Bell JF, III, Gaddis LR, Hawke BR, Giguere TA, and the LROC Science Team (2012) A search for potential newly discovered lunar pyroclastic deposits with LROC Data. J Geophys Res 117:E00H25

Hagerty JJ, Lawrence DJ, Hawke BR, Vaniman DT, Elphic RC, Feldman WC (2006) Refined thorium abundances for lunar red spots: Implications for evolved, nonmare volcanism on the Moon. J Geophys Res 111:E06002

Hagerty JJ, Lawrence DJ, Hawke BR, Gaddis LR (2009) Thorium abundances on the Aristarchus plateau: Insights into the composition of the Aristarchus pyroclastic glass deposits. J Geophys Res 114:E04002

Halliday AN, Lee DC, Christensen JN, Rehkämper M, Yi W, Luo X, Hall CM, Ballentine CJ, Pettke T, Stirling CH (1998) Applications of multiple collector-ICPMS to cosmochemistry, geochemistry and paleoceanography. Geochim Cosmochim Acta 62:919–940
Hallis LJ, Anand M, Greenwood RC, Miller MF, Franchi IA, Russell SS (2010) The oxygen isotope composition, petrology and geochemistry of mare basalts: Evidence for large-scale compositional variation in the lunar mantle. Geochim Cosmochim Acta 74:6885–6899
Haloda J, Tycová P, Korotev RL, Fernandes VA, Burgess R, Thöni M, Jelenc M, Jakes P, Gabzdyl P, Kosler J (2009) Petrology, geochemistry, and age of low-Ti mare-basalt meteorite Northeast Africa 003-A: A possible member of the Apollo 15 mare basaltic suite. Geochim Cosmochim Acta 73:3450–3470
Harada Y, Goossens S, Matsumoto K, Yan J, Ping J, Noda H, Haruyama J (2016) The deep lunar interior with a low-viscosity zone: Revised constraints from recent geodetic parameters on the tidal response of the Moon. Icarus 276:96–101
Hauri EH, Weinreich T, Saal AE, Rutherford MC, Van Orman JA (2011) High pre-eruptive water contents preserved in lunar melt inclusions. Science 333:213–215
Hawke BR, Coombs CR, Gaddis LR, Lucey PG, Owensby PD (1989) Remote sensing and geologic studies of localized dark mantle deposits on the Moon, Proc Lunar Planet Sci Conf 19:255–268
Head JW (1974) Orientale multi-ringed basin interior and implications for the petrogenesis of lunar highland samples. The Moon 11:327–356
Head III JW, Coffin MF (1997) Large igneous provinces: a planetary perspective. Geophys Monogr Am Geophys Union 100:411–438
Head III JW, Hess PC (1978) Geologic characteristics of lunar highland volcanic domes (Gruithuisen and Mairan region and possible eruption conditions. Proc Lunar Planet Sci Conf 9:488–490
Head III JW, Wilson L (1992) Lunar mare volcanism: Stratigraphy, eruption conditions, and the evolution of secondary crusts. Geochim Cosmochim Acta 56:2155–2175
Head III JW, Wilson L, Hiesinger H, van der Bogert C, Chen Y, Dickson JL, Gaddis LR, Haruyama J, Jawin ER, Jozwiak LM, Li C, Liu J, Morota T, Needham DH, Ostrach LR, Pieters CM, Prissel TC, Qian Y, Qiao L, Rutherford MR, Scott DR, Whitten JL, Xiao L, Zhang F, Ziyuan O (2023) Lunar mare basaltic volcanism: Volcanic features and emplacement processes. Rev Mineral Geochem 89:453–507
Helmke PA, Blanchard DP, Haskin LA, Telander K, Weiss C, Jacobs JW (1973) Major and trace elements in igneous rocks from Apollo 15. The Moon 8:129–148
Herwartz D, Pack A, Friedrichs B, Bischoff A (2014) Identification of the giant impactor Theia in lunar rocks. Science 344:1146–1150
Herzog GF, Moynier F, Albarède F, Berezhnoy AA (2009) Isotopic and elemental abundances of copper and zinc in lunar samples, Zagami, Pele's hairs, and a terrestrial basalt. Geochim Cosmochim Acta 73:5884–5904
Hess PC (1989) Origin of Igneous Rocks, Harvard Univ Press, Cambridge, Mass
Hess PC (1994) Petrogenesis of lunar troctolites. J Geophys Res Planets 99:19083–19093
Hess PC (2000) On the source regions for mare picrite glasses. J Geophys Res Planets 105:4347–4360
Hess PC, Rutherford MJ, Guillemette RN, Ryerson FJ, Tuchfeld HA (1975) Residual products of fractional crystallization of lunar magmas: An experimental study. Proc Lunar Sci Conf 6:895–910
Hiesinger H, Head III JW, Wolf U, Jaumann R, Neukum G (2003) Ages and stratigraphy of mare basalts in Oceanus Procellarum, Mare Nubium, Mare Cogitum, and Mare Insularum. J Geophys Res 108:5065
Hiesinger H, Head III JW, Wolf U, Jaumann R, Neukum G (2011) Ages and stratigraphy of lunar mare basalts: A synthesis. Geol Soc Am Spec Pap 477:1–51
Hiesinger H, van der Bogert CH, Michael G, Schmedemann N, Iqbal W, Robbins SJ, Ivanov B, Williams J-P, Zanetti M, Plescia J, Ostrach LR, Head III JW (2023) The lunar cratering chronology. Rev Mineral Geochem 89:401–451
Hinthorne JR, Conrad RL, Andersen CA (1975) Lead–lead and trace element abundances in lunar troctolite, 76535. Lunar Sci Conf VI:373–375
Hirschmann MM (2012) Magma ocean influence on early atmosphere mass and composition. Earth Planet Sci Lett 341:48–57
Hopkins SS, Prytulak J, Barling J, Russell SS, Coles BJ, Halliday AN (2019) The vanadium isotopic composition of lunar basalts. Earth Planet Sci Lett 511:12–24
Horgan BH, Cloutis EA, Mann P, Bell III JF (2014) Near-infrared spectra of ferrous mineral mixtures and methods for their identification in planetary surface spectra. Icarus 234:132–154
Horgan BH, Bennett KA, Gaddis LR, Greenhagen BT, Allen C, Hayne PO, Bell III JF, Paige DA (2015) Complex explosive volcanic activity on the Moon in Oppenheimer Crater. AGU Fall Meeting Abstracts:#P31H-03
Hubbard NJ, Gast PW (1971) Chemical composition and origin of nonmare lunar basalts. Proc Lunar Sci Conf 2:999–1020
Hubbard NJ, Rhodes JM, Gast PW, Bansal BM, Shih C-Y, Wiesmann H, Nyquist LE (1973) Lunar rock types: The role of plagioclase in non-mare and highland rock types. Proc Lunar Sci Conf 4:1297–1312
Hubbard NJ, Rhodes JM, Wiesmann H, Shih CY, Bansal BM (1974) The chemical definition and interpretation of rock types returned from the non-mare regions of the Moon. Proc Lunar Sci Conf 5:1227–1246
Hui H, Neal CR, Shih C-Y, Nyquist LE (2013) Petrogenetic association of the oldest lunar basalts: Combined Rb–Sr isotopic and trace element constraints. Earth Planet Sci Lett 373:150–159

Humayun M, Clayton RN (1995) Precise determination of the isotopic composition of potassium: Application to terrestrial rocks and lunar soils. Geochim Cosmochim Acta 59:2115–2130
Huneke JC, Wasserburg GJ (1975) Trapped ^{40}Ar in troctolie 76535 and evidence for enhanced ^{40}Ar–^{39}Ar age plateaus. Lunar Sci Conf 6:417–419
Hurwitz DM, Kring DA (2014) Differentiation of the South Pole–Aitken basin impact melt sheet: Implications for lunar exploration. J Geophys Res Planets 119:1110–1133
Husain L, Schaeffer OA(1975) Lunar evolution: The first 600 million years. Geophys Res Lett 2:29–32
Isaacson PJ, Pieters CM, Besse S, Clark RN, Head III JW, Klima RL, Mustard JF, Petro NE, Staid MI, Sunshine JM, Taylor LA, Thaisen KM, Tompkins S (2011) Remote compositional analysis of lunar olivine-rich lithologies with Moon Mineralogy Mapper (M3) spectra. J Geophys Res Planets 116:E00G11
Ivanov MA, Head III JW, Bystrov A (2016) The lunar Gruithuisen silicic extrusive domes: Topographic configuration, morphology, ages, and internal structure. Icarus 273:262–283
Jessberger EK, Kirsten T, Staudacher T (1977) One rock and many ages—Further K–Ar data on consortium breccia 73215. Proc Lunar Sci Conf 8:2567–2580
Johannes W, Holtz F (1996) Petrogenesis and Experimental Petrology of Granitic Rocks. Springer, Berlin
Jolliff BL (1991) Fragments of quartz monzodiorite and felsite in Apollo 14 soil particles. Proc Lunar Planet Sci Conf 21:101–118
Jolliff BL, Floss C, McCallum IS, Schwartz JM (1999) Geochemistry, petrology, and cooling history of 14161,7373: A plutonic lunar sample with textural evidence of granitic-fraction separation by silicate-liquid immiscibility. Am Mineral 84:821–837
Jolliff BL, Gillis JJ, Haskin L, Korotev RL, Wieczorek MA (2000) Major lunar crustal terranes: Surface expressions and crust-mantle origins. J Geophys Res 105:4197–4216
Jolliff BL, Wieczorek MA, Shearer CK, Neal CR (eds) (2006) New Views of the Moon. Reviews in Mineralogy and Geochemistry vol. 60. Mineralogical Society of America
Jolliff BL, Wiseman SA, Lawrence SJ, Tran TN, Robinson MS, Sato H, Hawke BR, Scholten F, Oberst J, Hiesinger H, Bogert CHvd, Greenhagen BT, Glotch TD, Paige DA (2011) Non-mare silicic volcanism on the lunar far side at Compton-Belkovich. Nat Geosci 4:566–571
Jónasson K (2007) Silicic volcanism in Iceland: Composition and distribution within the active volcanic zones. J Geodyn 43:101–117
Joy KH, Arai T (2013) Lunar meteorites: new insights into the geological history of the Moon. Astron Geophys 54:4.28–4.32
Joy KH, Gross J, Korotev RL, Zeigler RA, McCubbin FM, Snape JF, Curran NM, Pernet-Fisher JF, Arai T (2023) Lunar meteorites. Rev Mineral Geochem 89:509-562
Jozwiak LM, Head III JW, Neumann GA, Wilson L (2017) Observational constraints on the identification of shallow lunar magmatism: Insights from floor-fractured craters. Icarus 283:224–231
Kato C, Moynier F (2017) Gallium isotopic evidence for extensive volatile loss from the Moon during its formation. Sci Adv 3:e1700571
Kato C, Moynier F, Valdes MC, Dhaliwal JK, Day JMD (2015) Extensive volatile loss during formation and differentiation of the Moon. Nat Commun 6:7617
Kato S, Morota T, Yamaguchi Y, Watanabe SI, Otake H, Ohtake M (2017) Magma source transition of lunar mare volcanism at 2.3 Ga. Meteorit Planet Sci 52:1899–1915
Kesson SE, Ringwood AE (1976) Mare basalt petrogenesis on a dynamic Moon. Earth Planet Sci Lett 30:155–163
Kleine T, Touboul M, Bourdon B, Nimmo F, Mezger K, Palme H, Jacobsen SB, Yin QZ, Halliday AN (2009) Hf–W chronology of the accretion and early evolution of asteroids and terrestrial planets. Geochim Cosmochim Acta 73:5150–5188
Klima RL, Pieters CM, Boardman JW, Green RO, Head III JW, Isaacson PJ, Mustard JF, Nettles JW, Petro NE, Staid MI, Sunshine JM, Taylor LA, Tompkins S (2011) New insights into lunar petrology: Distribution and composition of prominent low-Ca pyroxene exposures as observed by the Moon Mineralogy Mapper (M3) J Geophys Res Planets 116:E00G06
Klima RL, Cahill J, Hagerty J, Lawrence D (2013) Remote detection of magmatic water in Bullialdus Crater on the Moon. Nat Geosci 6:737–741
Korotev RL, Zeigler RA, Jolliff BL, Irving AJ, Bunch TE (2009) Compositional and lithological diversity among brecciated lunar meteorites of intermediate iron concentration. Meteorit Planet Sci 44:1287–1322
Kramer GY, Jolliff BL, Neal CR (2008a) Distinguishing HA Mare Basalts Using Clementine UVVIS and Lunar Prospector GRS Data: Mare Moscoviense and Mare Nectrais. J Geophys Res 113:E01002
Kramer GY, Jolliff BL, Neal CR (2008b) Searching for high-aluminamarebasalts using Clementine UVVIS and Lunar Prospector GRS data: Mare Fecunditatis and Mare Imbrium. Icarus 198:7–18
Kramer GY, Kring DA, Nahm AL, Pieters CM (2013) Spectral and photogeologic mapping of Schrödinger Basin and implications for post-South Pole-Aitken impact deep subsurface stratigraphy. Icarus 223:131–148
Krawczynski MJ, Grove TL (2012) Experimental investigation of the influence of oxygen fugacity on the source depths for high titanium lunar ultramafic magmas. Geochim Cosmochim Acta 79:1–19
Kruijer TS, Kleine T (2017) Tungsten isotopes and the origin of the Moon. Earth Planet Sci Lett 475:15–24

Laneuville M, Wieczorek MA, Breuer D, Tosi N (2013) Asymmetric thermal evolution of the Moon. J Geophys Res Planets 118:1435–1452
Laneuville M, Taylor J, Wieczorek M (2018) Distribution of radioactive heat sources and thermal history of the Moon. J Geophys Res:Planets 123:3144–3166
Laul JC, Wakita H, Showalter DL, Boynton WV, Schmitt RA (1972) Bulk, rare earth, and other trace elements in Apollo 14 and 15 and Luna 16 samples. Proc Lunar Sci Conf 3:1181–1200
Lawrence DJ, Feldman WC, Barraclough BL, Binder AB, Elphic RC, Maurice S, Miller MC, Prettyman TH (2000) Thorium abundances on the lunar surface. J Geophys Res 105:20307–20331
Lawrence DJ, Elphic RC, Feldman WC, Prettyman T, Gasnault O, Maurice S (2003) Small-area thorium features on the lunar surface. J Geophys Res 108:5102
Lawrence DJ, Puetter RC, Elphic RC, Feldman WC, Hagerty JJ, Prettyman TH, Spudis PD (2007) Global spatial deconvolution of Lunar Prospector Th abundances. Geophys Res Lett 34:L03201
Leich DA, Kohl SB, Kirschbaum AR, Niemeyer S, Phinney D (1975) Rare gas constraints on the history of Boulder l, Station 2, Apollo 17. The Moon 14:407–444
Li H, Zhang N, Huang J, Dygert N (2016) Revisit the lunar overturn model with the ilmenite rheology experiment results. AGU Fall Meeting:#DI33A-08
Lin Y, Tronche EJ, Steenstra ES, van Westrenen W (2017) Experimental constraints on the solidification of a nominally dry lunar magma ocean. Earth Planet Sci Lett 471:104–116
Lin Y, Hui H, Xia X, Shang S, van Westrenen W (2020) Experimental constraints on the solidification of a hydrous lunar magma ocean. Meteorit Planet Sci 55:207–230
Lindsay FN, Herzog GF, Albarède F (2011) Cu and Fe isotope abundances in low Ti lunar basalts. 74th Annu Meteorit Soc Meet: abstract #5186
Ling Z, Jolliff BL, Wang A, Li C, Liu, J, Zhang J, LiB, Sun L, Chen J, Xiao L, Liu J, Peng W, Cui X, He Z, Liu J (2015) Correlated compositional and mineralogical investigations at the Chang′ e-3 landing site. Nat Commun 6:8880
Liu Y, Spicuzza MJ, Craddock PR, Day JMD, Valley JW, Dauphas N, Taylor LA (2010) Oxygen and iron isotope constraints on near-surface fractionation effects and the composition of lunar mare basalt source regions. Geochim Cosmochim Acta 74:6249–6262
Liu Y, Patchen A, Taylor LA (2011) Lunar highland breccias MIL 090034/36/70/75: A significant KREEP component. Lunar Planet Sci Conf 42:1261
Longhi J, Walker D, Hays JF (1978) The distribution of Fe and Mg between olivine and lunar basaltic liquids. Geochim Cosmochim Acta 42:1545–1558
Longhi J (1987) On the connection between mare basalts and picritic volcanic glasses. Proc Lunar Planet Sci Conf 17 in J Geophys Res Solid Earth 92:E349–E360
Longhi J (1992) Experimental petrology and petrogenesis of mare volcanics. Geochim Cosmochim Acta 56:2235–2251
Longhi J, Durand SR, Walker D (2010) The pattern of Ni and Co abundances in lunar olivines. Geochim Cosmochim Acta 74:784–798
Loper DE, Werner CL (2002a) On lunar asymmetries 1: Tilted convection and crustal asymmetry. J Geophys Res 107(E6):5046
Loper DE, Werner CL (2002b) On lunar asymmetries 2: Origin and distribution of mare basalts and mascons. J Geophys Res 107(E6):5045
Ludwig KR (2003) Isoplot 3.00: A geochronological toolkit for Microsoft Excel. Berkeley Geochronology Center, Berkeley
Lugmair GW, Marti K, Kurtz JP, Scheinin NB (1976) History and genesis of lunar troctolite 76535 or: How old is old. Lunar Planet Sci Conf Proc 7:2009–2033
Lunatic Asylum (1970) Mineralogic and isotopic investigations on lunar rock 12013. Earth Planet Sci Lett 9:137–163
Ma M-S, Schmitt RA, Warner RD, Taylor GJ, Barker S, Keil K (1980) Aluminous mare basalts and basaltic-textured KREEPy rocks from Apollo 14 coarse fines. Lunar Planet Sci Conf 11:652–654
Maaløe S, McBirney AR (1997) Liquid fractionation. Part IV: Scale models for liquid fractionation of calc-alkaline magmas. J Volcanol Geother Res 76:111–125
Magna T, Wiechert U, Halliday AN (2006) New constraints on the lithium isotope compositions of the Moon and terrestrial planets. Earth Planet Sci Lett 243:336–353
Malin MC (1974) Lunar red spots: Possible pre-mare materials. Earth Planet Sci Lett 21:331–341
Marks NE, Borg LE, Shearer CK, Cassata WS (2019) Geochronology of an Apollo 16 clast provides evidence for a basin-forming impact 4.3 billion years ago. J Geophys Res Planets 124:2465–2481
Marschall HR, Wanless VD, Shimizu N, Pogge von Strandmann PAE, Elliott T, Monteleone BD (2017) The boron and lithium isotopic composition of mid-ocean ridge basalts and the mantle. Geochim Cosmochim Acta 207:102–138
Marvin UB, Lindstrom MM, Holmberg BB, Martinez RR (1991) New observations on the quartz monzodiorite–granite suite. Proc Lunar Planet Sci 21:119–135
McCord TB, Clark RN, Hawke, McFadden LA, Owensby PD, Pieters CM, Adams JB (1981) Moon: Near-infrared Spectral Reflectance, a First Good Look.J Geophys Res 86:10883–10892
McCubbin FM, Steele A, Hauri EH, Nekvasil H, Yamashita S, Hemley RJ (2010) Nominally hydrous magmatism on the Moon. Proc Natl Acad Sci 107:11223–11228

McCubbin FM, Jolliff BL, Nekvasil H, Carpenter PK, Zeigler RA, Steele A, Elardo SM, Lindsley DH (2011) Fluorine and chlorine abundances in lunar apatite: Implications for heterogeneous distributions of magmatic volatiles in the lunar interior. Geochim Cosmochim Acta 75:5073–5093

McCubbin FM, Barnes JJ, Ni P, Hui H, Klima RL, Burney D, Day JMD, Magna T, Boyce JW, Tartèse R, Vander Kaaden KE, Steenstra E, Elardo SM, Zeigler RA, Anand M, Liu Y (2023) Endogenous lunar volatiles. Rev Mineral Geochem 89:729–786

McKay GA, Wiesmann H, Nyquist LE, Wooden JL, Bansal BM (1978) Petrology, chemistry, and chronology of 14078-Chemical constraints on the origin of KREEP. Proc Lunar Planet Sci Conf 9:661–687

McKay GA, Wiesmann H, Bansal BM, Shih CY (1979) Petrology, chemistry, and chronology of Apollo 14 KREEP basalts. Proc Lunar Planet Sci Conf 10:181–205

McLeod CL, Brandon AD, Armytag RMG (2014) Constraints on the formation age and evolution of the Moon from 142Nd-143Nd systematics of Apollo 12 basalts. Earth Planet Sci Lett 396:179–189

Melosh HJ, Kendall J, Horgan B, Johnson BC, Bowling T, Lucey PG, Taylor GJ (2017) South Pole–Aitken basin ejecta reveal the Moon's upper mantle. Geology 45:1063–1066

Meyer C, Williams IS, Compston W (1989) Zircon-containing rock fragments within Apollo 14 breccia indicate serial magmatism from 4350 to 4000 million years. *In:* Moon in transition: Apollo 14, KREEP, and evolved lunar rocks, p 75–78

Meyer C, Williams IS, Compston W (1996) Uranium-lead ages for lunar zircons: Evidence for a prolonged period of granophyre formation from 4.32 to 3.88 Ga. Meteoritics Planet Sci 31:370–387

Miljković K, Wieczorek MA, Collins GS, Laneuville M, Neumann GA, Melosh HJ, Solomon SC, Phillips RJ, Smith DE, Zuber MT (2013) Asymmetric distribution of lunar impact basins caused by variations in target properties. Science 342:724–726

Millet MA, Dauphas N, Greber ND, Burton KW, Dale CW, Debret B, Macpherson CG, Nowell GM, Williams HM (2016) Titanium stable isotope investigation of magmatic processes on the Earth and Moon. Earth Planet Sci Lett 449:197–205

Mills RD, Simon JI, Alexander CMO'D, Wang J, Hauri EH (2017) Water in alkali feldspar: The effect of rhyolite generation on the lunar hydrogen budget. Geochem Perspect Lett 3:115–123

Moynier F, Albarède F, Herzog GF (2006) Isotopic composition of zinc, copper, and iron in lunar samples. Geochim Cosmochim Acta 70:6103–6117

Nakamura N, Tatsumoto M, Nunes PD, Unruh DM, Schwab AP, Wildeman TR (1976) 4.4 b.y .-old clast in Boulder 7, Apollo 17: A comprehensive chronological study by U–Pb, Rb–Sr and Sm–Nd methods. Proc Lunar Sci Conf 7:2309–2333

Neal CR (2001) Interior of the Moon: The presence of garnet in the primitive deep lunar mantle. J Geophys Res 106:27865–27885

Neal CR (2017) Lunar LIPs: What story are they telling us? Lunar Planet Sci Conf 48:1912

Neal CR (2018) A new look at Apollo 17 basaltic samples 45 years on. Lunar Planet Sci Conf 49:1807

Neal CR, Kramer GY (2006) The petrogenesis of Apollo 14 high-Al basalts. Am Mineral 91:1521–1535

Neal CR, Taylor LA (1989a) The nature of barium partitioning between immiscible melts: A comparison of experimental and natural systems with reference to lunar felsite petrogenesis. Proc Lunar Planet Sci Conf 19:209–218

Neal CR, Taylor LA (1989b) Metasomatic products of the lunar magma ocean: The role of KREEP dissemination. Geochim Cosmochim Acta 53:529–541

Neal CR, Taylor LA (1992) Petrogenesis of mare basalts: A record of lunar volcanism. Geochim Cosmochim Acta 56:2177–2211

Neal CR, Donohue P, Fagan AL, O'Sullivan K, Oshrin J, Roberts S (2015) Distinguishing between basalts produced by endogenic volcanism and impact processes: A non-destructive method using quantitative petrography of lunar basaltic samples. Geochim Cosmochim Acta 148:62–80

Needham DH, Kring DA (2017) Lunar volcanism produced a transient atmosphere around the ancient Moon. Earth Planet Sci Lett 478:175–178

Nemchin AA, Pidgeon RT, Whitehouse MJ, Vaughan JP, Meyer C (2008) SIMS U-Pb study of zircon from Apollo 14 and 17 breccias: implications for evolution of lunar KREEP. Geochim Cosmochim Acta 72:668–689

Nemchin AA, Whitehouse MJ, Grange ML, Muhling JR (2011) On the elusive isotopic composition of lunar Pb. Geochim Cosmochim Acta 75:2940–2964

Newcombe ME, Brett A, Beckett JR, Baker MB, Newman S, Guan Y, Eiler JM, Stolper EM (2017) Solubility of water in lunar basalt at low pH_2O. Geochim Cosmochim Acta 200:330–352

Nielsen SG, Auro M, Righter K, Davis D, Prytulak J, Wu F, Owens JD (2019) Nucleosynthetic vanadium isotope heterogeneity of the early solar system recorded in chondritic meteorites. Earth Planet Sci Lett 505:131–140

Nicholis MG, Rutherford MJ (2009) Graphite oxidation in the Apollo 17 orange glass magma: Implications for the generation of a lunar volcanic gas phase. Geochim Cosmochim Acta 73:5905–5917

Norman MD, Yaxley GM, Bennett VC, Brandon AD (2006) Magnesium isotopic composition of olivine from the Earth, Mars, Moon, and pallasite parent body. Geophys Res Lett 33:L15202

Nyquist LE, Shih C-Y (1992) The isotopic record of lunar volcanism. Geochim Cosmochim Acta 56:2213–2234

Nyquist LE, Bansal BM, Wiesmann H (1975) Rb–Sr ages and initial Sr-87/Sr-86 for Apollo 17 basalts and KREEP basalt 15386. Proc Lunar Sci Conf 6:1445–1465

Nyquist LE, Bansal BM, Wooden JL, Wiesmann H (1977) Sr-isotopic constraints on the petrogenesis of Apollo 12 mare basalts. Proc Lunar Sci Conf 8:1383–1415

Nyquist LE, Reimold WU, Bogard DD, Wooden JL, Bansal BM, Wiesmann H, Shih C-Y (1981) A comparative Rb–Sr, Sm–Nd, and K–Ar study of shocked norite 78236: Evidence of slow cooling in the lunar crust? Proc Lunar Planet Sci 12B:67–97

Nyquist LE, Wiesmann H, Bansal B, Shih C-Y, Keith JE, Harper CL (1995) ^{146}Sm–^{142}Nd formation interval for the lunar mantle. Geochim Cosmochim Acta 59:2817–2837

Nyquist LE, Bogard DD, Shih C-Y (2001) Radiometric chronology of the Moon and Mars. *In:* The Century of Space Science. Springer, Dordrecht, p 1325–1376

Oberli F, Huneke JC, Wasserburg GJ (1979) U–Pb and K–Ar systematics of cataclysm and precataclysm lunar impactites. Lunar Planet Sci Conf 10:940–942

Ohtake M, Takeda H, Matsunaga T, Yokota Y, Haruyama J, Morota T, Yamamoto S, Ogawa Y, Hiroi T, Karouji Y, Saiki K, Lucey PG (2012) Asymmetric crustal growth on the Moon indicated by primitive farside highland materials. Mat Geosci 5:384–388

Paige DA, Siegler MA (2016) New constraints on lunar heat flow rates from LRO diviner lunar radiometer experiment polar observations. Lunar Planet Sci Conf 47:2753

Paniello RC, Day JMD, Moynier F (2012) Zinc isotopic evidence for the origin of the Moon. Nature 490:376–379

Papanastassiou DA, Wasserburg GJ (1971) Rb–Sr ages of igneous rocks from the Apollo 14 mission and the age of the Fra Mauro formation. Earth Planet Sci Lett 12:36–48

Papanastassiou DA, Wasserburg GJ (1975) Rb–Sr study of a lunar dunite and evidence for early lunar differentiates. Proc Lunar Planet Sci Conf 6:1467–1489

Papanastassiou DA, Wasserburg GJ (1976) Rb–Sr age of troctolite 76535. Proc Lunar Planet Sci Conf 7:2035–2054

Papike JJ, Hodges FN, Bence AE, Cameron M, Rhodes JM (1976) Mare basalts: crystal chemistry, mineralogy, and petrology. Rev Geophys 14:475–540

Papike JJ, Ryder G, Shearer CK (1998) Lunar samples. Rev Mineral Geochem 36:1–234

Parmentier EM, Zhong S, Zuber MT (2002) Gravitational differentiation due to initial chemical stratification: origin of lunar asymmetry by the creep of dense KREEP? Earth Planet Sci Lett 201:473–480

Petford N (1996) Dykes or diapirs. Trans R Soc Edinburgh: Earth Sci 87:105–114

Petford N, Gallagher K (2001) Partial melting of mafic (amphibolitic) lower crust by periodic influx of basaltic magma. Earth Planet Sci Lett 193:483–499

Petro NE, Isaacson PJ, Pieters CM, Jolliff BL, Carter LM, Klima RL (2013) Presence of OH/H_2O associated with the lunar Compton-Belkovich volcanic complex identified by the Moon Mineralogy Mapper (M3) Lunar Planet Sci Conf 44:2688

Pidgeon RT, Nemchin AA, Van Bronswijk W, Geisler T, Meyer C, Compston W, Williams IS (2007) Complex history of a zircon aggregate from lunar breccia 73235. Geochim Cosmochim Acta 71:1370–1381

Pidgeon RT, Nemchin AA, Kamo SL (2011) Comparison of structures in zircons from lunar and terrestrial impactites. Can J Earth Sci 48:107–116

Pieters CM, McCord TB, Zisk SH, Adams JB (1973) Lunar black spots and the nature of the Apollo 17 landing area, J Geophys Res 78:5867–5875

Pieters CM, Besse S, Boardman J, Buratti B, Cheek L, Clark RN, Combe JP, Dhingra D, Goswami JN, Green RO, Head III JW, Isaacson P, Klima R, Kramer G, Lundeen S, Malaret E, McCord T, Mustard J, Nettles J, Petro NE, Runyon C, Staid M, Sunshine J, Taylor LA, Thaisen K, Tompkins S, Whitten J (2011) Mg-spinel lithology: A new rock type on the lunar farside. J Geophys Res Planets 116:E00G08

Pieters CM, Hanna KD, Cheek L, Dhingra D, Prissel T, Jackson C, Moriaty D, Parman S, Taylor LA (2014) The distribution of Mg-spinel across the Moon and constraints on crustal origin. Am Mineral 99:1893–1910

Poitrasson F, Halliday AN, Lee DC, Levasseur S, Teutsch N (2004) Iron isotope differences between Earth, Moon, Mars and Vesta as possible records of contrasted accretion mechanisms. Earth Planet Sci Lett 223:253–266

Poitrasson F, Zambardi T, Magna T, Neal CR (2019) A reassessment of the iron isotope composition of the Moon and its implications for the accretion and differentiation of terrestrial planets. Geochim Cosmochim Acta 267:257–274

Powell BN, Aitken FK, Weiblen PW (1973) Classification, distribution, and origin of lithic fragments from the Hadley-Apennine region. Proc Lunar Sci Conf. 4:445–460

Premo WR, Tatsumoto M (1991) U–Th–Pb isotopic systematics of lunar norite 78235. Proc Lunar Planet Sci Conf 21:89–100

Premo WR, Tatsumoto M (1992) U–Th–Pb, Rb–Sr, and Sm–Nd isotopic systematics of lunar troctolitic cumulate 7653—Implications on the age and origin of this early lunar, deep-seated cumulate. Proc Lunar Planet Sci Conf 22:381–397

Pringle EA, Moynier F (2017) Rubidium isotopic composition of the Earth, meteorites, and the Moon: Evidence for the origin of volatile loss during planetary accretion. Earth Planet Sci Lett 473:62–70

Prissel TC, Gross J (2018) Re-examining the petrogenesis of lunar troctolites. Lunar Planet Sci Conf 49:2583

Prissel TC, Gross J (2019) Establishing new co-magmatic trends among the lunar highlands. 50th Lunar Planet Sci Conf 50:3106

Prissel TC, Gross J (2020) On the petrogenesis of lunar troctolites: New insights into cumulate mantle overturn & mantle exposures in impact basins. Earth Planet Sci Lett 551:116531

Prissel TC, Parman SW, Jackson CRM, Rutherford MJ, Hess PC, Head JW, Cheek L, Dhingra D, Pieters CM (2014) Pink Moon: The petrogenesis of pink spinel anorthosites and implications concerning Mg-suite magmatism. Earth Planet Sci Lett 403:144–156

Prissel TC, Parman SW, Head III JW (2016a) Formation of the lunar highlands mg-suite as told by spinel. Am Mineral 101:1624–1635

Prissel TC, Whitten JL, Parman SW, Head III JW (2016b) On the potential for lunar highlands Mg-suite extrusive volcanism and implications concerning crustal evolution. Icarus 277:319–329

Prytulak J, Nielsen SG, Ionov DA, Halliday AN, Harvey J, Kelley KA, Niu YL, Peate DW, Shimizu K, Sims KWW (2013) The stable vanadium isotope composition of the mantle and mafic lavas. Earth Planet Sci Lett 365:177–189

Qiao L, Head III JW, Xiao L, Wilson L, Dufek JD (2018) The role of substrate characteristics in producing anomalously young crater retention ages in volcanic deposits on the Moon: Morphology, topography, subresolution roughness, and mode of emplacement if the Sosigenes lunar irregular mare patch. Meteorit Planet Sci 53:778–812

Qiao L, Head III JW, Ling Z, Wilson L, Xiao L, Dufek JD, Yan J (2019) Geological characterization of the Ina shield volcano summit pit crater on the Moon: Evidence for extrusion of waning-stage lava lake magmatic foams and anomalously young crater retention ages. J Geophys Res Planets 124:1100–1140

Qiao L, Head III JW, Wilson L, Ling Z (2020) The Cauchy 5 small, low-volume lunar shield volcano: Evidence for volatile exsolution-eruption patterns and Type 1/Type 2 hybrid irregular mare patch formation. J Geophys Res Planets 125:e2019JE006171

Quick JE, James OB, Albee AL (1981) Petrology and petrogenesis of lunar breccia 12013. Proc Lunar Planet Sci Conf 12B:117–172

Rankenburg K, Brandon AD, Neal CR (2006) Neodymium isotope evidence for a chondritic composition of the Moon. Science 312:1369–1372

Rapp JF, Draper DS (2018) Fractional crystallization of the lunar magma ocean: Updating the dominant paradigm. Meteorit Planet Sci 53:1432–1455

Renggli CJ, King PL, Henley RW, Norman MD (2017) Volcanic gas composition, metal dispersion and deposition during explosive volcanic eruptions on the Moon. Geochim Cosmochim Acta 206:296–311

Robinson KL, Taylor GJ (2014) Heterogeneous distribution of water in the Moon. Nat Geosci 7:401–408

Robinson KL, Treiman AH, Joy KH (2012) Basaltic fragments in lunar feldspathic meteorites: Connecting sample analyses to orbital remote sensing. Meteorit Planet Sci 47:387–399

Robinson KL, Hellebrand E, Taylor GJ (2015) The physical setting for felsite formation. Lunar Planet Sci 46:1623

Rolf T, Zhu MH, Wünnemann K, Werner SC (2017) The role of impact bombardment history in lunar evolution. Icarus 286:138–152

Rutherford M, Papale M (2009) Origin of basalt fire-fountain eruptions on Earth versus the Moon. Geology 37:219–222

Rutherford MJ, Hess PC, Ryerson FJ, Campbell HW, Dick PA (1976) The chemistry, origin and petrogenetic implications of lunar granite and monzonite. Proc Lunar Sci Conf 7:1723–1740

Ryder G (1976) Lunar sample 15405: ReHessmnant of a KREEP basalt-granite differentiated pluton. Earth Planet Sci Lett 29:255–268

Ryder G (1987) Petrographic evidence for nonlinear cooling rates and a volcanic origin for Apollo 15 KREEP basalts. J Geophys Res Solid Earth 92:E331–E339

Ryder G (1988) Quenching and disruption of lunar KREEP lava flows by impacts. Nature 336:751–754

Ryder G (2002) Mass flux in the ancient EarthMoon system and benign implications for the origin of life on Earth. J Geophys Res Planets 107:e2019JE006171

Ryder G, Martinez RR (1991) Evolved hypabyssal rocks from Station 7, Apennine Front, Apollo 15. Proc Lunar Planet Sci Conf 21:137–150

Saal AE, Hauri EH, Lo Cascio M, Van Orman JA, Rutherford MC, Cooper RF (2008) Volatile content of lunar volcanic glasses and the presence of water in the Moon's interior. Nature 454:192–195

Sakamaki T, Ohtani E, Urakawa S, Suzuki A, Katayama Y, Zhao D (2010) Density of high-Ti basalt magma at high pressure and origin of heterogeneities in the lunar mantle. Earth Planet Sci Lett 299:285–289

Salisbury JW, Walter LS (1989) Therm infrared (2.5–13.5 μm) spectroscopic remote sensing of igneous rock types on particulate planetary surfaces. J Geophys Res 94:9192–9202

Salpas PA, Taylor LA, Lindstrom MM (1987) Apollo 17 KREEPy basalts: Evidence for nonuniformity of KREEP. Proc Lunar Planet Sci Conf 18, in J Geophys Res Solid Earth 92:E340–E348

Sato M (1976) Oxygen fugacity and other thermochemical parameters of Apollo 17 high-Ti basalts and their implications on the reduction mechanism. Proc Lunar Sci Conf 7:1323–1344

Schauble EA (2004) Applying stable isotope fractionation theory to new systems. Rev Mineral Geochem 55:65–111

Schoenberg R, Zink S, Staubwasser M, von Blanckenburg F (2008) The stable Cr isotope inventory of solid Earth reservoirs determined by double spike MC-ICP-MS. Chem Geol 249:294–306

Schultz PH, Spudis PD (1983) Beginning and end of lunar mare volcanism. Nature 302:233–236

Sedaghatpour F, Teng FZ, Liu Y, Sears DWG, Taylor LA (2013) Magnesium isotopic composition of the Moon. Geochim Cosmochim Acta 120:1–16

Sedaghatpour F, Jacobsen SB (2019) Magnesium stable isotopes support the lunar magma ocean cumulate remelting model for mare basalts. PNAS 116:73–78

Seddio SM, Jolliff BL, Korotev RL, Zeigler RA (2013) Petrology and geochemistry of lunar granite 12032,366–19 and implications for lunar granite petrogenesis. Am Mineral 98:1697–1713
Seddio SM, Jolliff BL, Korotev RL, Carpenter PK (2014) Thorite in an Apollo 12 granite fragment and age determination using the electron microprobe. Geochim Cosmochim Acta 135:307–320
Seddio SM, Korotev RL, Jolliff BL, Wang A (2015) Silica polymorphs in lunar granite: Implications for granite petrogenesis on the Moon. Amer Mineral 100:1533–1543
Seitz HM, Brey GP, Weyer S, Durali S, Ott U, Münker C, Mezger K (2006) Lithium isotope compositions of Martian and lunar reservoirs. Earth Planet Sci Lett 245:6–18
Shaulis BJ, Righter M, Lapen,TJ, Jolliff BL, Irving AJ (2017) 3.1 Ga crystallization age for magnesian and ferroan gabbro lithologies in the Northwest Africa 773 clan of lunar meteorites. Geochim Cosmochim Acta 213:435–456
Shearer CK, Papike JJ (1993) Basaltic magmatism on the Moon: A perspective from volcanic picritic glass beads. Geochim Cosmochim Acta 57:4785–4812
Shearer CK, Papike JJ (2005) Early crustal building processes on the moon: Models for the petrogenesis of the magnesian suite. Geochim Cosmochim Acta 69:3445–3461
Shearer CK, Papike JJ, Galbreath KC, Shimizu N (1991) Exploring the lunar mantle with secondary ion mass spectrometry: A comparison of lunar picritic glass beads from the Apollo 14 and Apollo 17 sites. Earth Planet Sci Lett 102:134–147
Shearer CK, Hess P, Wieczorek M, Pritchard M, Parmentier EM, Borg L, Longhi J, Elkins-Tanton L, Neal CR, Antonenko I, Canup R, Halliday A, Grove T, Hager B, Lee D-C,Wiechert U (2006) Thermal and magmatic evolution of the Moon. Rev Mineral Geochem 60:365–518
Shearer CK, Borg LE, Burger PV, Connelly JN, Bizarro M (2012) Timing and duration of the Mg-suite episode of lunar crustal building. Part 1: Petrography and mineralogy of a norite clast in 15445. Lunar Planet Sci Conf 43:1421
Shearer CK, Elardo SM, Petro NE, Borg LE, McCubbin FM (2015) Origin of the lunar highlands Mg-suite: An integrated petrology, geochemistry, chronology, and remote sensing perspective. Am Mineral 100:294–325
Shervais JW, Taylor LA (1983) Breccia Guidebook No. 5:14305: NASA Planetary Materials Branch, Publication No. 68, JSC 19267, Johnson Space Center, Houston
Shih C-Y, Nyquist LE, Bogard DD, Wooden JL, Bansal BM, Wiesmann H (1985) Chronology and petrogenesis of a 1.8 g lunar granitic clast: 14321, 1062. Geochim Cosmochim Acta 49:411–426
Shih C-Y, Nyquist LE, Bansal BM, Wiesmann H (1992) Rb–Sr and Sm–Nd chronology of an Apollo 17 KREEP basalt. Earth Planet Sci Lett 108:203–215
Shih C-Y, Nyquist LE, Wiesmann H (1993) K–Ca chronology of lunar granites. Geochim Cosmochim Acta 57:4827–4841
Shih C-Y, Nyquist LE, Bogard DD, Wiesmann H (1994) K–Ca and Rb–Sr dating of two lunar granites: Relative chronometer resetting. Geochim Cosmochim Acta 58:3101–3116
Shirai N, Ebihara M, Sekimoto A, Yamaguchi A, Nyquist L, Shih C-Y, Park J, Nagao K (2012) Geochemistry of lunar highland meteorites MIL 090034, 090036 and 090070. Lunar Planet Sci Conf 43:2003
Shirley KA, Zanetti M, Jolliff BL, van der Bogert CH, Hiesinger H (2016) Crater size–frequency distribution measurements and age of the Compton-Belkovich Volcanic Complex. Icarus 273:214–223
Shuster DL, Balco G, Cassata WS, Fernandes VA, Garrick-Bethell I, Weis BP (2010) A record of impacts preserved in the lunar regolith. Earth Planet Sci Lett 290:155–165
Siegler MA, Smrekar SE (2014) Lunar heat flow: Regional prospective of the Apollo landing sites. J Geophys Res Planets 119:47–63
Siegler MA, Miller RS, Keane JT, Laneuville M, Paige DA, Matsuyama I, Lawrence DJ, Crotts A, Poston MJ (2016) Lunar true polar wander inferred from polar hydrogen. Nature 531:480–484
Simon JI, DePaolo DJ (2010) Stable calcium isotopic composition of meteorites and rocky planets. Earth Planet Sci Lett 289:457–466
Simon SB, Papike JJ, Laul JC (1988) Chemistry and petrology of the Apennine Front, Apollo 15, Part 1: KREEP basalts and plutonic rocks. Proc Lunar Planet Sci Conf 18:187–201
Simon JI, Renne PR, Mundil R (2008) Implications of pre-eruptive magmatic histories of zircons for U–Pb geochronology of silicic extrusions. Earth Planetary Sci Lett 266:182–194
Simon JI, Shih C-Y, Nyquist LE (2011) K–Ca and Rb–Sr dating of lunar granite 14321 revisited. Lunar Planet Sci Conf 42:2754
Simon JI, Weis D, DePaolo DJ, Renne PR, Mundil R, Schmitt AK (2014) Assimilation of preexisting Pleistocene intrusions at Long Valley by periodic magma recharge accelerates rhyolite generation: rethinking the remelting model. Contrib Mineral Petrol 167:955
Simon JI, Jordan MK, Tappa MJ, Schauble EA, Kohl IE, Young ED (2017) Calcium and titanium isotope fractionation in refractory inclusions: Tracers of condensation and inheritance in the early solar protoplanetary disk. Earth Planet Sci Lett 472:277–288
Simon JI, Christoffersen R, Wang J, Mouser MD, Mills RD, Ross DK, Alexander CMO'D (2020) Volatiles in lunar felsite clasts: Impact related delivery of hydrous material to a dry Moon. Geochim Cosmochim Acta 276:299–326
Singletary S, Grove T (2008) Origin of lunar high-titanium ultramafic glasses: A hybridized source? Earth Planet Sci Lett 268:182–189
Singoi S, Quick JE, Clemens-Knott D, Mayer A, Demarchi G, Mazzucchelli M, Negrini L, Rivalenti G (1994), Chemical evolution of a large mafic intrusion in the lower crust, Ivrea–Verbano Zone, northern Italy. J Geophys Res 99:21,575–21,590

Sisson TW, Ratajeski K, Hankins WB, Glazner AF (2005) Voluminous granitic magmas from common basaltic sources. Contrib Mineral Petrol 148:635–661
Smith JV, Anderson AT, Newton RC, Olsen EJ, Wyllie PJ (1970) Petro logic history of the moon inf erred from petrography, mineralogy, and petrogenesis of Apollo 11 rocks. Proc Lunar Sci Conf 1:897–925
Snape JF, Curran NM, Whitehouse MJ (2018) Ancient volcanism on the Moon: Insightss from Pb isotopes in the MIL 13317 and Kalahari 009 lunar meteroites. Earth Planet Sci Lett 502:84–95
Snyder GA, Taylor LA, Neal CR (1991) The sources of mare basalts: A model involving lunar magma ocean crystallization, plagioclase flotation, and trapped instantaneous residual liquid. *In:* Mare Volcanism and Basalt Petrogenesis: Astounding Fundamental Concepts. LPI Tech Rpt 91–03:53–54
Snyder GA, Taylor LA, Neal CR (1992) A chemical model for generating the sources of mare basalts: Combined equilibrium and fractional crystallization of the lunar magmasphere. Geochim Cosmochim Acta 56:3809–3823
Snyder GA, Lee D-C, Taylor LA, Halliday AN, Jerde EA (1994) Evolution of the upper mantle of the Earth's Moon: Neodymium and strontium isotopic constraints from high-Ti mare basalts. Geochim Cosmochim Acta 58:4795–4808
Snyder GA, Neal CR, Taylor LA (1995) Processes involved in the formation of magnesian-suite plutonic rocks from the highlands of the Earth's Moon. J Geophys Res 100:9365–9388
Snyder GA, Taylor LA, Patchen A, Nazarov MA, Semenova TS (1999) Mineralogy and petrology of a primitive spinel troctolite and gabbros from Luna 20, eastern highlands of the Moon. Lunar Planet Sci Conf 30:1491
Snyder GA, Borg LE, Nyquist LE, Taylor LA (2000) Chronology and isotopic constraints on lunar evolution. *In:* Origin of the Earth and Moon. University of Arizona Press, p 361–395
Sokol A, Fernandes V, Schulz T, Bischoff A, Burgess R, Clayton R, Münker C, Nishiizumi K, Palme H, Schultz L, Weckwerth G, Mezger K, Horstmann M (2008) Geochemistry, petrology and ages of the lunar meteorites Kalahari 008 and 009: New constraints on early lunar evolution. Geochim Cosmochim Acta 72:4845–4873
Sossi PA, Moynier F (2017) Chemical and isotopic kinship of iron in the Earth and Moon deduced from the lunar Mg-suite. Earth Planet Sci Lett 471:125–135
Sossi PA, O'Neill HStC (2017) The effect of bonding environment on iron isotope fractionation between minerals at high temperature. Geochim Cosmochim Acta 196:121–143
Sossi PA, Nebel O, O'Neill HStC, Moynier F (2018) Zinc isotope composition of the Earth and its behaviour during planetary accretion. Chem Geol 477:73–84
Speyerer EJ, Robinson MS, Denevi BW, LROC Science Team (2011) Lunar Reconnaissance Orbiter Camera global morphological map of the Moon. Lunar Planet Sci Conf 42:2387
Spicuzza MJ, Day JMD, Taylor LA, Valley JW (2007) Oxygen isotope constraints on the origin and differentiation of the Moon. Earth Planet Sci Lett 253:254–265
Sprung P, Kleine T, Scherer EE (2013) Isotopic evidence for chondritic Lu/Hf and Sm/Nd of the Moon Earth Planet Sci Lett 380:77–87
Stadermann A, Zanetti M, Jolliff B, Hiesinger H (2015) Revisiting the youngest mare basalts on the Moon: Analysis of primary and secondary crater distributions in the region south of Aristarchus Crater. Lunar Planet Sci Conf 46:1269
Staudacher T, Jessberger EK, Flohs I, Kirsten T (1979) $^{40}Ar/^{39}Ar$ age systematics of consortium breccia 73255. Proc Lunar Planet Sci Conf 10:745–762
Steenstra ES, Seegers AX, Eising J, Tomassen BGJ, Webers FPF, Berndt J, Klemme S, Mateev S, van Westrenen W (2018) Evidence for a sulfur-undersaturated lunar interior from the solubility of sulfur in lunar melts and sulfide–silicate partitioning of siderophile elements. Geochim Cosmochim Acta 231:130–156
Stettler A, Eberhardt P, Geiss J, Grogler N (1974) $^{39}Ar–^{40}Ar$ ages of samples from the Apollo 17 station 7 boulder and implications for its formation. Earth Planet Sci Lett 23:453–461
Stoeser DB, Ryder G, Marvin UB (1975) Lunar granite clasts with unique ternary feldspars. Lunar Sci Conf 6:780–782
Stolper E (1982) Water in silicate glasses: an infrared spectroscopic study. Contrib Mineral Petrol 81:1–17
Stolper E, Newman S (1994) The role of water in the petrogenesis of Mariana trough magmas. Earth Planet Sci Lett 121:293–325
Sun Y, Li L, Zhang Y (2017) Detection of Mg-spinel bearing central peaks using M3 images: Implications for the petrogenesis of Mg-spinel. Earth Planet Sci Lett 465:48–58
Takeda H, Yamaguchi A, Bogard DD, Karouji Y, Ebihara M, Ohtake M, Saiki K, Arai T (2006) Magnesian anorthosites and a deep crustal rock from the farside crust of the moon. Earth Planet Sci Lett 247:171–184
Tatsumoto M, Unruh DM (1976) KREEP basalt age: Grain by grain U–Th–Pb systematics study of the quartz monzodiorite clast 15405,88. Proc Lunar Sci Conf 7:2107–2129
Taylor SR, Jakes P (1974) The geochemical evolution of the Moon. Proc Lunar Sci Conf 5:1287–1305
Taylor LA, Shervais JW, Hunter RH, Shih C, Bansal B, Wooden J, Nyquist L, Laul L (1983) Pre-4.2 AE mare-basalt volcanism in the lunar highlands. Earth Planet Sci Lett 66:33–47
Taylor LA, Patchen A, Mayne RG, Taylor DH (2004) The most reduced rock from the moon, Apollo 14 basalt 14053: Its unique features and their origin. Am Mineral 89:1617–1624
Taylor DJ, McKeegan KD, Harrison TM (2009) Lu–Hf zircon evidence for rapid lunar differentiation. Earth Planet Sci Lett 279:157–164
Taylor GJ, Martel LM, Spudis PD (2012) The Hadley-Apennine KREEP basalt igneous province. Meteorit Planet Sci 47:861–879
Teng FZ (2017) Magnesium isotope geochemistry. Rev Mineral Geochem 82:219–287

Teng F-Z, Li W-Y, Ke S, Marty B, Dauphas N, Huang S, Wu F-Y, Pourmand A (2010) Magnesium isotopic composition of the Earth and chondrites. Geochim Cosmochim Acta 74:410–4166
Terada K, Anand M, Sokol AK, Bischoff A, Sano Y (2007) Cryptomare magmatism 4.35 Gyr ago recorded in lunar meteorite Kalahari 009. Nature 450:849–852
Thiessen F, Nemchin AA, Snape JF, Bellucci JJ, Whitehouse MJ (2018) Apollo 12 breccia 12013: Impact-induced partial Pb loss in zircon and its implications for lunar geochronology. Geochim Cosmochim Acta 230:94–111
Tomascak PB, Magna T, Dohmen R (2016) Advances in lithium isotope geochemistry. Springer International Publishing, Cham, Switzerland
Treiman AH, Maloy AK, Shearer Jr CK, Gross J (2010) Magnesian anorthositic granulites in lunar meteorites Allan Hills A81005 and Dhofar 309: Geochemistry and global significance. Meteorit Planet Sci 45:163–180
Treiman AH, Kulis MJ, Glazner AF (2019) Spinel-anorthosites on the Moon: Impact melt origins suggested by enthalpy constraints. Am Mineral 104:370–384
Turner G (1970) ^{40}Ar–^{39}Ar age determination of lunar rock 12013. Earth Planet Sci Lett 9:177–180
Turner G, Cadogan PH (1975) The history of lunar bombardment inferred from ^{40}Ar–^{39}Ar dating of highland rocks. Proc Lunar Sci Conf 6:1509–1538
Unruh DM, Stille P, Patchett PJ, Tatsumoto M (1984) Lu-Hf and Sm–Nd evolution in lunar mare basalts. Proc Lunar Planet Sci Conf 14. J Geophys Res Solid Earth 89:B459–B477
Valdes MC, Moreira M, Foriel J, Moynier F (2014) The nature of Earth's building blocks as revealed by calcium isotopes. Earth Planet Sci Lett 394:135–145
Valencia SN (2017) Compositional analysis of Apollo 12 granitic breccia 12013: Insights into proto-lithologies. Chapter 3. In The evolution of igneous rocks on the Moon: Insights from lunar meteorites and Apollo 12. Ph. D. Dissertation, Washington University in St. Louis
Valley JW, Spicuzza MJ, Ushikubo T (2014) Correlated $\delta^{18}O$ and [Ti] in lunar zircons: a terrestrial perspective for magma temperatures and water content on the Moon. Contrib Mineral Petrol 167:956
Vaughan WM, Head III JW (2014) Impact melt differentiation in the South Pole-Aitken basin: Some observations and speculations. Planet Space Sci 91:101–106
Vaughan WM, Head III JW, Wilson L, Hess PC (2013) Geology and petrology of enormous volumes of impact melt on the Moon: A case study of the Orientale basin impact melt sea. Icarus 223:749–765
Wagner R, Head III JW, Wolf U, Neukum G (2002) Stratigraphic sequence and ages of volcanic units in the Gruithuisen region of the Moon. J Geophys Res 107:5104
Wagner R, Head III JW, Wolf U, Neukum G (2010) Lunar red spots: Stratigraphic sequence and ages of domes and plains in the Hansteen and Helmet regions on the lunar near side. J Geophys Res 115:E06015
Wang K, Jacobsen SB (2016) Potassium isotopic evidence for a high-energy giant impact origin of the Moon. Nature 538:487–490
Wang ZZ, Liu SA, Liu J, Huang J, Xiao Y, Chu ZY, Zhao XM, Tang L (2017) Zinc isotope fractionation during mantle melting and constraints on the Zn isotope composition of Earth's upper mantle. Geochim Cosmochim Acta 198:151–167
Warren PH (1985) The magma ocean concept and lunar evolution. Annu Rev Earth Planet Sci 13:201–240
Warren PH (1988) The origin of pristine KREEP-Effects of mixing between urKREEP and the magmas parental to the Mg-rich cumulates. Proc Lunar Planet Sci Conf 18:233–241
Warren PH (1989) KREEP: major-element diversity, trace-element uniformity (almost). *In:* Moon in transition: Apollo 14, KREEP, and evolved lunar rocks. LPI Tech Rept 89–03, p 149–153
Warren PH (1993) A concise compilation of petrologic information on possibly pristine nonmare Moon rocks. Am Mineral 78:360–376
Warren PH, Taylor GJ, Keil K, Kallemeyn GW, Shirley DN, Wasson JT (1983) Seventh foray: Whitlockite-rich lithologies, a diopside-bearing troctolitic anorthosite, ferroan anorthosites, and KREEP. Proc Lunar Planet Sci Conf 14. J Geophys Res 88:B151–B164
Warren PH, Jerde EA, Kallemeyn GW (1987) Pristine Moon rocks: A "large" felsite and a metal-rich ferroan anorthosite. Proc Lunar Planet Sci Conf 17. J Geophys Res 92:E303–E313
Webb GS, Neal CR (2019) Quantitative textural analysis of thin sections cut from the interior and exterior of lunar sample 14053. Lunar Planet Sci Conf 50:2534
Weitz CA, Head III JW, Pieters CM (1998) Lunar regional dark mantle deposits:Geologic, multispectral, and modeling studies. J Geophys Res 103:22725–22759
Weitz C, Staid M, Gaddis L, Besse S, Sunshine JM (2017) Investigation of lunar spinels at Sinus Aestuum. J Geophys Res Planets 122:2013–2033
Weyer S, Anbar AD, Brey GP, Münker C, Mezger K, Woodland AB (2005) Iron isotope fractionation during planetary differentiation. Earth Planet Sci Lett 240:251–264
Whitaker EA (1972) Lunar color boundaries and their relationship to topographic features: A preliminary survey. The Moon 4:348–355
Whitehouse MJ, Nemchin AA (2009) High precision, high accuracy measurement of oxygen isotopes in a large lunar zircon by SIMS. Chem Geol 261:32–42
Whitten JL, Head III JW (2015) Lunar cryptomaria: Physical characteristics, distribution, and implications for ancient volcanism. Icarus 247:150–171

Wiechert U, Halliday AN (2007) Non-chondritic magnesium and the origins of the inner terrestrial planets. Earth Planet Sci Lett 256:360–371
Wiechert U, Halliday AN, Lee DC, Snyder GA, Taylor LA, Rumble D (2001) Oxygen isotopes and the Moon-forming giant impact. Science 294:345–348
Wieczorek MA, Weiss BP, Breuer D, Cébron D, Fuller M, Garrick-Bethell I, Gattacceca J, Halekas JS, Hemingway DJ, Hood LL, Laneuville M, Nimmo F, Oran R, Purucker ME, Rückriemen T, Soderlund KM, Tikoo1 SM (2023) Lunar magnetism. Rev Mineral Geochem 89:207–241
Wiesli RA, Beard BL, Taylor LA, Johnson CM (2003) Space weathering processes on airless bodies: Fe isotope fractionation in the lunar regolith. Earth Planet Sci Lett 216:457–465
Wilcox BB, Lucey PG, Hawke BR (2006) Radiative transfer modeling of compositions of lunar pyroclastic deposits. J Geophys Res 111:E09001
Wilson LW, Head III JW (1981) Ascent and eruption of basaltic magma on the Earth and Moon. J Geophys Res 86:2971–3001
Wilson LW, Head III JW (2003) Deep generation of magmatic gas on the Moon and implications for pyroclastic eruptions. Geophys Res Lett 30:1605
Wilson L, Head III JW (2017a) Generation, ascent and eruption of magma on the Moon: New insights into source depths, magma supply, intrusions and effusive/explosive eruptions (Part 1: Theory). Icarus 283:146–175
Wilson L, Head III JW (2017b) Eruption of magmatic foams on the Moon: Formation in the waning stages of dike emplacement events as an explanation of "irregular mare patches". Icarus 335:113–127
Wilson L, Hawke BR, Giguere TA, Petrycki ER (2011) An igneous origin for Rima Hyginus crater on the Moon. Icarus 215:584–595
Wood JA, Dickey JS, Marvin UB, Powell BN (1970) Lunar anorthosites and a geophysical model of the Moon. Proc Lunar Sci Conf 1:965–988
Xue Z, Xiao L, Neal CR, Xu Y (2019) Oldest high-Ti basalt and magnesian crustal materials in feldspathic lunar meteorite Dhofar 1428. Geochim Cosmochim Acta 266:74–108
Yamamoto S, Nakamura R, Matsunaga T, Ogawa Y, Ishihara Y, Morota T, Hirata N, Ohtake M, Hiroi T, Yokota Y, Haruyama J (2010) Possible mantle origin of olivine around lunar impact basins detected by SELENE. Nat Geosci 3:533–536
Yamamoto S, Nakamura R, Matsunaga T (2012) Olivine-rich exposures in the South Pole-Aitken Basin. Icarus 218:331–334
Young ED, Kohl IE, Warren PH, Rubie DC, Jacobson SA, Morbidelli A (2016) Oxygen isotopic evidence for vigorous mixing during the Moon-forming giant impact. Science 351:493–496
Yu S, Tosi N, Schwinger S, Maurice M, Breuer D, Xiao L (2019) Overturn of ilmenite-bearing cumulates in a rheologically weak lunar mantle. J Geophys Res Planets 124:418–436
Zambardi T, Poitrasson F, Corgne A, Méheut M, Quitté G, Anand M (2013) Silicon isotope variations in the inner solar system: Implications for planetary formation, differentiation and composition. Geochim Cosmochim Acta 121:67–83
Zhang N, Parmentier EM, Liang Y (2013) A 3-D numerical study of the thermal evolution of the Moon after cumulate mantle overturn: The importance of rheology and core solidification. J Geophys Res Planets 118:1789–1804
Zhang N, Dygert N, Liang Y, Parmentier EM (2017) The effect of ilmenite viscosity on the dynamics and evolution of an overturned lunar cumulate mantle. Geophys Res Lett 44:6543–6552
Zhao Y, De Vries J, van den Berg AP, Jacobs MHG, van Westrenen W (2019) The participation of ilmenite-bearing cumulates in lunar mantle overturn. Earth Planet Sci Lett 511:1–11
Zhai M, Nakamura E, Shaw DM, Nakano T (1996) Boron isotope ratios in meteorites and lunar rocks. Geochim Cosmochim Acta 60:4877–4881

ELECTRONIC ANNEX

Figures and tables referred to by the prefix "EA" are in an electronic annex available at https://apenninus.u-aizu.ac.jp/NVM2-EA.html